NTNU – Trondheim
Norwegian University of
Science and Technology

Electrolytic Removal of Chloride from Acidic Nitrate Solutions

Maiken Sandland

Chemical Engineering and Biotechnology
Submission date: June 2014
Supervisor: Geir Martin Haarberg, IMTE
Co-supervisor: Frode Seland, IMT

Norwegian University of Science and Technology
Department of Materials Science and Engineering

Declaration

I, Maiken Sandland, hereby declare that the work described in this report has been carried out independently and in accordance with the regulations at NTNU.

Trondheim, June 2014.

Maiken Sandland

Preface

This report describes the work carried out during the master thesis (TMT4900), at the Norwegian University of Science and Technology in the spring of 2014.
The experimental work is carried out by the author, at the Department of Materials Science and Engineering.

The scope of this project is outlined in collaboration with my supervisors; Professor Geir Martin Haarberg and Associate professor Frode Seland, as a continuation of the specialization project (TMT4500) carried out during the fall of 2013.

I would like to thank both of my supervisor, Associate professor Frode Seland and Professor Geir Martin Haarberg, for guidance during this project.

Further, I would like to give a special thanks to Siri Marie Skaftun for helping me in the lab, supporting me when problems have occurred and for always being available for questions and discussions. Also, thank you to Anita Reksten for providing me with iridium oxide powder and helping me at the lab and with the XRD analysis.

A big thank you goes to the department for giving me the opportunity of attending the 7th KIFEE conference in Kyoto, Japan, presenting my project work. I will never forget this great experience.

A thank you also goes to Kjell Røkke and Elin Albertsen for helping me with equipment and for always being available for a quick talk. To Julian Tolchard helping me with both SEM, EDS and XRD. And to Permascand, for providing me with electrode material.

To Andreas, for always making me smile when I come home. Thank you for being the "housewife" in our relationship, when I did not have the time or energy.

Last but not least, my family deserves a big thank you for giving me the opportunity and the push I needed to apply for a study at NTNU. Your support through out my years of studying has been invaluable.

Abstract

Aqueous chemical industry often use solutions which contain chloride. In some processes, like the chlor-alkali or the chlorate process, the chloride is desirable. In other processes, like metal production, water treatment and fertilizer production, the presence of chloride is unfortunate. The presence of chlorine is damaging both for the production inventory and for the environment. The amount of chloride present in the process water in the production needs therefore to be reduced.

The aim of this thesis was to study the feasibility of electrolytic removal of chloride, from an acidic nitrate solution, using a customized dimensionally stable anode (DSA) with an active component of iridium oxide.

Voltammetry was carried out using different electrode set ups and electrode materials. Both a rotating disc electrode (RDE) and a rotating ring disc electrode (RRDE) were utilized. The RDE was used for kinetic studies of the chlorine and oxygen evolution, using a commercial titanium supported IrO_2-Ta_2O_5 electrode. The RRDE was used for current efficiency measurements, both a Pt-Pt electrode (both disc and ring in platinum), and an IrO_2-Pt electrode (iridium oxide coated glassy carbon disc, platinum ring) were used.

Prior to the electrolysis experiments, a titanium supported IrO_2-Ta_2O_5 electrode was prepared by thermal decomposition. Different application techniques of the coating were investigated, including painting and dip coating. The synthesized electrodes were analysed by scanning electron microscopy (SEM), energy dispersive spectroscopy (EDS) and X-ray diffraction (XRD), and compared to a similar commercial electrode from Permascand.

The electrolysis experiments were carried out in both a stagnant cell and in a designed flow cell, testing both a synthetic electrolyte and process water. Different working electrodes were utilized, including the synthesized IrO_2-DSA and a commercial RuO_2/IrO_2-mesh.

The voltammetry experiments using both a RDE and a RRDE indicated that chlorine evolution on iridium oxide based electrodes was only to small degree affected by mass transport.

The electrolysis experiments showed proof of concept, yielding a reduction in the chloride content in the process water of 23 % and a current efficiency of 3 %, using the flow cell and the commercial RuO_2/IrO_2-mesh electrode. The synthesized electrode showed low selectivity towards chlorine evolution. This was found to be most likely due to low crystallinity and/or high porosity of the IrO_2-Ta_2O_5 coating. During long time, stagnant electrolysis in the process water a white deposit was formed on the counter electrode. This deposit was analysed by EDS indicating a high content of calcium phosphate.

Sammendrag

Vannbasert kjemisk industri har ofte oppløsninger som inneholder til dels større eller mindre mengder klorid. I noen prosesser er dette ønskelig, som i klor-alkali og kloratprosessen. Mens i andre prosesser, som metalutvinning, vannrensing og gjødselproduksjon, er tilstedeværelsen av klorid mindre heldig. Tilstedeværelsen av klorgass vil være skadelig både for produksjonsinventar og andre omgivelser. Mengden klorid som er tilstede i prosessvannet i produksjonen bør derfor reduseres.

Formålet med denne oppgaven var å studere muligheten for elektrolytisk fjerning av klorid, fra en vandig nitratløsning, ved bruk av en tilpasset DSA-elektrode med iridiumoksid som aktiv komponent.

Voltammetri ble utført på forskjellige elektrodematerialer og ved bruk av forskjellige elektrodeoppsett. Både en roterende-disk-elektrode (RDE) og en roterende-ring-disk-elektrode (RRDE) ble benyttet. Den første for å studere reaksjonskinetikken for klor- og oksygenutvikling på en titanelektrode belagt med IrO_2-Ta_2O_5. RRDE ble benyttet for måling av strømutbytte, ved bruk av både en Pt-Pt elektrode (disc og ring bestående av platina) og en IrO_2-Pt elektrode (disc bestående av glasskarbon belagt med IrO_2, ring i platina).

I forkant av elektrolyseforsøkene ble det tillaget titanelektroder belagt med IrO_2-Ta_2O_5 ved bruk av metoden kalt termisk dekomponering. Forskjellige metoder for påføring av belegget ble benyttet, deriblant påføring ved bruk av pensel og ved dypping av titansubstratet. De syntetisk fremstilte elektrodene ble undersøkt ved bruk av SEM, EDS og XRD og deretter sammenlignet med en lignende, kommersiell elektrode fra det Svenske selskapet Permascand.

Elektrolyseforsøkene, i både syntetisk elektrolytt og i prosessvann, ble utført i en stillestående celle og også i en strømningscelle. Forskjellige arbeidselektroder ble benyttet; både den syntetisk fremstilte IrO_2-DSA elektroden og en kommersiell RuO_2/IrO_2-elektrode ble testet.

Voltammetriforsøkene ga indikasjoner på at klorutvikling på elektroder basert på iridiumoksid kun i liten grad påvirkes av massetransport.

Elektrolyseforsøkene ga lovende resultater ved bruk av RuO_2/IrO_2-oksidelektroden, med en reduksjon i kloridkonsentrasjon i prosessvannet på 23 % og et strømutbytte på 3 % i strømningscellen. Den syntetisk fremstilte elektroden viste lav selektivitet for klorutvikling. Dette var antatt å være som følge av lav krystallinitet i belegget og /eller på grunn av høy porøsitet i titansubstratet. Ved langtidselektrolyse ble det observert et hvitt belegg på motelektroden. Analyse ved bruk av EDS antydet at belegget for det meste besto av kalsiumfosfat.

Table of contents

Symbols and abbreviations

	Unit	Explanation
a_i	-	Activity of species i
b	mv	Tafel slope
CE		Counter Electrode
CE_x		Current Efficiency
c_i	mol dm^{-3}	Concentration
CV		Cyclic Voltammetry
E	V	Potential
E_p	V	Peak potential
E_{REF}	V	Potential of the reference electrode
E^{rev}	V	Reversible potential
E^0	V	Standard potential
EDS		Energy Dispersive Spectroscopy
f	Hz	Frequency
F	C mol^{-1}	Faraday constant
i	A cm^{-2}	Current density
i_{lim}	A cm^{-2}	Limiting current density
i_0	A cm^{-2}	Exchange current density
LSV		Linear Sweep Voltammetry
N_0	-	Collection efficiency
M	g mol^{-1}	Molar weight
Q	C	Charge
R	J mol^{-1} K^{-1}	Ideal gas constant
RDE		Rotating disc electrode
RHE		Reversible Hydrogen Electrode
RRDE		Rotating ring disc electrode
SEM		Scanning Electron Microscopy
T	K	Temperature
t	s	Time
U	V	Total cell voltage

WE		Working Electrode
W_{el}	kWh kg^{-1}	Electrical consumption
β	-	Asymmetry parameter
γ_i	-	Activity coefficient
ΔH^0	kJ mol^{-1}	Enthalpy
η	V	Overpotential
ν	m^2 s^{-1}	Kinematic viscosity
ν_s	mV s^{-1}	Sweep rate
ω	rad s^{-1}	Angular velocity

1 Introduction

Chlorine is one of the most important commodity products in the chemical industry, with an annual worldwide capacity of approximately 52 million tons (in 2003) [1]. Most of the chlorine today [2] is produced from an aqueous sodium chloride solution by use of electrolysis, in the chlor-alkali process. Another important process involving the electrolysis of chloride is the chlorate process. This process is quite similar to the chlor-alkali process, except from the fact that the chlorine that is formed at the anode will dissolve in the electrolyte, forming hypochlorite at a pH of approximately 4 (at the anode) [3]. The hypochlorite will further react and chlorate is formed in a chemical reaction [4]. The main part of the chlorine produced today is raw materials for plastic production and bleaching agents.

Chlorine production is an energy demanding processes, and because of this, there is a lot of ongoing research on how to lower the energy consumption [5]. In the chlor-alkali process, the raw material is a concentrated salt solution, thus the current efficiency for chlorine evolution can be as high as 95-97 % in a membrane cell [4]. For electrolytes containing low amounts of chloride, on the other hand, there is a challenge to achieve a sufficient current efficiency.

Chloride containing solutions is not only used in the chlor-alkali or chlorate process. Chloride is also often present in the aqueous solutions used for metal electrowinning (of Co and Ni) and fertilizer production. The presence of chloride may cause problems in the production process. In the electrowinning of cobalt and nickel, chlorine gas will be evolved as on the anode. The presence of chlorine is damaging for production inventory, as corrosion will increase with the presence of chlorine. In addition, the chlorine evolved is a big problem regarding health, environment and safety. The amount of chloride present in the process water needs therefore to be reduced, either by chemicals or electrolytically. Regardless, removal of chloride is a big cost for the industry, and the ratio between profit and cost need optimization.

Traditionally, chlorine was produced using graphite anodes [6]. These anodes degraded during operation, producing both carbon dioxide and carbon monoxide in addition to chlorine and oxygen. Furthermore, the graphite anodes showed relatively low electrical conductivity and there was a problem regarding bubble formation and a high overpotential for chlorine evolution on these anodes, increasing the cell voltage. A start of the solution to these problems came as

the Belgian scientist Henri Bernard Beer discovered what today is known as the dimensionally stable anode (DSA) [7]. These electrodes are as the name indicates, electrodes which will keep their geometric shape during operation. A DSA consists of a metal substrate, usually titanium, and an electrocatalytically active coating. The active coating components used in the chlorine industry today are usually ruthenium oxide and/ or iridium oxide. The development of DSA electrodes introduced electrodes with high electrical conduction and enhanced selectivity that were both mechanical and chemically stable during long-time operation. Thus, there are a lot of ongoing research, finding the most suitable electrodes for different operations and enhancing the existing quality of these electrodes.

The aim of this project is to study the feasibility of chloride removal by electrolysis using a customized DSA electrode with iridium oxide as the active component. The electrolytic removal of chloride will take place in an acidic nitrate solution containing low amounts of chloride.

The kinetics of the reactions taking place during the electrolysis is examined by voltammetry. The voltammetry experiments is executed using both a rotating disc electrode (RDE) and a rotating ring disc electrode (RRDE). The RDE is a commercial titanium supported IrO_2-Ta_2O_5 electrode. Two different RRDE were tested. The first a Pt-Pt, which is an electrode with both the disc and ring in platinum. The second one, an IrO_2-Pt, which has an IrO_2 coated glassy carbon disc, and a platinum ring.

The preparation of a titanium supported IrO_2-Ta_2O_5 electrode by thermal decomposition is investigated by different application techniques of the coating. Including application by brush and dip coating. The surface morphology of the electrodes synthesized in house is studied by scanning electron microscopy (SEM) and energy dispersive spectroscopy (EDS). The electrodes is also analysed by X-ray diffraction (XRD), to confirm the elements present in the coating. The analysis of the electrodes is compared with the commercial IrO_2-DSA used for RDE experiments.

Electrolysis is carried out in solutions containing different concentration of chloride, and also in process water containing approximately 1400 ppm of chloride (in addition to other components). The electrolysis is carried out in both a stagnant cell and in a designed flow cell.

Different working electrodes are tested, including an IrO_2-DSA synthesised in house and a commercial RuO_2/IrO_2-mesh.

2 Theory

2.1 Electrochemical cells

In general, an electrochemical cell is defined as two electrodes separated by at least one electrolyte phase [8].

Consider a general half-reaction taking place at one of the electrodes in the cell (2.1). Then the Nernst equation (2.2) will provide the connection between the electrode potential (E), vs. a given reference electrode, and the concentration of the participating species [8]. In equation (2.2), E^0 is the standard potential of the reaction, n is the number of electrons transferred per mole of O reacted, F is Faraday constant, R is the molar gas constant, T is the temperature in Kelvin and a_i is the activity of species, i.

$$O + ne^- \Leftrightarrow R \tag{2.1}$$

$$E = E^0 - \frac{RT}{nF} \cdot \ln \frac{a_R}{a_O} \tag{2.2}$$

If other potential losses are neglected, the measured/ induced potential is only determined by the reversible potential (calculated from the Nernst equation) and the overpotential, η as shown in equation (2.3). A type of loss that is neglected in the following equations is the so called ohmic potential loss (also known as iR drop). This loss is dependent on the electrolyte conductivity, the distance between the reference and the working electrode and the magnitude of the current [9].

The overpotential can be divided into many different subcategories, two of them are the activation overpotential and the concentration overpotential. For large values of the overpotential the activation overpotential can be expressed as Tafels equation (2.4), and the concentration overpotential can be expressed as in equation (2.5). The *b* in both equation (2.4) and (2.5) is known as the Tafel slope. This parameter is dependent both on the electrode material and the reaction taking place on this material. The Tafel slope can be calculated by equation (2.6), where β is what is known as the asymmetry parameter.

$$E_{measured/induced} = \left|E^{rev}\right| + \left|\eta\right| \tag{2.3}$$

$$\eta = b \cdot \log \frac{\left|i\right|}{\left|i_0\right|} \tag{2.4}$$

$$\eta = b \cdot \log \frac{\left|i_{\lim} - i\right|}{\left|i_{\lim}\right|} \tag{2.5}$$

$$b = -\frac{\ln(10) \cdot RT}{\beta nF} \tag{2.6}$$

In the equations above, i_0 is the exchange current density, and i_{lim} is the limiting current density.

2.1.1 Three electrode setup

A sketch of a three electrode setup used in electrochemical measurements is shown in Figure 2.1. The working electrode (WE) is the electrode where the studied reaction is taking place. The current is measured between the working electrode and the counter electrode (CE). The potential between the working electrode and the reference electrode (REF) is controlled by a potentiostat. To reduce the ohmic voltage drop in the electrolyte, the reference is placed close to the working electrode, but a too small distance between WE and REF may cause errors in the measurements [10].

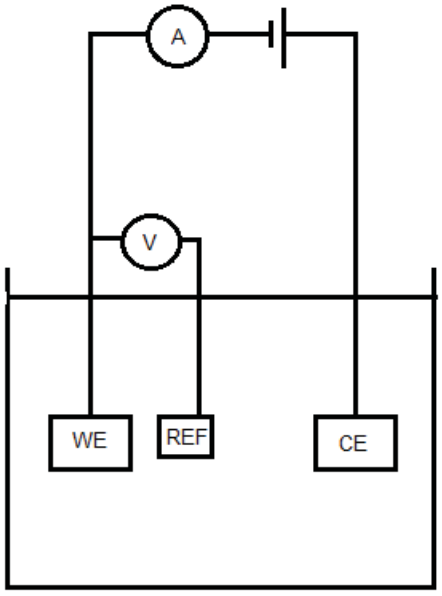

Figure 2.1: Three-electrode setup.

2.1.2 The reversible hydrogen electrode

A Reversible Hydrogen Electrode (RHE) is similar to the Standard Hydrogen Electrode (SHE). The SHE consists of a platinised platinum sheet immersed in an acidic solution of unit activity of hydrogen ions in contact with hydrogen gas at a pressure of one atmosphere [11]. In the RHE on the other hand, the platinum sheet is immersed in an acidic solution of the same concentration as the electrolyte holds. The glass chamber, which contains the RHE, is immersed directly in to the electrolyte without the use of a salt bridge. The electrode potential on the RHE is dependent on the pH in the electrolyte and can be calculated from equation (2.7) (the equation is valid for a temperature of 25 degrees Celsius).

$$E_{REF}[V] = E^{rev}_{H^+/H_2} = -0.0591 \cdot pH \tag{2.7}$$

As described above, the pH in the reference chamber of the RHE is the same as the pH in the electrolyte, and the measured potential will therefore not depend on the pH. The measured potential is then only dependent on the overpotential on the working electrode.

If the pH in the electrolyte and in the reference chamber is different from each other, a shift in the measured potential will be observed, according to equation (2.8).

$$\Delta E_{Measured}[V] = -0.0591 \cdot \left[pH_{WE} - pH_{REF} \right] \tag{2.8}$$

2.2 Chlorine evolution in acidic solution

Chlorine evolution carried out in an acidic, aqueous electrolyte yields the following anode and cathode reactions given in equation (2.9) and (2.10):

$$Cl_2(g) + 2e^- \leftarrow 2Cl^-(aq) \tag{2.9}$$

$$2H^+(aq) + 2e^- \rightarrow H_2(g) \tag{2.10}$$

Combining equation (2.9) and (2.10) gives the total main reaction (2.11):

$$2H^+(aq) + 2Cl^-(aq) \rightarrow Cl_2(g) + H_2(g) \tag{2.11}$$

Considering that the reactions are taking place in an aqueous solution there will also be a competing reaction of oxygen evolution (2.12), taking place on the anode. The evolution of oxygen on the anode will cause loss in the current efficiency for chlorine evolution.

$$\frac{1}{2}O_2(g) + 2H^+ + 2e^- \leftarrow H_2O(aq) \tag{2.12}$$

The standard potential for the chlorine evolution is 1.36 V while the standard potential for oxygen evolution is only 1.23 V. From these numbers, the oxygen evolution is said to be thermodynamically more favorable. Even though the oxygen evolution is thermodynamically preferred it shows a much higher overpotential, and it is possible to produce chlorine over a restricted range of acidic solution [12].

By using Nernst equation it can be seen that the reversible potential of oxygen evolution depends on the pH (2.13) while the reversible potential of the chlorine evolution only depends on the chloride concentration (2.14).

$$E^{rev}_{O_2/H_2O} = E^{o}_{O_2/H_2O} - \frac{RT \cdot \ln(10)}{F} \cdot pH \tag{2.13}$$

$$E^{rev}_{Cl_2/Cl^-} = E^{o}_{Cl_2/Cl^-} - \frac{RT \cdot \ln(10)}{F} \cdot \log c_{Cl^-} \tag{2.14}$$

Lowering of the pH will cause the reversible potential of the oxygen evolution to go to more anodic potentials, this will lead to an increase in the current efficiency for chlorine evolution. In addition, according to the Pourbaix diagram for chlorine (shown in Figure 2.2), chlorine gas is more stable at low pH. Figure 2.2 is a simplified Pourbaix diagram constructed from calculations based on data in SI Chemical Data [13]. The calculations are based only on the most stable compounds. The diagram is valid for a chloride concentration of 20 mM. An increase in the chloride concentration will move the line separating the green and blue area to lower potentials.

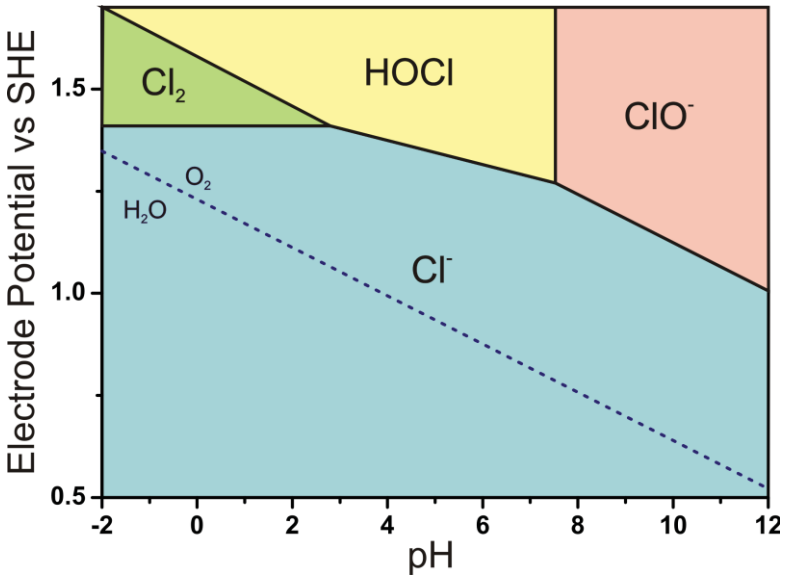

Figure 2.2: Pourbaix diagram showing the stability of chlorine in water (containing 20mM of chloride).

As this project is using an aqueous nitrate solution as the electrolyte, other electrode reactions of interest may be the oxidation of ammonium ions (2.15) and the reduction of nitrate ions (2.16). These reactions have a standard potential of 1.35 V and 0.96 V respectively.

$$NH_3OH^+ + 2H^+ + 2e^- \rightarrow NH_4^+ + H_2O \quad (2.15)$$

$$NO_3^- + 4H^+ + 3e^- \rightarrow NO(g) + 2H_2O \quad (2.16)$$

As mentioned, the evolution of oxygen gas will lower the current efficiency for chlorine evolution. The current efficiency can be calculated from equation (2.17) [11]. The total charge, Q_{tot}, is found as the integral of the current versus time curve, recorded for the electrolysis. The charge associated with the evolution of chlorine, here noted Q_x, is calculated from Faraday's law (2.18) using z=1 and n as the reduction in moles of chloride ions.

$$CE_x = \frac{Q_x}{Q_{tot}} \quad (2.17)$$

$$Q_x = n \cdot z \cdot F \quad (2.18)$$

2.3 Dimensionally stable anode (DSA) and chlorine evolution

The Dimensionally Stable Anodes (DSA) are, as the name indicates, electrodes that maintain their shape during operation. DSA electrodes consist of a thin active coating deposited on a metal substrate, usually a valve metal like titanium. The coating consists of metal oxides, usually one active component and one stabilizing component, formed by thermal decomposition.

Traditionally chlorine was produced using graphite anodes, the new DSAs now used in the chlorine industry are made by coating titanium with a mixture of titanium oxide and ruthenium oxide (TiO_2 + RuO_2) [4]. Figure 2.3 shows that the anodic overvoltage for chlorine evolution is higher on graphite than on the DSA coated with ruthenium oxide. In chlorine production from electrolysis, oxygen evolution is a competing reaction causing lowering of the current efficiency.

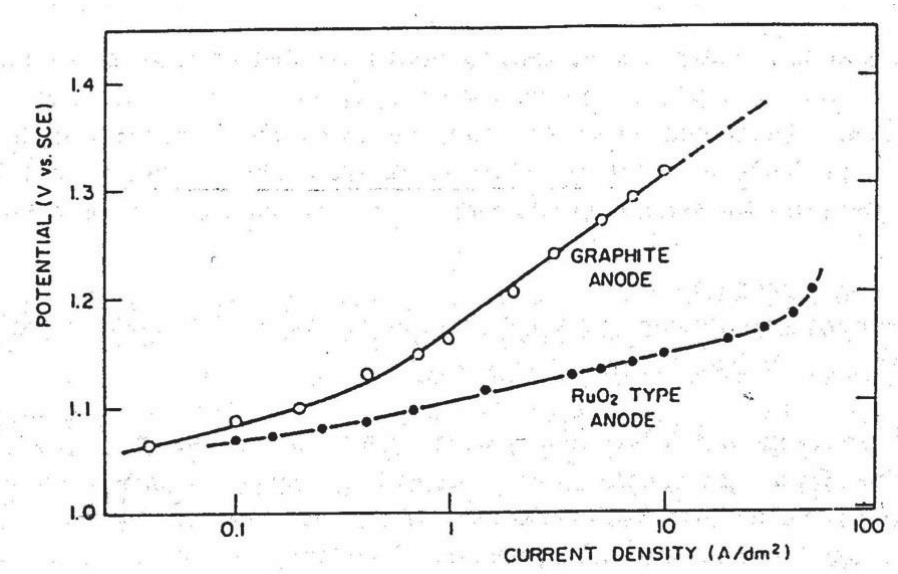

Figure 2.3: Anodic overvoltage for chlorine evolution on graphite and ruthenium oxide coated DSA [4].

The reader is referred to section 3.2 for more a more thorough description of the DSA, its history, composition and other aspects of importance.

2.4 Voltammetry

2.4.1 Linear sweep voltammetry

In linear sweep voltammetry the potential at the working electrode is changed linearly with time while simultaneously measuring the current. This gives a recording of current versus potential, which is equivalent to recording current versus time.

2.4.2 Cyclic voltammetry

In cyclic voltammetry the potential at the working electrode is changed with a triangular waveform with time, while simultaneously measuring the current. The characteristic waveform of the potential is shown in Figure 2.4.

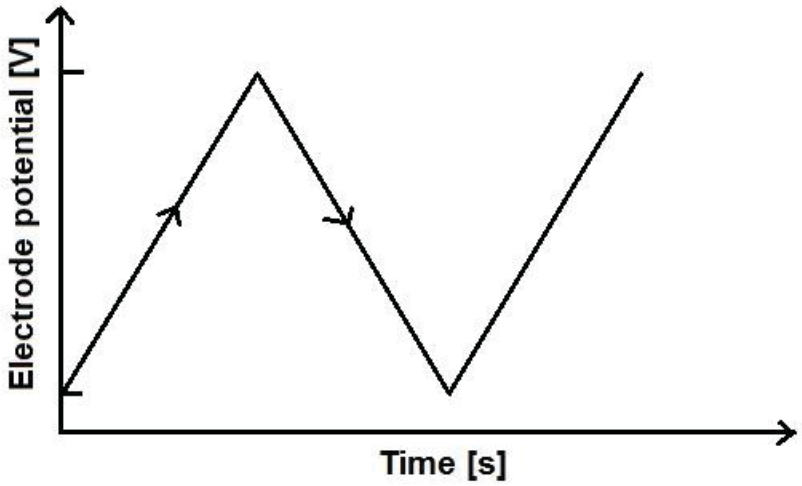

Figure 2.4: Cyclic voltammetry waveform – potential versus time at the working electrode. The sweep rate is the rate of change in potential with time.

In aqueous solutions the positive and negative turn-round potential is usually chosen to lie between the hydrogen and oxygen evolution potentials. If there are no redox-active couples between this potential region in the aqueous solution, the observed current is due to the formation and dissolution of chemisorbed hydride and oxide layers on the electrode surface. In addition, the charging or the discharging of the double layer will lead to a small change in the observed current when the potential is changed. When the potential is swept in cathodic direction a current arises due to the chemisorption of hydrogen atoms on the surface of the electrode, and if the cathodic potential is sufficiently large, hydrogen gas will be formed. Correspondingly, if the potential is swept in the anodic direction, a current originates as oxide

layers are formed on the electrode surface. In addition, if the anodic potential is sufficiently large oxygen gas will be formed. When the potential is reversed the chemisorbed hydrogen atoms will desorb and the oxide layer will be reduced. An effect in the current will also be noticeable if the electrolyte contains electrochemically active species that may react on the electrode surface. [11]

Why there may be observed a peak in the cyclic voltammogram is described by Hamann and Hamnett [11]. The surface concentration of the reacting species falls as the potential rises further from the potential where electron transfer is initiated. The concentration is decreased from the bulk concentration towards zero. This decrease in concentration, initially cause the concentration gradient to increase and therefore the current, which is proportional to the concentration gradient, increases. The Nernst diffusion layer thickness is also increasing with time and at higher potential, when the electron transfer is fast and the current has reached its diffusion-limited value. An increase in the diffusion layer thickness will lead to a decrease in the current. When the sweep rate is increased there is less time for the diffusion layer to grow, leading to a steeper concentration gradient and a larger current. A plot of the peak current density versus the square root of the scan rate may provide information about the diffusion coefficient or the bulk concentration depending on what is known. Such calculations were executed during the authors project work during the fall of 2013 [14].

A cyclic voltammogram of platinum in 0.5 M aqueous sulphuric acid solution is shown in Figure 2.5. The figure is taken from [15]. In this voltammogram a scan rate of 50 mVs^{-1} has been used.

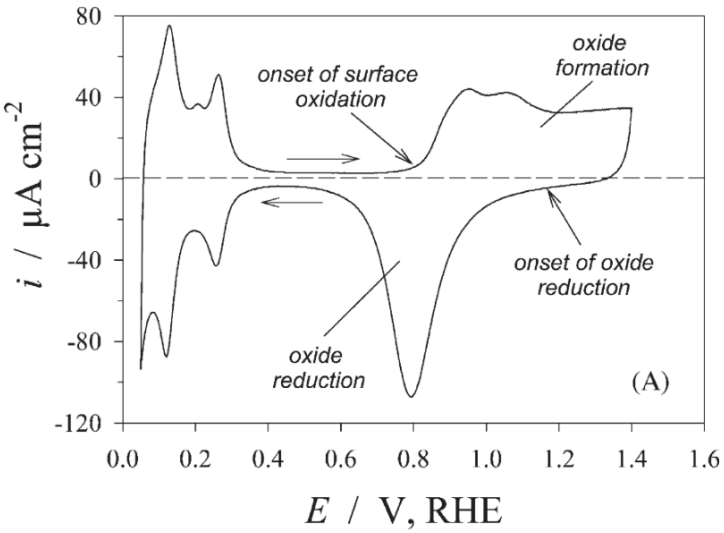

Figure 2.5: Cyclic voltammogram of platinum in 0.5 M sulphuric acid with a sweep rate of 50 mVs^{-1} at 298 K [15].

2.5 Rotating disc electrode (RDE) and rotating ring-disc electrode (RDE)

2.5.1 Rotating disc electrode

In an electrochemical reaction, it is essential with the supply of reactant and the removal of product from the electrode surface. There are three phenomena which contribute to such mass transport, and those are: diffusion, convection and migration [16].

In the laboratory, it is possible to design experiments where diffusion of the species in the solution is controlled. This can be done by using a rotating disc electrode (RDE) [16].

The rotating disc electrode consists of a disc of the electrode material surrounded by an insulating material [8]. The construction is attached to a motor and rotated at a certain frequency, f, where the parameter of interest is the angular velocity, $\omega = 2\pi f$ [8]. The construction is rotated about an axis perpendicular to the surface of the disc as shown in Figure 2.6 [17]. The rotating structure drags the fluid at its surface along with it and the solution is then thrown outward. As shown in Figure 2.7 [17] there is a thin layer near the surface of the electrode which is left unstirred, this is called the Nernst diffusion layer. Within this layer, diffusion is the only mode of mass transport. The thickness of this layer is defined by the rotation speed [11]; stronger convection decreases the Nernst diffusion layer thickness.

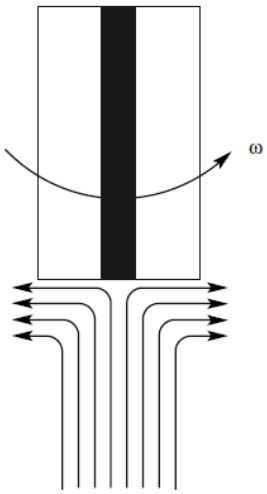

Figure 2.6: Solution movement caused by the use of a rotating disc electrode (RDE), the figure is taken from [17].

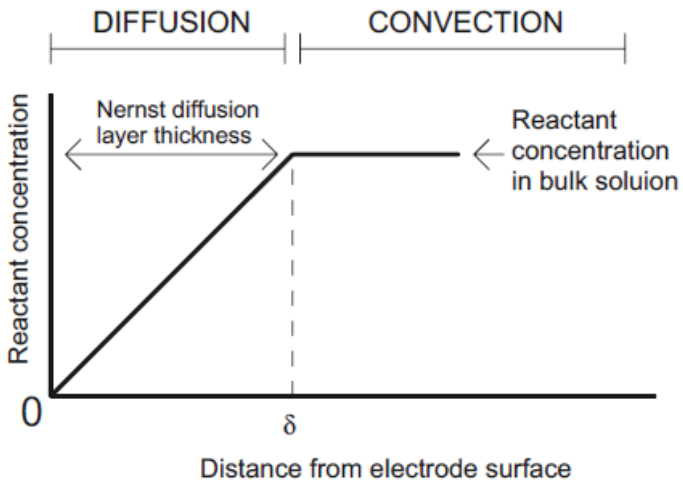

Figure 2.7: The Nernst diffusion layer model for an oxidation at a rotating disc electrode, the figure is taken from [17].

For a totally mass-transfer-limited condition at the rotating disc electrode, the Levich equation (2.19) is valid [8]:

$$i_{\text{lim}} = 0.620nFD^{2/3}\omega^{1/2}\nu^{-1/6}c^{0} \qquad (2.19)$$

where i_{lim} is the limiting current density, n is the number of electrons transferred, F is Faradays constant, D is the diffusion coefficient, ν is the kinematic viscosity and c^0 is the bulk concentration.

2.5.2 Rotating ring disc electrode

A rotating ring-disc electrode is similar to the rotating disc electrode, but in addition to the disc, it also contains a ring electrode. An insulating material separates both of these electrodes. The disc and the ring electrode can be controlled independently of each other, this is helpful in that way that the ring electrode may provide additional information about processes occurring on the disc electrode. An example of a ring-disc electrode is shown in Figure 2.8.

Figure 2.8: A rotating ring-disc electrode (RRDE) [18].

A ring-disc electrode can be used to calculate current efficiency. This is done (for instance) by using a potential on the electrodes so that the species oxidized on the disc will be reduced once they reach the ring electrode. By analysing the current responses on the disc and ring, the current efficiency can be calculated. When calculating the current efficiency it is important to take into account that only a fraction of the species formed on the disc electrode will reach the ring. Some of the species will escape into the bulk of the electrolyte. Therefore, the ring current will be a fraction of the disc current. This fraction is called the collection efficiency and the experimental value can be calculated according to equation (2.20) [19]. Here i_R is the current density on the ring electrode, and i_D is the current density on the disc electrode.

$$N_o = -\frac{i_R}{i_D} \tag{2.20}$$

2.6 Potentiometric titration

To measure the concentration of chloride in a solution, potentiometric titration can be used. In this method, a silver ring electrode is used to measure the potential difference in a chloride containing solution, while silver nitrate is added. The silver ring electrode consists of a silver electrode with a reference electrode based on silver – silver chloride in a 1 molar potassium nitrate solution. The total cell can be written as follows [20].

$$Ag(s) \mid AgCl(s), 1M\ KNO_3 \parallel Cl^-(aq), AgCl(s) \mid Ag(s) \tag{2.21}$$

The potential in the left half cell will always be constant, while the potential in the right half cell will change with the addition of silver ions to the solution. The electrode potential of the $Ag^+/Ag(s)$ half cell will be given by Nernst equation (2.22):

$$E^{rev}_{Ag^+/Ag(s)} = E^0_{Ag^+/Ag(s)} - \frac{RT}{F}\ln\frac{1}{a_{Ag^+}} \tag{2.22}$$

If it is assumed that the activity of the silver ions is equal to the concentration of the silver ions, then activity of the silver ions can be given from the solubility product of silver chloride (K_{sp}) (2.23).

$$a_{Ag^+} = c_{Ag^+} = \frac{K_{sp}(AgCl)}{c_{Cl^-}} \tag{2.23}$$

As the silver nitrate is added, the titration curve is plotted (potential as a function of added silver nitrate). The volume of silver nitrate at the point of inflection is used to calculate the amount of chloride in the solution as follows (2.24).

$$c_{Cl^-}(ppm) = \frac{V_{ekv}\cdot c_{AgNO_3}\cdot MW_{Cl}}{m_{solution}}\cdot 10^6 \tag{2.24}$$

where V_{ekv} is the amount of silver nitrate added at the inflection point of the titration curve in litres, c_{AgNO3} is the concentration of silver nitrate, MW_{Cl} is the molecular weight of chloride in grams per mole and $m_{solution}$ is the sample weight in grams.

An example of a titration curve is shown in Figure 2.9 below:

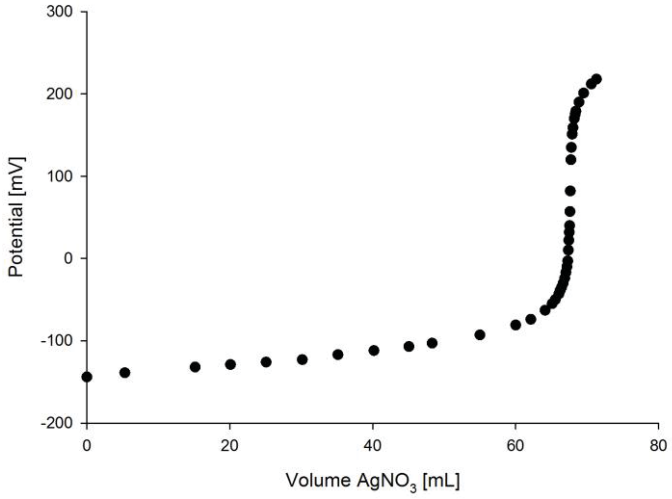

Figure 2.9: Example of a potentiometric titration curve. Potential in mV plotted versus amount of 0.1 M silver nitrate added, in mL.

2.7 SEM and EDS

When using Scanning Electron Microscopy (SEM), the area to be studied is irradiated with a thin, focused electron beam. Different signals can be detected when the electron beam hits the surface of the sample. An image of the different signals is presented in Figure 2.10 [21].

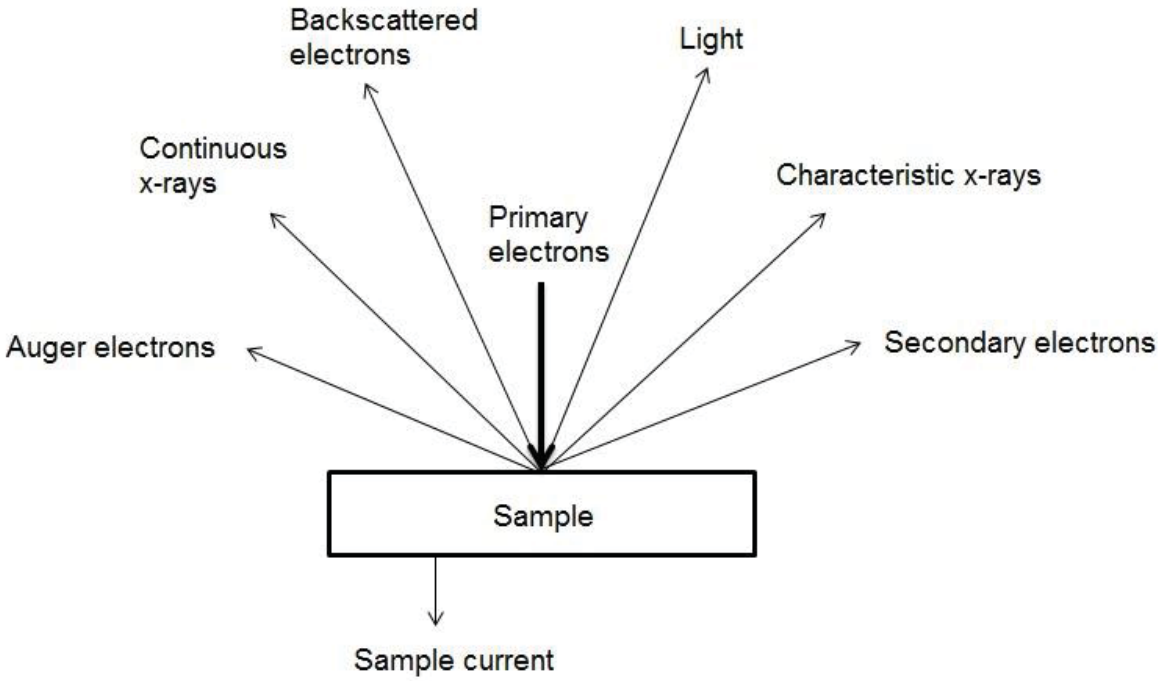

Figure 2.10: Signals which can be detected by the SEM.

The secondary electrons are used for topography imaging. Energy Dispersive X-ray Spectroscopy (EDS), which is used for element analysis purposes, detects the characteristic x-rays of the sample being analysed. The emission volume of the characteristic x-rays are much bigger than that for the secondary electrons [22]. This means that there is not only the surface of the sample that are being analysed when using EDS, but a much bigger volume.

2.8 XRD

Each crystalline solid has its own characteristic X-ray pattern, a "fingerprint", which can be used for identification. XRD can be used for both qualitative and quantitative analysis, in addition to crystallite size and structure analysis (lattice parameters).

Diffraction occurs when a wave hits a number of regularly spaced obstacles that are capable of scattering the wave [23]. Diffraction is also a consequence of how two or more scattered waves interfere with each other. Two scattered waves, both in phase, will mutually reinforce one another and constructive interference originates. A diffracted beam is one formed by multiple scattered waves that constructively interfere with one another.
X-rays are electromagnetic radiation of wavelength 1Å (10^{-10} m) [24]. When X-rays hit a crystal (which have atoms placed in a periodic structure) the rays are scattered producing a diffraction pattern. This diffraction pattern contains information about the atomic structure in the crystal [25]. Amorphous materials do not have the periodic arrangement of atoms like the crystals do have, so they do not produce a diffraction pattern.

3 Literature

3.1 Industrial application of chlorine evolution

Chlorine evolution is the side reaction in both cobalt and nickel electrowinning in chloride electrolytes and in seawater electrolysis for hydrogen production. There are two processes where chlorine gas is the main product; these are the chlorate process and the chlor-alkali process.

3.1.1 The chlor-alkali process

Chlorine gas can be produced by use of electrolysis in the chlor-alkali process. In this process chlorine gas is produced from an aqueous solution of sodium chloride. In addition to the chlorine gas formed at the anode, hydrogen gas and sodium hydroxide is formed at the cathode. The main reaction is shown in equation (3.1) [4].

$$2NaCl + 2H_2O = 2NaOH + Cl_2(g) + H_2(g) \qquad (3.1)$$

If the chlorine gas produced at the anode is mixed with the sodium hydroxide formed at the cathode, hypochlorite will be formed according to equation (3.2) [4]. This reaction can be prevented by separation of the electrolyte in the anode and the cathode compartments. The separation is done by using a diaphragm, a membrane or so called mercury cells.

$$Cl_2(g) + 2OH^- = ClO^- + H_2O \qquad (3.2)$$

As chlorine gas is produced from an aqueous solution, oxygen evolution on the anode will always be lowering the current efficiency. To supress the oxygen evolution a dimensionally stable anode (DSA) [6] is used.

The major part of the chlorine produced is used as raw material for plastic production [4].

3.1.2 The chlorate process

The production of chlorate is today a large industry. Chlorate is mostly produced in the form of sodium chlorate ($NaClO_3$), by use of electrolysis. The sodium chlorate is further used in the production of chlorine dioxide (ClO_2) – used in the bleaching industry. The raw material used in the chlorate electrolysis is sodium chlorate in an almost neutral electrolyte [4]. The chloride ions in the electrolyte will oxidize to chlorine gas, but will immediately dissolve in the electrolyte by hydrolysis and form hypochlorite. The hypochlorite acid dissociates and the chlorate is further formed in a chemical reaction. The electrode reactions, (3.3) and (3.4), as well as the total cell reaction (3.5) and the chlorate forming reaction (3.6) are shown below [4].

$$2Cl^-(aq) \rightarrow Cl_2(g) + 2e^- \quad (3.3)$$

$$2H_2O + 2e^- \rightarrow H_2(g) + 2OH^- \quad (3.4)$$

$$H^+ + Cl^- + H_2 \rightarrow HClO + H_2 \quad (3.5)$$

$$2HClO + ClO^- = ClO_3^- + 2Cl^- + 2H^+ \quad (3.6)$$

Similar to the chlor-alkali process the anodes used in the chlorate electrolysis process are usually Dimensionally Stable Anodes (DSA).

Ann Cornell worked with electrode reactions in chlorate electrolysis in her doctoral thesis [3]. The DSA used in the experiments was the type normally used in the chlorate process, a RuO_2(30%)–TiO_2(70%)/Ti electrode. When comparing an acidic electrolyte to a chlorate electrolyte using an anode rotating at 3000 rpm, experiments showed only a straight line for the acidic electrolyte with a Tafel slope normal to that of chlorine evolution. For the chlorate electrolyte, experiments showed a clear dependency of pH at low potentials. At a pH close to neutral the chlorate electrolyte showed a steep gradient of the polarization curve between 0.95-1.1 V. Cornell described this as a self-retarding effect of the oxygen evolution which locally increases the pH close to the anode and therefore increases the reversible potential of for the oxygen evolution.

3.2 Dimensionally stable anode (DSA)

Trasatti has published quite a few papers on electrocatalysis and the explanation of the word varies to some degree. Two of these explanations are: "*the dependence of the electrode reaction rate on the nature of the electrode material*" [26] and "*the optimization of electrode processes by careful choice of electrode material"* [27]. From both of these explanations it can be seen that electrocatalysis involves the optimization of the electrode material; the electrocatalyst. Trasatti also gives an extensive list of the requirements of electrocatalysts [28]:

- *High surface area*
- *High electrical conduction*
- *Good electrocatalytic properties*
- *Long-term mechanical and chemical stability*
- *Minimised gas bubble problems*
- *Enhanced selectivity*
- *Availability and low cost*
- *Health safety*

A new era, changing from graphite anodes to more intricate electrodes, started in the 1950's.

3.2.1 History

The dimensionally stable anode (DSA) was invented by Henri Bernard Beer in the search of finding a reliable electrocatalyst suitable for the production of chlorine to substitute the former graphite anodes [6]. In the 1950's, Beer had already been searching for a better anode material for chlorine evolution for about 20 years. And in 1956 he discovered, by an accident, that titanium did not anodically dissolve in chloride containing electrolyte [6]. This was the start of what today is known as the dimensionally stable anode (DSA). Beer used titanium as the base of a new anode and started the search of a coating that that could be electrical conducting as well as electrocatalytically active and chemically inert. An advantage with the use of titanium was the "self-healing" quality that it held [6]. When titanium was exposed to air, a protecting titanium oxide film was formed. In an article in the Journal of the Electrochemical Society [6] Beer described the process of searching for a proper coating. The first coatings, which were made of platinum, showed promising results. However, these anodes were very expensive and also the platinum coating had a tendency of becoming passive during operation. Later Beer

discovered that the use of ruthenium oxide, the cheapest of the platinum metal oxides, was possible. In 1967, Beer improved the ruthenium oxide coating by mixing it with titanium oxide giving a more stable electrode, which showed an extraordinary electrocatalytic activity towards chlorine production. De Nora now owns the patent of Beer and production of DSA for chlorate and chlor-alkali industry has been a multi-billion business for many years.

3.2.2 Metal substrate, coating composition and preparation

Choice of a metal substrate

In the literature [29, 30] the metals most often mentioned as possible metal substrates are: titanium, tantalum, zirconium and niobium. The requirements for the substrate are conduction and stability. Vercesi et. al [29] investigated the performance of the base metal, influencing the activity loss of oxygen evolving DSAs. They found that the pretreatment of the base metal in order to create a roughened surface (by for instance sandblasting or chemically etching) was very important. In addition the replacement of titanium by tantalum improved the service life of the electrode during oxygen evolution in acidic media by a factor of 14. As tantalum is very expensive titanium represents the best alternative when cost, in addition to performance, is taken into consideration. The work mentioned above also stated that zirconium cannot be expected to be a good metal substrate.

Choice of coating composition

As described above, different coatings were examined during the development of the DSA. Hayfield [31] summarized some of the activity when going from Pt/Ir electrodes to ruthenium oxide based electrodes. In an article in "Platinum Metals Review" [31], Hayfield described a switch from pure platinum to a 70/30 Pt/Ir coating during the year of 1965. What was not known at that time was the fact that the coating also contained some iridium oxide, which is a great electrocatalyst for chlorine evolution, and so this 70/30 Pt/Ir coating was applied to electrodes in the chlorate plants. This coating was then later replaced by ruthenium oxide based coatings in the search of finding successful electrodes for mercury type chlor-alkali cells.

Today, the coating of a DSA usually consists of a mix of metal oxides. The most important component is the active and conductive one (usually RuO_2, IrO_2 or Pt). In addition to the active component the coating also consists of a stabilizing component, which should ensure a high dispersion of the active component, protect the substrate from corrosion and strengthen the

cohesion of the coating [32]. The stabilizing component can either be conducting or non conducting [30]. This mix usually lowers the electrocatalytic activity, but as this increases the lifetime of the electrode such a mix is more economical. During Comninellis and Vercesi's study [30] of different coatings they found that, in terms of electrochemical stability, IrO_2 was a better choice for the conducting component, compared to RuO_2. In addition, they concluded that coating consisting of 70mol% IrO_2 and 30mol% Ta_2O_5 on a titanium substrate exhibits the best activity towards oxygen evolution (compared to other mixtures of IrO_2, RuO_2, Pt, TiO_2, ZrO_2 and Ta_2O_5).

When it comes to chlorine evolution, the industry usually apply a mixture of RuO_2 and TiO_2 (a customary composition is 30mol% RuO_2 and 70mol% TiO_2). Literature shows that a mixture of these two components exhibits a better selectivity towards chlorine evolution than an electrode of a pure RuO_2 coating [33]. This may be due to the oxidation of pure RuO_2 to volatile RuO_4 (see section 3.2.4). In addition, doping with other elements has shown improved efficiency in the favor of either chlorine evolution or oxygen evolution. Oxides such as SnO_2, Sb_2O_3, CdO, SeO_2 and TeO_2 are known to behave as oxygen evolution inhibitors and therefore increases the chlorine selectivity [33]. And opposite, electrodes doped with MnO_2 are reported to decrease the overpotential for oxygen evolution [34].

Preparation

The first coatings Beer prepared were galvanically deposited on to the titanium substrate, later he developed a thermochemical process for deposition of the oxide coating [6]. The thermochemical process involved dissolution of the desired metals as their salts in an organic liquid, the solution was then applied to the etched substrate and the solvent was then evaporated.

The making of a DSA today has not changed significantly from the procedure in the 1960's. The preparation includes several steps, which are the dissolution of precursors, pretreatment of base metal, application of coating to substrate, solvent evaporation at low temperature and finally annealing. A flow chart of the procedure is shown in Figure 3.1. This figure is taken from the thesis of Torjus Åkre [35].

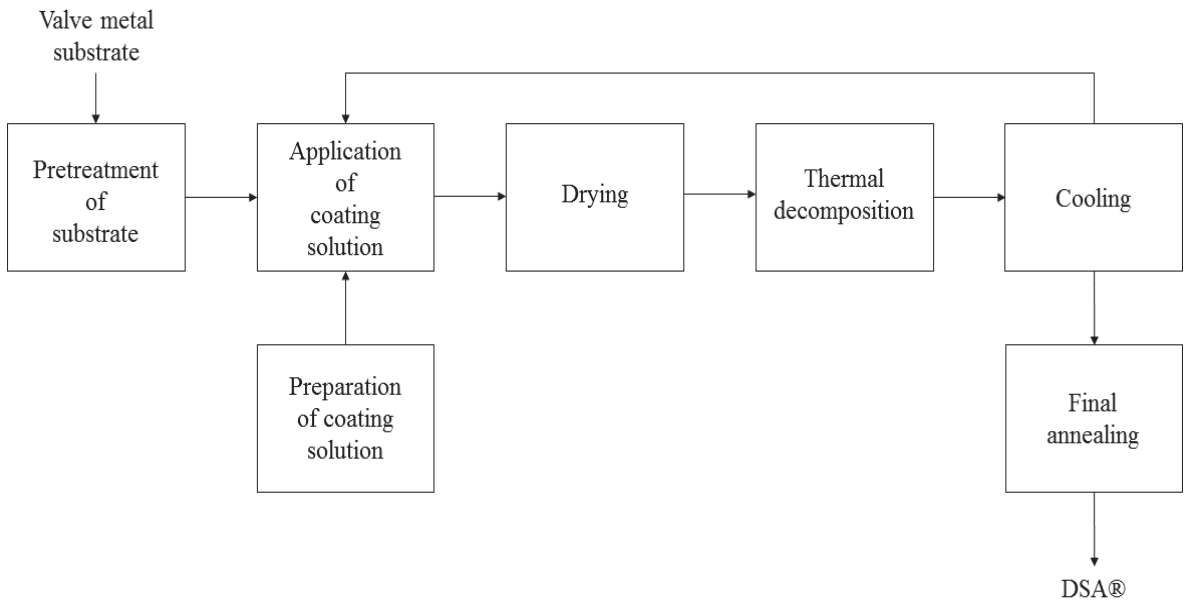

Figure 3.1: Preparation of DSA, the figure is taken from [35].

The procedure for the preparation of dimensionally stable anodes is described in various articles [36, 37] and Trasatti and Lodi has made a table of suggested procedures for preparation of different types of the DSA [38]. All the stated references above uses chloride salts of the metal oxide as precursors for the painting solution, which is applied by brush, dipping or spraying to the pretreated metal substrate. After this, the solution is evaporated at low temperature, before the annealing step takes place at a temperature between 400-500°C [32].

3.2.3 Mechanism of oxygen and chlorine evolution

Oxygen evolution

The oxygen evolution reaction is a widely studied reaction, yet several characteristics remain unresolved. Trasatti [39] highlights three possible reasons for this:

- The oxygen evolution reaction is very sensitive to the nature and structure of the electrode surface, because of the high energy intermediates.
- The electrode surface can undergo changes at the potentials required to form oxygen.
- As the surface of the electrode changes, the kinetic parameters may be time dependent.

As the points above state, the electrocatalytic activity for oxygen evolution is dependent on the nature of the catalyst. This can be shown by a volcano plot (Figure 3.2). The volcano plot indicates that the best oxide material is one where the adsorption enthalpy (ΔH) of an

intermediate is not to high, nor too low [28]. In Figure 3.2 it can be seen that oxides of Ru, Ir and Pt are the best electrocatalysts for oxygen evolution.

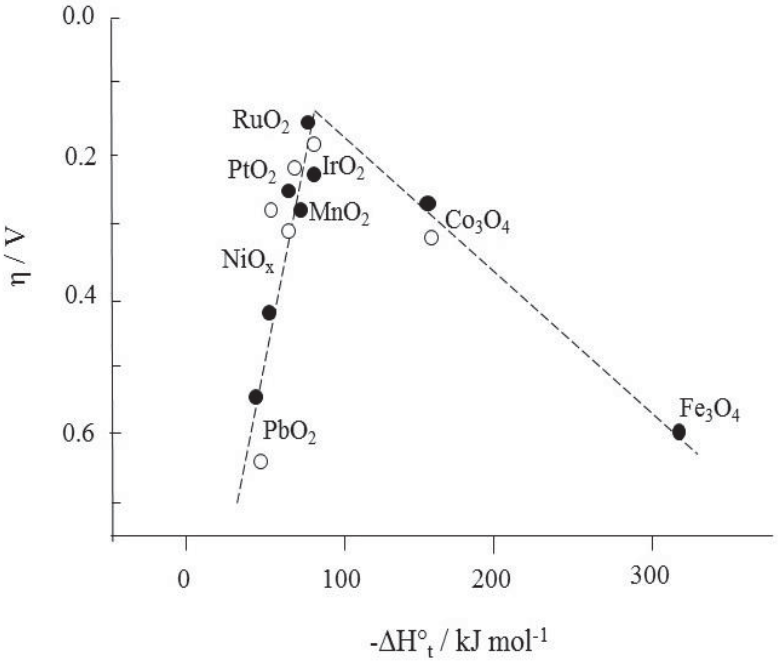

Figure 3.2: Electrocatalytic activity towards oxygen evolution reaction at different oxide electrodes. The electrocatalytic activity is given as a function of the enthalpy of the lower-to-higher oxide transition. The figure is taken from [28].

There are many different mechanisms that have been suggested for the oxygen evolution reaction. One of these is the "electrochemical oxide path" [34, 36]. The mechanism is shown in equations (3.7)-(3.10); here S denotes an active surface site.

$$S + H_2O \rightarrow S - OH + H^+ + e^- \tag{3.7}$$

$$S - OH \rightarrow S - O + H^+ + e^- \tag{3.8}$$

$$S - OH + S - OH \rightarrow S - O + S + H_2O \tag{3.9}$$

$$S - O + S - O \rightarrow O_2 + 2S \tag{3.10}$$

A break in the Tafel line may be observed when going to higher overpotentials. This has been explained as a change in the reaction mechanism [34], and later shown experimentally by Hu et al. [40], where experiments showed that oxygen evolution (at room temperature) on a Ti supported IrO_2-Ta_2O_5 electrode gave a Tafel slope of 60 mV dec^{-1} in the low current density

areas, and increased to 130 mV dec^{-1} in the high current density areas. Another paper [41] reports only a single Tafel slope for the Ti supported IrO_2-Ta_2O_5 electrode (70mol% Ir) of 70 mV dec^{-1}. Oxygen evolution on pure IrO_2 in sulphuric acid has been reported to be close to 60 mV dec^{-1}. [34, 42]

Chlorine evolution

Chlorine evolution on rutile oxides has been studied by DFT calculations by Hansen et al. [43]. By constructing a Sebatier volcano plot they found that RuO_2 is close to an ideal catalyst for chlorine evolution, and that the oxygen evolution always require a higher overpotential than the chlorine evolution.

The mechanism of chlorine evolution on oxide materials is a frequently debated topic. A review by Trasatti [12] highlights some of the mechanisms proposed from 1972 - 1984. An example of a mechanism proposed by Krishtalik in 1975 is given in equation (3.11)-(3.13).

$$Cl^- \Leftrightarrow Cl_{ads} + e^- \tag{3.11}$$

$$Cl_{ads} \rightarrow (Cl_{ads})^+ + e^- \tag{3.12}$$

$$(Cl_{ads})^+ + Cl^- \Leftrightarrow Cl_2 \tag{3.13}$$

As mentioned, there are many different mechanisms proposed for the chlorine evolution reaction. All of these [12, 34] mechanisms proceeds with low Tafel slopes in the range of 30 to 40 mV. The Tafel slope has been reported to increase as the chloride concentration decreases [44].

3.2.4 Stability and wear of RuO_2-typed DSAs

As mentioned, the RuO_2-typed DSA electrodes are widely used in the chlorine industry. These electrodes, however, suffer from a lack of stability and corrode heavily during oxygen evolution [45]. This is due to the volatile intermediate RuO_4 (or H_2RuO_5), which is formed in the oxygen evolution in acidic media, according to the following reaction [46, 47]:

$$RuO_2 + 2H_2O \rightarrow RuO_4 + 4H^+ + 4e^- \tag{3.14}$$

The start of wear and the onset of formation of RuO_4 at the anode is accosiated with a break in the Tafel slope, this has been defined as a "critical anode potential" [3]. Above this potential the anode is not stable and will corrode. This critical potential was experimentally determined to 1.2 V versus Ag/AgCl in a chlorate electrolyte, by Cornell et al [48]. They also found that the critical anode potential decreased with increasing chloride concentration in the electrolyte.

It has been shown that the wear rate of anodes coated with a mixture of RuO_2 and TiO_2 is enhanced when the polarization is disconnected and then connected again [34].

RuO_2 based anodes used in the industry are found to be operative in more than 10 years [49].

When it comes to choosing the active oxide in the DSA, IrO_2 is known to be more stable compared to RuO_2 [30].

3.2.5 Voltammetry on IrO_2 and RuO_2

Cyclic voltammetry on noble metal oxides like iridium oxide and ruthenium oxide gives quite distinctive curves. Examples of such voltammograms are given in Figure 3.3. The voltammograms were obtained by Aaron Marshall [50].

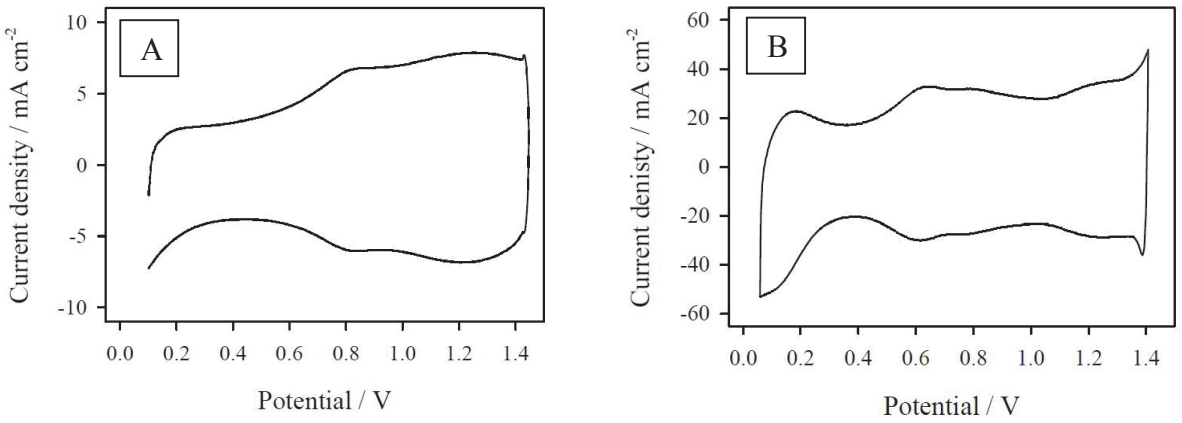

Figure 3.3: Cyclic voltammograms of IrO_2 (A) and RuO_2(B)in 0.5 M H_2SO_4. The figures are taken from the thesis of Aaron Marshall [50].

The wave formed peaks located at the voltammograms of IrO_2 and RuO_2 is due to solid state redox transitions. For iridium oxide, the peaks correspond to the redox transitions of Ir^{3+}/Ir^{4+}

and Ir^{4+}/Ir^{6+} [50]. For ruthenium oxide there are three redox transitions, Ru^{2+}/Ru^{3+}, Ru^{3+}/Ru^{4+} and Ru^{4+}/Ru^{6+} [50]. The process for IrO_2 is given by (3.15) [51], and the process for RuO_2 is given by (3.16) [51].

$$IrO_a(OH)_b \rightleftarrows IrO_{a+\delta}(OH)_{b-\delta} + \delta H^+ + \delta e^- \quad (3.15)$$

$$RuO_a(H_2O)_b \rightleftarrows RuO_{a+\delta}(H_2O)_{b-\delta} + 2\delta H^+ + 2\delta e^- \quad (3.16)$$

3.2.6 Kinetics and selectivity of chlorine evolution

As mentioned in section 2.2, oxygen evolution is a parasitic reaction in chlorine electrolysis. The chlorine evolution occurs with low overpotential on most materials, compared to the overpotential of the oxygen evolution reaction, which greatly depends on the electrode material. Making the anode material highly important regarding selectivity.

RuO_2 based anodes are among the best catalysts for chlorine evolution. Trasatti and Lodi reviewed the electrode material in "Electrodes of conductive metallic oxides, part B" [34]. The ruthenium oxide content in a RuO_2-TiO_2/Ti electrode was found to influence the activity of the coating. The activity towards chlorine evolution decreased drastically at a content lower than 20-30 mol%. The ruthenium oxide content also influenced the competing oxygen evolution. As the oxide content decreased the overpotentials and the Tafel slopes for the oxygen evolution increased. Below about 20 mol% RuO_2 there was observed a steep increase in both overpotentials and Tafel slopes [34, 52]. It was also shown by Arikawa [53] that the chlorine evolution selectivity was highest for an anode rich on titanium oxide compared to an anode rich on ruthenium oxide. In the same article it was proposed that for the RuO_2-TiO_2/Ti anodes, the anode containing 40% RuO_2 and 60% TiO_2 gave the best chlorine evolution ratio (RuO_2 content tested: 100%, 80%, 60%, 40% and 20%).

Aspects other than the anode material may also influence the chlorine selectivity. The selectivity for chlorine evolution over oxygen evolution was found to increase with increasing acidity, chloride concentration, temperature and current density [34].

3.2.6.1 Dilute chloride solutions

In the chlor-alkali process, the raw material is a saturated brine. That is, an aqueous solution containing approximately 26 wt% of NaCl. The use of a concentrated chloride solution yields a current efficiency of approximately 95-97 % [4]. The selectivity of the chlorine evolution in dilute brines, on the other hand, are confirmed to be much lower than that in concentrated solutions [47]. Arikawa [53] tested a RuO_2/Ti electrode and also he found that both the selectivity of the chlorine evolution as well as the current density was dependent on the chloride concentration in the electrolyte. Both the current density of chlorine evolution and the chlorine evolution ratio was remarkably lower in the solution containing low amounts of chloride (0.3 M NaCl, ~500 ppm Cl^-).

There are not a lot of information on chlorine evolution in dilute solutions. In 1972 Kuhn and Mortimer [54] did some research on dilute brines (0.5 – 1 M) of pH 2, on ruthenium dioxide electrodes. Using rotating disc electrodes, they found that the chlorine efficiency increased with higher rotation speed. This indicated that diffusion limitation of chloride ions was occurring. Kuhn and Mortimer also tested different electrode materials, and found that for dilute chloride solutions, electrodes based on IrO_2 would be preferable to those based on RuO_2 when considering current efficiency.

3.3 Oxide powders as electrocatalysts

The DSA is, as described above, usually prepared “in situ” on metallic substrates by thermal decomposition. It is also possible to form oxide electrocatalysts by synthesizing powders of the oxide material, mix the powder in an ink and then apply the catalyst on a to a support material. This last method is widely used in the PEM fuel cell/ water electrolysis research [55] and it is also useful for characterization of different oxide catalysts. The preparation of oxide powders can be done in many different ways, some of the methods are mentioned briefly below.

3.3.1 Synthesis of oxide powders

Sol-gel method

In this method [56] a liquid based colloidal solution (sol) is transformed into a solid gel phase. Inorganic salts or organic metal alkoxides are exposed to hydrolysis and polymerization reactions [50].

Polyol method

In the polyol method [55, 57], a polyol (e.g. ethylene glycol) is used as both the solvent and the reducing agent. The metallic particles are prepared by the reduction of metal precursors in the polyol. The mixture is then heated and the metallic part of the solution is precipitated [58]. The advantage of this method is the possibility to form nanosized particles.

Aqueous Hydrolysis

In aqueous hydrolysis [59] a metal hydroxide is formed by reacting inorganic precursor salts with an aqueous sodium hydroxide solution. The metal oxide is further formed by condensation reactions of the formed complexes.

4 Experimental

All glass equipment used in the experiments described below (except for the volumetric equipment) were cleaned in a hydrogen peroxide bath prior to the experiments. The bath was made from 1 part hydrogen peroxide (30wt%) and 3 parts distilled water, in addition 1 vol% of concentrated sulphuric acid was added.

Unless anything else is mentioned a Gamry600 potentiostat was used in all experiments. A water bath of the type Neslab GP-400 and a rotating electrode setup from Pine instruments were used in all voltammetry experiments, as shown in Figure 4.1.

Figure 4.1: Experimental setup used in the voltammetry experiments.

A list of the chemicals used is given in Table 4.1 below. During all the experiments the electrolyte contained 3.2 wt-% ammonium nitrate and the pH was adjusted with nitric acid. Unless anything else is stated, the pH of the electrolyte was 1.4. Ammonium chloride was added as the source of chloride.

Table 4.1: Electrolyte components.

Chemical compound	Purity/ Quality	Production company
Ammonium nitrate, NH_4NO_3	Pro analysi	Merck
Ammonium chloride, NH_4Cl	Pro analysi	Fluka
Nitric acid, HNO_3	Pro analysi	Merck
Deionised water	15,0 mΩ cm	Milipore

4.1 The reference electrode

For all the voltammetry experiments a three electrode setup was used, with a reversible hydrogen electrode (RHE) as the reference. A detailed description on how this was prepared can be found in Appendix A.

In the electrolysis experiments, a two electrode setup was utilized.

4.2 Rotating disc electrode (RDE) experiments

Voltammetry was executed using a rotating disc electrode setup from Pine instruments, as shown in Figure 4.2. The disc electrode was an IrO_2-DSA (Figure 4.2), that is a dimensionally stable anode coated with iridium oxide (IrO_2) and tantalum oxide (Ta_2O_5). The coating consisted of at least 50 % iridium oxide. The disc was delivered from the Swedish company Permascand (electrode number: PSC 202Y). In all these experiments a platinum mesh, with a large surface area, was used as the counter electrode.

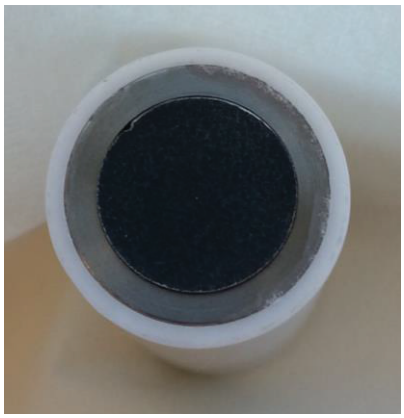

Figure 4.2: IrO_2 - Ta_2O_5/Ti electrode from Permascand in a rotating disc setup.

The experimental parameters for the cyclic voltammetry executed with a rotating disc electrode setup are shown in Table 4.2. For every experimental parameter six different rotation speeds were tested (100, 400, 900, 1600, 2500 and 3600 rpm) and three cycles were run, sweeping the potential from 400 mV to 1800 mV. In these experiments, the current was measured as a function of the potential. The results are given as current density versus potential, using the geometric surface area of the electrode (0.95 cm^2).

Table 4.2: Experimental parameters for the rotating disc electrode (RDE) experiments.

Sweep rate [mV s^{-1}]	**Chloride concentration [ppm]**	**pH**	**Temperature [°C]**
100, 20	0, 100, 1000, 10000	1.4	35
100, 20	1000	1.4	60*
100, 20	1000	0	35*

***** The results of these experiments showed a large degree of inconsistency and was therefore not further processed.

SEM and EDS analyses were carried out to examine the disc electrode both before and after experiments.

4.3 Rotating ring-disc electrode (RRDE) experiments

In the following experiments a VMP3 Multi potentiostat from BioLogic was used. The data were collected by the EC-lab software. In every experiment the ring was made of platinum, while the disc was either platinum or iridium oxide on a glassy carbon disc.

4.3.1 Pt disc, Pt ring (Pt-Pt electrode)

The active surface area of the platinum electrodes was determined by experiments (see Appendix B) to be 0.53 cm^2 for the disc and 0.51 cm^2 for the ring. For comparison, the geometric dimensions of the electrodes can be found in Appendix C. Both the disc and the ring were unpolished.

The electrode was thoroughly rinsed in deionized water, prior to each experiment.

In the experiments using a Pt disc and a Pt ring, the disc electrode was cycled between 0 mV and 2000 mV (3 cycles) while the ring potential was set at a constant potential of 1100 mV or 1000 mV. The experimental parameters are shown in Table 4.3. All experiments were executed at room temperature (~25°C).

Table 4.3: Experimental parameters for the Pt-Pt rotating ring disc electrode (RRDE) experiments. T=25°C.

Chloride concentration [ppm]	**pH**	**Temperature [°C]**	**Potential on ring [mV]**	**Sweep rate [mV s^{-1}]**	**Rotation rate [rpm]**
1000	1.4	25, 35	1100	10, 100	0, 100, 400, 900, 1600, 2500
1000	1.4	35	1000	10, 100	400
10000	1.4	22, 35	1100	10	0, 100, 400, 900, 1600, 2500
10000	1.4	45	1100	100	400, 2500, 4900

4.3.2 IrO_2 on glassy carbon disc, Pt ring (Pt-IrO_2 electrode)

To make the iridium oxide catalyst, 2 mg of iridium oxide powder (made by the hydrolysis method by Anita Reksten, affiliated XRD data are given in Appendix D) was mixed with 1 mL of deionized water adjusted to have a pH of 2 using sulphuric acid (the mixture is further referred to as ink). The ink was then placed in an ultrasonic bath until the mixture was uniform (approximately 40 min). 20 µL of the ink was further placed on the polished glassy carbon disc using a micro pipette, and left to dry under nitrogen purging. A coating of 15 µL Nafion (0.05 wt%) was placed on top of the catalyst and the electrode was again left to dry under nitrogen purging.

For the platinum ring, the active surface area was determined by experiments (see Appendix B) and resulted in an area of 0.51 cm^2. For the IrO_2 on the glassy carbon disc the current was normalized with respect to the total charge (see Appendix B).

In the experiments using an IrO_2 disc and a Pt ring, the disc was first characterized by voltammetry in sulphuric acid, as shown in Table 4.4. This was then followed by voltammetry in an electrolyte containing 1000 ppm of chloride, as shown in *Table* 4.5. All the experiments were executed at room temperature (~25°C).

Table 4.4: Characterization of the IrO_2 coated glassy carbon disc electrodes. T=25°C.

Experiment	**Electrolyte**	**Lower potential limit [mV]**	**Upper potential limit [mV]**	**Sweep rate [mV s^{-1}]**	**Rotation rate [rpm]**
CV*	0.5 M H_2SO_4	0	1400	10, 20, 50, 100, 200, 500	0
LSV*	0.5 M H_2SO_4	1000	1700	0.083	0

Table 4.5: Experimental parameters for the Pt-IrO_2 rotating ring disc electrode (RRDE) experiments. T=25°C.

Experiment	Concentration of chloride [ppm]	Lower potential limit, disc [mV]	Upper potential limit, disc [mV]	Potential, ring [mV]	Sweep rate [mV s^{-1}]	Rotation rate [rpm]
CV *	1000	0	1400	not in use	10, 20, 50, 100, 200, 500	0
LSV *	0, 1000	1300	1700	not in use	0.083	0
CV	1000	0	1700	1100	100	0, 100, 400, 900, 1600, 2500
CV	1000	0	1700	1000	100	100, 900, 2500
LSV	1000	1300	1700	1100	0.083	400, 1600

** In these experiments, a Gamry 600 potentiostat was used. This was only connected to the disc.*

4.4 Preparation of dimensionally stable anodes

IrO_2-Ta_2O_5/Ti (IrO_2-DSA) electrodes were prepared by thermal decomposition as described in the doctoral thesis by Kenji Kawaguchi [60]. The titanium substrate was pre-treated by ultrasonic cleaning in acetone and was further etched in 10 wt% oxalic acid for 60 minutes at 90°C. A precursor solution was prepared by dissolving $H_2IrCl_6 \cdot 6H_2O$ and $TaCl_5$ in butanol containing 6 vol% hydrochloric acid. This was done so that the total metal concentration of Ir and Ta was 70 mg cm^{-3}, and the iridium content was 70 mol%.

The pre-treated substrate was then dipped into the precursor solution, dried for 10 minutes at 120°C and then heated for 20 minutes at 470°C. The dipping procedure was repeated five times.

In addition to an electrode fit for the flow cell (substrate shown in Figure 4.3) two circular electrodes were made for examination by SEM, EDS and XRD.

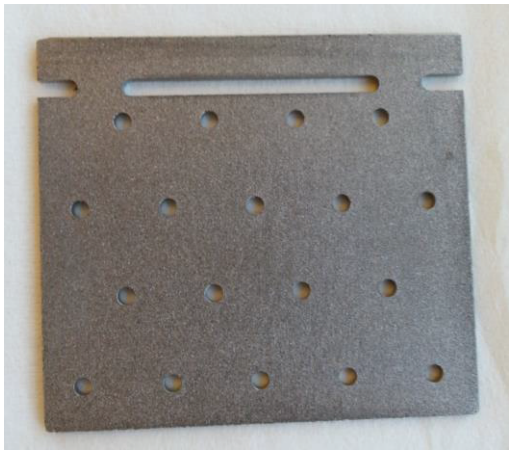

Figure 4.3: Titanium electrode made for flow cell, without coating.

Two additional spherical electrodes were made by a slightly different procedure. In this method, the pre-treated substrate was painted with the precursor solution. The electrodes were further dried for 10 minutes at 120°C and the heated for 20 min at 500°C. The brushing and heat treatment procedure was repeated until a coverage of approximately 2 mg coating per cm^2 was achieved.

4.5 Ex-situ characterization of electrodes

The surface morphology of the RDE from Permascand as well as the electrodes synthesized in house were observed using a Hitachi Model S-3400N low vacuum scanning electron microscope (LV-SEM). An accelerating voltage of 15 keV was used, and the working distance was set to approximately 11 mm. Elemental analyses of the same samples were executed by use of energy dispersive spectroscopy (EDS).

The electrodes were also analysed by grazing incidence X-ray diffraction (XRD). This is a diffraction technique used for characterization of thin films. In this type of XRD, the incident angle of the incoming X-rays is very small in order to maximize the signal from the thin film. Grazing incidence diffraction is therefore a surface sensitive technique, in contrast to "standard" XRD.

In addition to the use of SEM, EDS and XRD, the electrodes synthesized in house were electrochemically characterized by cyclic voltammetry in 0.5 M H_2SO_4.

4.6 Electrolysis

For the electrolysis experiments, a new flow cell made from PVC was designed. A drawing and a picture of the cell are given in Figure 4.4. The anode and cathode compartments are separated as shown in Figure 4.5. This prevents the gases evolved at each side to mix. The electrode shown in Figure 4.3 were made to fit exactly into the anode compartment so that the entire amount of electrolyte which flows through this compartment is in contact with the electrode. The anode compartment was designed with the following dimensions; 5 cm wide, 4.5 cm high and 0.4 cm deep. The counter electrode utilized in the electrolysis experiments was either platinum or steel.

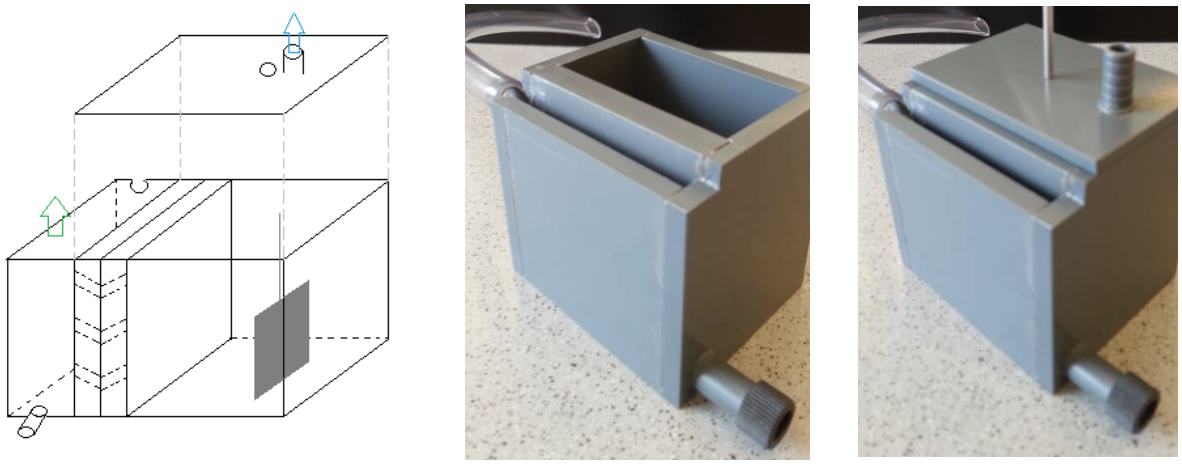

Figure 4.4: Flow cell.

Figure 4.5: Separator of anode and cathode compartment in flow cell.

The electrolyte flows through the anode compartment from a reservoir placed above the cell. A drain tube is used to control the flow of electrolyte through the cell.

The flow cell was first tested with the synthesized IrO_2-electrode. The preliminary experiments were run potentiostatically (constant voltage) with a variety of flow rates (from 50 mL h^{-1} to 250 mL h^{-1}). Further testing was done galvanostatically (constant current) by using currents up to 50 mA.

The synthesized IrO_2-electrode was further tested in a stagnant cell. For comparison, the same experiments were carried out using a commercial RuO_2/IrO_2-mesh from Permascand (electrode number: PSC 102). In these experiments, different chloride concentrations of the electrolyte (3000 ppm and 10 000 ppm) was tested as well as the electrolysis time (1 and 15 hours) and current (50 mA, 100mA). The commercial RuO_2/IrO_2-mesh electrode is shown in Figure 4.6.

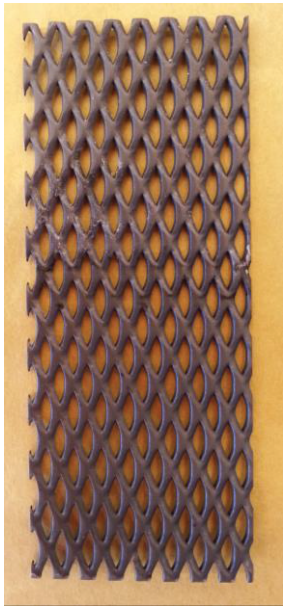

Figure 4.6: RuO2/IrO2 mesh electrode from Permascand (PSC 102).

In addition to the synthetic electrolyte, process water containing approximately 1400 ppm of chloride was tested in both the flow cell and the stagnant cell. In these experiments, the commercial RuO_2/IrO_2-mesh was used as the working electrode.

All of the experiments mentioned above were executed at room temperature. In addition to these, the commercial RuO_2/IrO_2-mesh was tested at 30°C and 60°C as well as in a stagnant electrolyte containing 3000 ppm of chloride, using a current of 100 mA.

The concentration of chloride in the solution before and after electrolysis was determined by potentiometric titration.

4.7 Potentiometric titration

Potentiometric titration with a standardized silver nitrate solution of 0.1 M was used to determine the content of chloride in the electrolyte.

Approximately 25 g of the electrolyte to be analysed in addition to a magnet was poured into a 250 mL beaker. For the solutions with low concentrations approximately 50 g of electrolyte was analysed in order to improve the accuracy of the procedure.

Silver nitrate was filled into a glass burette. A silver electrode was positioned in the beaker, after it was thoroughly cleaned with deionised water, and the magnetic stirrer was turned on. A small amount (about 2 mL for the electrolytes with high concentration of chloride) of the silver nitrate was added by use of the titrator and the cell potential was noted for each addition of silver nitrate. When the cell potential started to increase more rapidly, smaller amounts of silver nitrate were added.

The titration curve was plotted (potential as a function of added silver nitrate) and the volume of silver nitrate at the point of inflection was used to calculate the amount of chloride in the solution.

5 Results and discussions

5.1 Cyclic voltammetry

5.1.1 Supporting electrolyte

For characterization of the system, there were executed cyclic voltammetry in the supporting electrolyte (0.04 M HNO_3, 3.2 wt% NH_4NO_3). A cyclic voltammogram of platinum is shown in Figure 5.1 A, and a cyclic voltammogram of the commercial IrO_2-DSA (IrO_2-Ta_2O_5/Ti) from Permascand is shown in Figure 5.1 B.

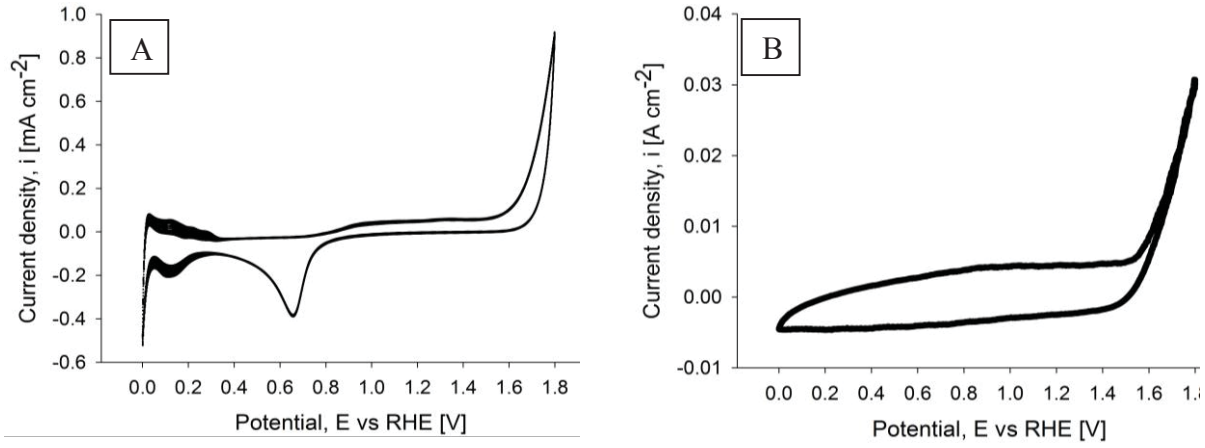

Figure 5.1: Cyclic voltammogram of different electrodes in supporting electrolyte (0.04 M HNO_3, 3.2 wt% NH_4NO_3). Cycled from 0 V to 1.8 V with a sweep rate of 100 mV s^{-1}. ***(A)*** *Platinum electrode.* ***(B)*** *Commercial IrO_2-DSA from Permascand, the electrode was rotated at 100 rpm.*

The base voltammogram of platinum in supporting electrolyte (Figure 5.1 A) can be divided into three sections. The area between 0 to 0.4 V is the region of hydrogen adsorption and desorption (underpotential deposition), and from 0.4 to approximately 0.75 is the double layer region. Platinum oxide is formed at a potential of approximately 0.8 V [11], leading in to oxygen evolution at potentials above 1.6 V. The platinum oxide that was formed, is reduced in the subsequent negative going scan giving a current reduction peak located at approximately 0.7 V.

In Figure 5.1 B there is a large current increase at approximately 1.6 V, this is due to oxygen evolution. The voltammogram of the DSA does not show any reduction peak, as was the case

for the voltammogram of platinum. On platinum, an oxide layer will be formed at high positive potentials during the potential sweep. This oxide layer has a rather low conductivity and so it will be reduced in the subsequent negative going scan. On the DSA, the oxide layer has a high conductivity and thus the reaction zone is limited to the surface of the oxide, impeding its reduction to metallic state. Consequently, no reduction peak will be present in the voltammogram of the DSA.

5.1.2 Addition of chloride

Both the platinum electrode and the IrO_2-DSA electrode were further tested in an electrolyte (0.04 M HNO_3, 3.2 wt% NH_4NO_3) containing a 1000 ppm of chloride. A cyclic voltammogram of the platinum electrode is shown in Figure 5.2 A, while a cyclic voltammogram of the commercial IrO_2-DSA is shown in Figure 5.2 B.

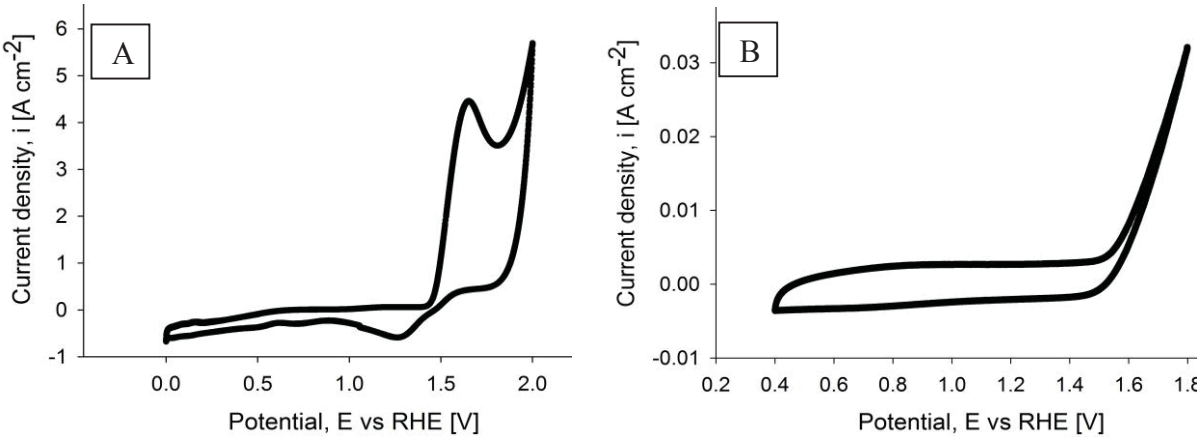

Figure 5.2: Cyclic voltammogram of different electrodes in an electrolyte (0.04 M HNO_3, 3.2 wt% NH_4NO_3) containing a 1000 ppm of chloride. Sweep rate of 100 mV s^{-1}. ***(A)*** *Platinum electrode cycled from 0 to 2 V.* ***(B)*** *Commercial IrO_2-DSA from Permascand cycled from 0 to 1.8 V., The IrO_2-DSA was rotated at 100 rpm.*

Comparison of Figure 5.1 A and Figure 5.2 A clearly shows that the current peak located at approximately 1.6 V in Figure 5.2 A depends on the presence of chloride in the electrolyte. A similar observation was reported in the project work of the author in the fall of 2013 [14], where it was found that the mentioned current peak increased with both chloride concentration in the electrolyte and sweep rate. A reduction peak at 1.3 V is observed in Figure 5.2 A and was found to increase in size with sweep rate as shown previously [14]. This peak corresponds to the

reduction of a soluble oxidation product not escaping the electrode surface prior to the negative going scan.

Experiments also showed that the current peak was dependent on the lower potential limit of the cyclic voltammogram [14]. A lower potential limit set at 1.0 V gave a drastic drop in the peak current for each cycle. The exact reason for this current peak is not known, but it seems to be connected to the surface state of the platinum electrode. If this peak is not related to the chlorine evolution, an alternative explanation may be the formation of a platinum-chloro-complex. Literature [61, 62] shows that chloride ions present in the electrolyte at an amount of as low as 10 ppm will cause a mass loss of the Pt electrode due to dissolution of Pt. This dissolution is related to the formation of Pt-chloride complexes. It is suggested that the loss of platinum in the presence of chloride is caused by the following reactions [63]

$$Pt + 4Cl^- \rightarrow PtCl_4^{2-} + 2e^- \tag{5.1}$$

$$Pt + 6Cl^- \rightarrow PtCl_6^{2-} + 4e^- \tag{5.2}$$

Yadav et al. [61] found that the presence of chloride increased the extension of the double layer region in the positive going scan in the CV, but not in the negative going scan. In addition, they found that the presence of chloride decreased the oxide reduction peak. Yadav et al. explained these phenomena by a strong retardation of oxide formation by adsorbed chloride ions.

Figure 5.1 B and Figure 5.2 B show the same features, and there is not easy to detect any difference in the voltammogram of the IrO_2-DSA as chloride is added. This is most likely due to the small content of chloride, causing oxygen evolution to be the dominating reaction. As discussed in Section 2.2, the oxygen evolution will always be competing with the chlorine evolution in aqueous solutions. The selectivity for chlorine evolution is dependent on several factors. Among these are the pH, chloride concentration and potential.

5.3 Rotating disc electrode (RDE) experiments

During the authors project work carried out in the fall of 2013 [14] it was found a linear relationship between the chloride concentration and the peak current density observed during cyclic voltammetry of platinum. This indicated that the chlorine evolution on platinum is most likely mass transport controlled. As an elaboration of this experiment there was carried out voltammetry using a rotating disc electrode in the present thesis. As the electrode, bot platinum and a commercial IrO_2-DSA was tested. The experiments using a platinum electrode (Figure 5.3) clearly showed an influence of rotation rate, indicating that the chlorine evolution on platinum is mass transport controlled.

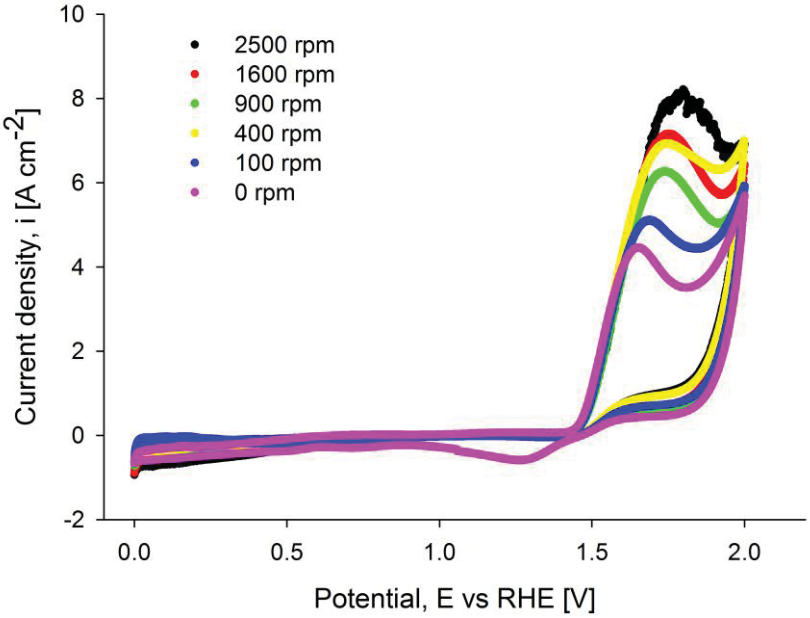

Figure 5.3: Cyclic voltammetry of a platinum electrode in an electrolyte (0.04 M HNO_3, 3.2 wt% NH_4NO_3) containing 1000 ppm chloride, for varying rotation rates at 35°C.

The RRDE experiments using an IrO_2-DSA (IrO_2-Ta_2O_5/Ti) indicated that chlorine evolution on this particularly electrode was only to a small degree dependent on the rotation rate, shown in Figure 5.4 and Figure 5.5. The experiments showed similar results for the electrolyte containing 0, 100 and 10 000 ppm of chloride.

In this project an electrolyte containing relatively small amounts of chloride (up to 10 000 ppm, ~0.3 M Cl^-) was used. This causing the oxygen evolution reaction to be the dominating reaction

taking place. Therefore, it could be that the chlorine evolution is in fact affected by mass transport, but that this effect is masked by the dominating oxygen evolution.

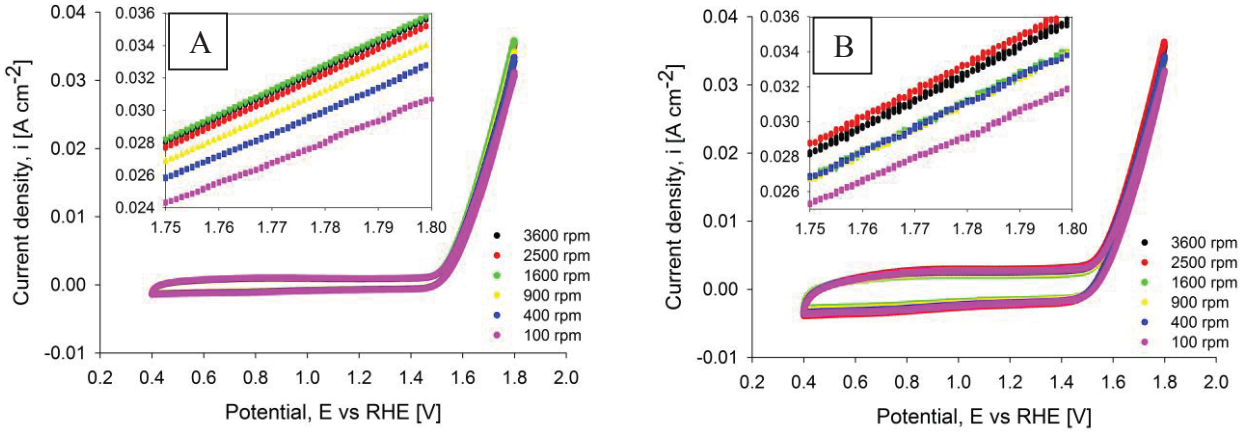

Figure 5.4: Cyclic voltammetry of IrO_2 – DSA (IrO_2-Ta_2O_5/Ti) in an electrolyte (0.04 M HNO_3, 3.2 wt% NH_4NO_3) containing 1000 ppm chloride, for varying rotation rates at 35°C. The insert represents a close up of the linear region. ***(A)*** *Sweep rate of 20 mV s^{-1}.* ***(B)*** *Sweep rate of 100 mV s^{-1}.*

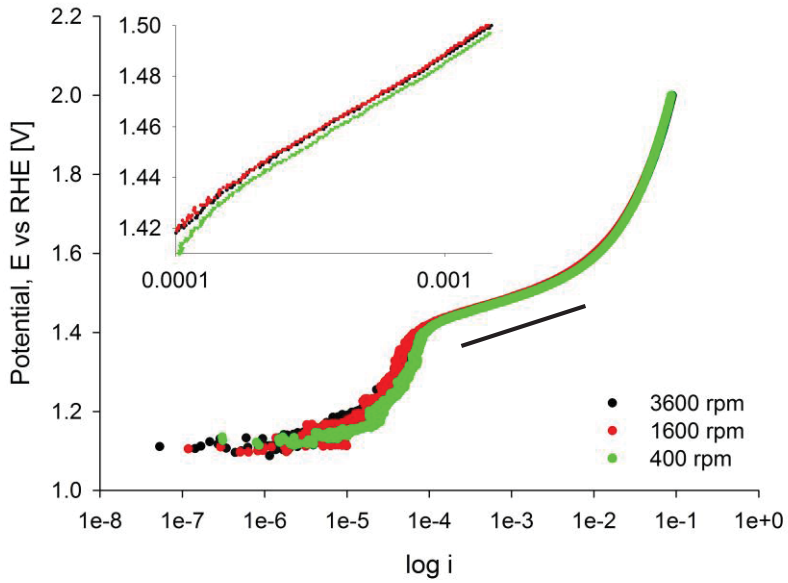

Figure 5.5: Linear sweep voltammetry of of IrO_2 – DSA (IrO_2-Ta_2O_5/Ti) in an electrolyte (0.04 M HNO_3, 3.2 wt% NH_4NO_3) containing 1000 ppm chloride, for a selection of rotational speeds (400, 1600, 3600 rpm). The potential was swept from 1.0 V to 2.0 V with a sweep rate of 1 mV s^{-1}. The black solid line represents the Tafel slope. The insert represents a close up of the linear region.

The linear sweep voltammetry presented as a Tafel plot (Figure 5.5), could be used for determining the anodic Tafel slope of the reaction taking place during the sweep. From literature [40, 41], the Tafel slope of the oxygen evolution reaction (in the low current density region) on Ti supported IrO_2-Ta_2O_5 electrodes was shown to lie in the region 60-70 mV dec^{-1}. The Tafel slope of the chlorine evolution reaction is determined to be about 40 mV dec^{-1} for IrO_2 typed electrodes [34]. Calculating the Tafel slope in Figure 5.5 gives a value of approximately 63 mV dec^{-1}. This indicates that the oxygen evolution reaction is dominating. The expected break in the Tafel slope (as discussed in Section 3.2.3) was not observed. This may be due to formation of gas on the electrode surface, masking this transition.

5.4 Rotating ring-disc electrode (RRDE) experiments

5.4.1 Pt disc, Pt ring

The main purpose for using the rotating ring disc electrode was to determine the current efficiency for chlorine evolution. While the potential was cycled on the disc, the potential on the ring was set to a constant potential of 1.1 V, and the current responses for both electrodes were recorded (Figure 5.6 and Figure 5.7). The idea of this experiment was to set the constant

potential of the ring so that the chlorine gas evolved at the disc would be reduced again at the ring as the electrode system was rotated. By analyzing the current responses from both the disc and the ring, a current efficiency could be calculated. Even though the potential at the ring was adjusted so that only chlorine gas would be reduced (ideally, negligible amounts of dissolved oxygen will be reduced at the ring at these potentials due to the irreversible nature of the oxygen reduction overpotential) it may be that the current response on the ring corresponded to another reaction. Such a reaction may be the dissolution of the platinum electrode. The same experiment executed in the supporting electrolyte (0.04 M HNO_3, 3.2 wt% NH_4NO_3), gave no current response on the ring during cyclic voltammetry on the disc. This indicates that the current response on the ring, detected in chloride containing electrolyte can be assumed to be related mostly to the chlorine evolution reaction.

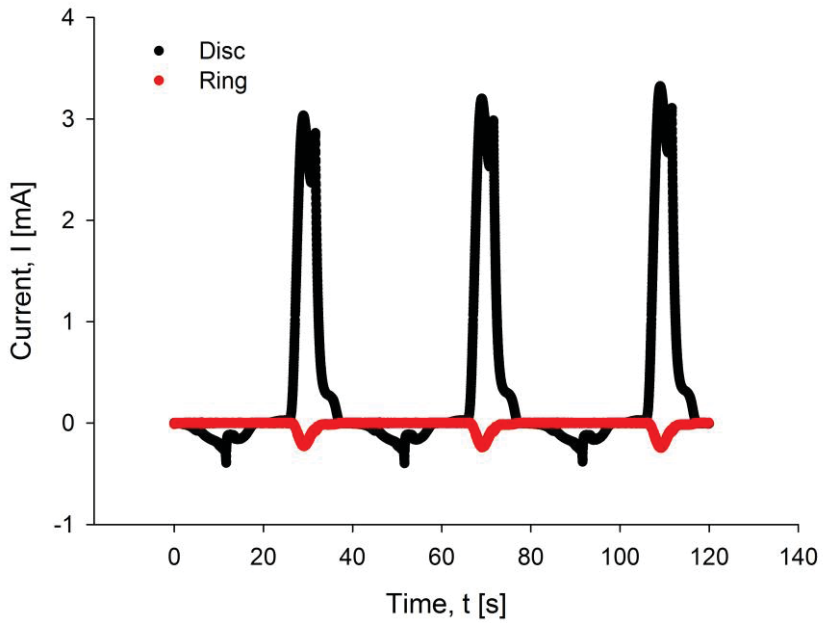

Figure 5.6: Current response as a function of time using a RRDE consisting of a Pt disc (back curve) and a Pt ring (red curve) in an electrolyte (0.04 M HNO_3, 3.2 wt% NH_4NO_3) containing 1000 ppm chloride at 35°C. Cyclic voltammetry from 0 V to 2 V with a sweep rate of 100 mV s^{-1} was executed at the disc, while a constant potential of 1.1 V was applied to the ring. Electrode rotating at 900 rpm.

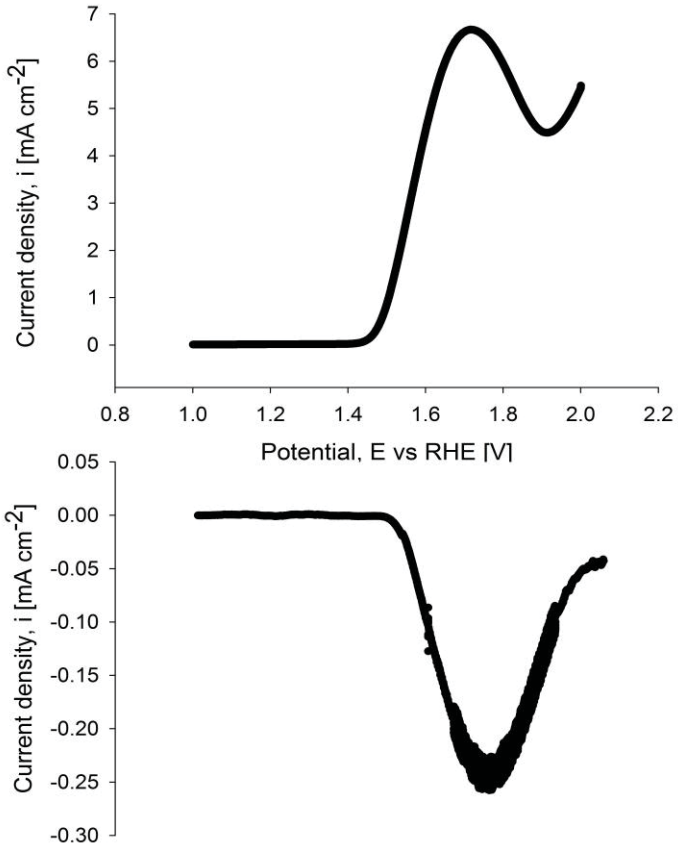

Figure 5.7: Current response as a function of potential using a RRDE consisting of a Pt-disc (top) and a Pt-ring (bottom) in an electrolyte (0.04 M HNO_3, 3.2 wt% NH_4NO_3) containing 1000 ppm chloride at 35°C. The figure shows only a part of the cyclic voltammogram which was executed on the disc, with a sweep rate of 10 mV s^{-1}. A constant potential of 1.1 V was applied to the ring. Electrode rotating at 400 rpm.

An interesting observation was made when the potential at the ring was changed to 1.0 V. As can be seen in Figure 5.8 a decrease in the ring potential of only 0.1 V resulted in a decrease in the current response peak from the ring. The author has not been able to identify the reason for this.

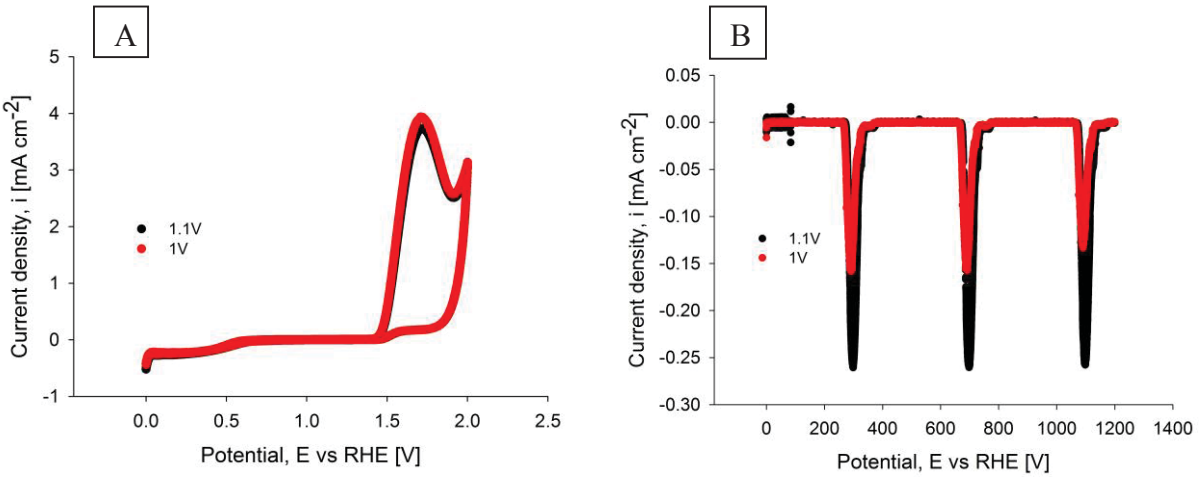

*Figure 5.8: Current responses on **(A)** disc (10 mV s^{-1}) and **(B)** ring, using a constant potential of 1.0 V on the ring. Electrode rotating at 400 rpm. Electrolyte (0.04 M HNO_3, 3.2 wt% NH_4NO_3) containing 1000 ppm of chloride.*

The influence of the upper reversal potential on the Pt-disc was examined in an electrolyte containing 10 000 ppm chloride at 45°C, with a sweep rate of 100 mV s^{-1}. With an upper reversal potential of 1.7 V instead of 2.0 V the current response on the ring became more stable. This is shown in Figure 5.9, and is most likely due to a more controlled gas evolution at a lower potential. For the upper reversal potential of 2.0 V, the maximum current on the disc was equal to approximately 37 mA (69.8 mA cm^{-2}) for all rotation rates. The same trend was observed when using an upper reversal potential of 1.7 V, this leading to maximum current on the disc, equal to approximately 17 mA (32.1 mA cm^{-2}). As can be seen in Figure 5.9, a higher upper reversal potential on the disc results in a larger current response on the ring. This is to be expected as the gas evolution on the disc will increase with increasing upper reversal potential. And so the current response on the ring will also increase as more chlorine gas is to be detected.

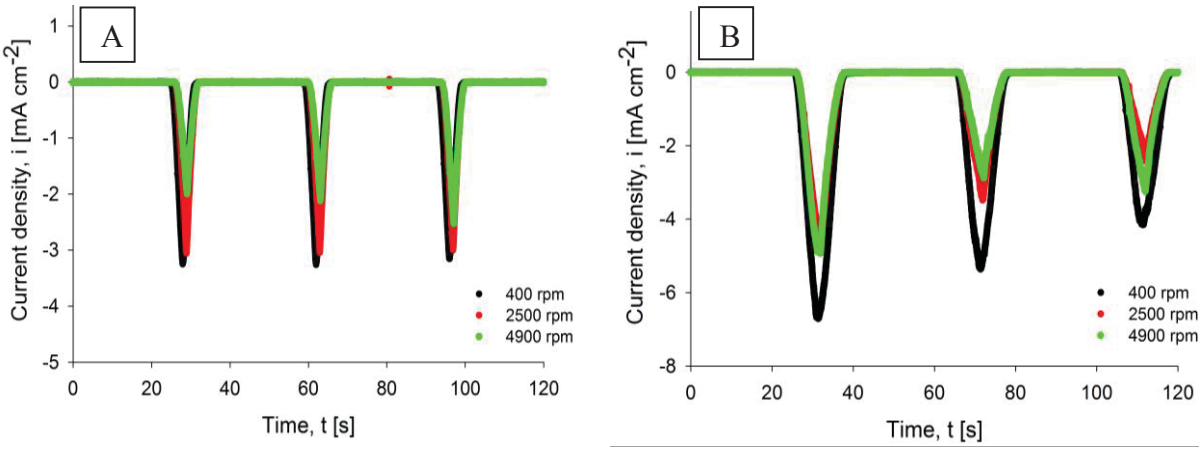

Figure 5.9: Experiments in an electrolyte (0.04 M HNO_3, 3.2 wt% NH_4NO_3) containing 10 000 ppm of chloride, at 45°C. Cyclic voltammetry (100 mV s^{-1}) on the Pt-disc was executed with varying upper reversal potential. The corresponding current response with a constant potential of 1.1 V on the ring is shown. Varying rotation rates (400, 2500 and 4900 rpm). ***(A)*** *Upper reversal potential of 1.7 V.* ***(B)*** *Upper reversal potential of 2.0 V.*

Assuming that it is actually only the chlorine gas that is being reduced at the ring electrode, the current efficiency of the chlorine evolution could be calculated. The current efficiency calculated for some of the experiments, is shown in Table 5.1. The theoretical collection efficiency of the electrode (26 % - Appendix C) was assumed to be close to the experimental value. An example of the calculation is given in (5.1).

$$CE = \frac{0.27mA}{0.26 \cdot 3.6mA} = 29\% \qquad (5.1)$$

As Table 5.1 shows, the current efficiency for chlorine evolution on platinum is for all experiments in the region between 23-32 %. The difference in the calculated value is relatively small. Because of this, it is difficult to say whether the current efficiency is dependent on rotation rate, temperature or chloride concentration. The variation in the current efficiency may be due to bubble formation on the electrode, causing the active surface area of the electrode to vary in the different experiments.

Table 5.1: Calculated current efficiencies for experiments carried out using the Pt-Pt RRDE. The sweep rate was 100 mV s^{-1} in all experiments.

Temperature [°C]	Chloride concentration [ppm]	Rotation rate [rpm]	Peak current, disc [mA]	Peak current, ring [mA]	CE [%]
35	1000	400	3.6	0.27	29
35	1000	900	3.0	0.25	32
35	1000	2500	4.2	0.25	23
22	1000	400	2.9	0.2	27
22	1000	900	3.5	0.28	31
22	1000	2500	4.0	0.33	32
45	10 000	400	37	3.1	32
45	10 000	2500	37	2.2	23

5.4.2 IrO_2 on glassy carbon disc, Pt ring

For characterisation of the IrO_2 disc on glassy carbon electrode, voltammetry was carried out in 0.5 M sulphuric acid as shown in Figure 5.10. These experiments were done without rotation of the electrode.

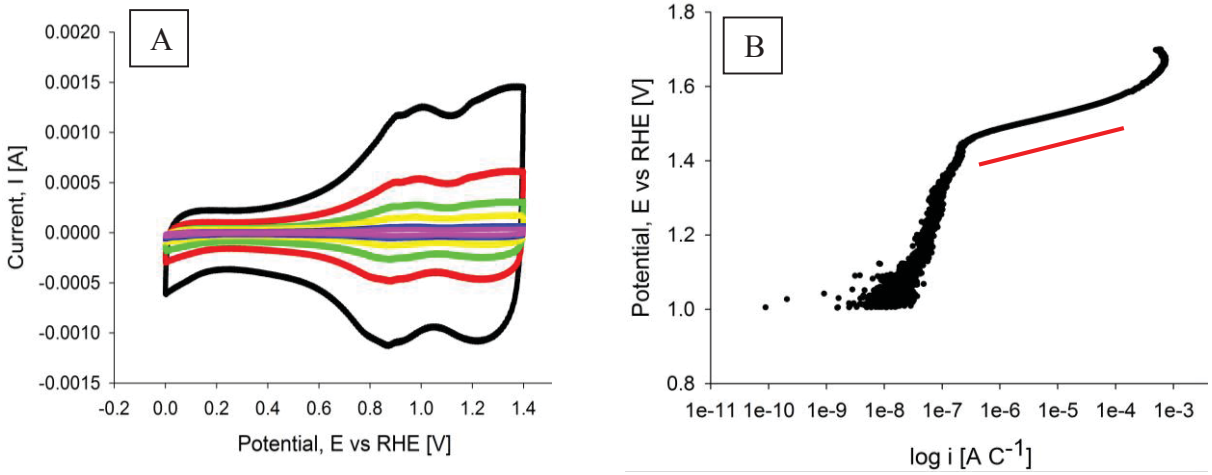

*Figure 5.10: Voltammetry of IrO_2 on glassy carbon in electrolyte containing 0.5 M H_2SO_4. **(A)** CV from 0 V to 1.4 V with varying sweep rate (10, 20, 50, 100, 200 and 500 mV s^{-1}). **(B)** Linear sweep voltammetry from 1 V to 1.7 V with a sweep rate of 5 mV min^{-1}. Red line representing the Tafel slope.*

Both the cyclic voltammogram and the linear sweep voltammogram given in Figure 5.10 looks similar to literature [50, 64], indicating that the IrO_2 layer on the electrode is active. Experiments executed in both of the doctoral theses mentioned above resulted in a Tafel slope of a little under 40 mV dec^{-1} when performing the same polarization measurements as stated in Figure 5.10 B. This is the same result obtained in the experiment performed in this project. This result is in contrast to other literature [34, 42] which state a Tafel slope of 58 – 60 mV dec^{-1} for IrO_2. An explanation for this deviation is not known.

The same experiments that were executed in the sulphuric acid were also performed in an electrolyte (0.04 M HNO_3, 3.2 wt% NH_4NO_3) containing 1000 ppm of chloride. These are shown in Figure 5.11.

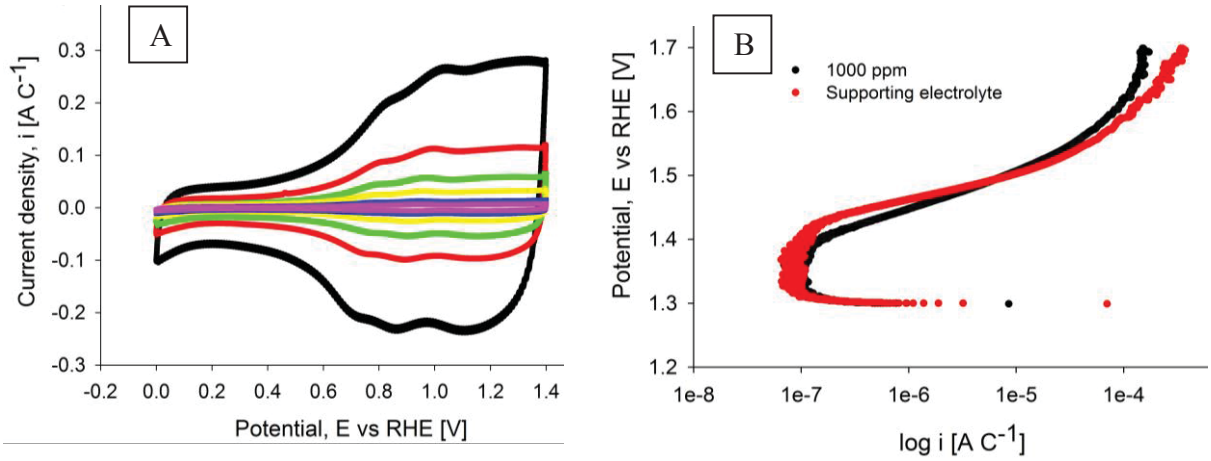

Figure 5.11: Voltammetry of IrO_2 on glassy carbon in an electrolyte (0.04 M HNO_3, 3.2 wt% NH_4NO_3) containing 1000 ppm of chloride. ***(A)*** *CV from 0 V to 1.4 V with varying sweep rate (10, 20, 50, 100, 200 and 500 mV s^{-1}).* ***(B)*** *Linear sweep voltammetry from 1 V to 1.7 V with a sweep rate of 5 mV min^{-1}. This also showing the same LSV in supporting electrolyte (0.04 M HNO_3, 3.2 wt% NH_4NO_3).*

Both the cyclic voltammogram and the linear sweep voltammogram in Figure 5.11 look similar to those from the thesis of Elizaveta Kuznetsova [65]. From the linear sweep voltammetry in Figure 5.11 B, Tafel slopes could be calculated. The Tafel slope of the supporting electrolyte was calculated to be close to 40 mV dec^{-1}. The same result which was obtained for Figure 5.10 B. The Tafel slope of the electrolyte containing 1000 ppm of chloride was calculated to be 55 mV dec^{-1}. This can be seen in Figure 5.12, where the Tafel slope is presented as a red solid line. The dashed red line marks the reversible potential of the chlorine evolution reaction for an

electrolyte containing 1000 ppm chloride. The reversible potential is determined by use of equation (2.14). As expected, the Tafel slope changed with the addition of chloride. Figure 5.12 shows that the Tafel slope belongs to the oxygen evolution reaction, and that a curvature above a potential of 1.45 V may be due to the production of chlorine. Regardless of this, the chloride in the electrolyte may also affect the oxygen evolution at lower potentials, and thus the Tafel slope will differ from the literature value for oxygen evolution.

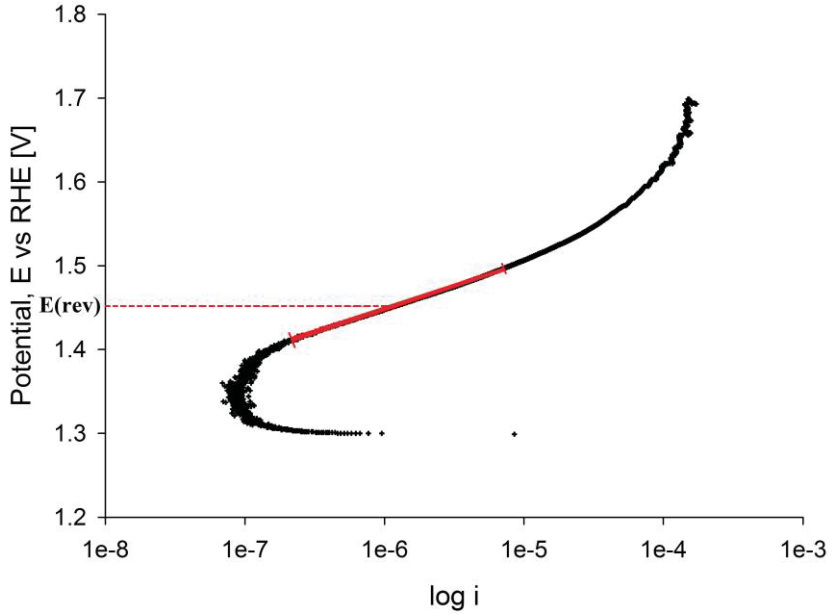

Figure 5.12: LSV of IrO_2 on glassy carbon in an electrolyte (0.04 M HNO_3, 3.2 wt% NH_4NO_3) containing 1000 ppm of chloride. The potential was swept from 1.3 V to 1.7 V with a sweep rate of 5 mV min^{-1}. The red solid line represents the Tafel slope, and the dashed line represents the reversible potential for the chlorine evolution reaction calculated from equation (2.13).

As for the commercial IrO_2-DSA, the rotation rate was found to have little effect on the chlorine evolution on IrO_2 on glassy carbon. This is shown for rotations of 400 rpm and 1600 rpm in Figure 5.13 and Figure 5.14.

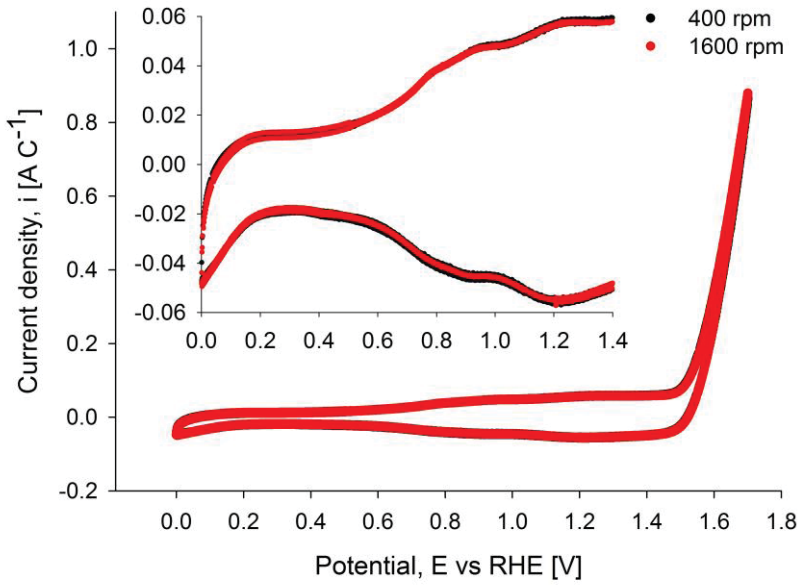

Figure 5.13: Cyclic voltammetry of IrO_2 on glassy carbon disc in an electrolyte (0.04 M HNO_3, 3.2 wt% NH_4NO_3) containing 1000 ppm of chloride. The potential was swept from 0 V to 1.7 V, with a sweep rate of 100 mV s^{-1}. The figure shows results for rotation rates of both 400 rpm and 1600 rpm. The potential of the inset is up to 1.4 V only.

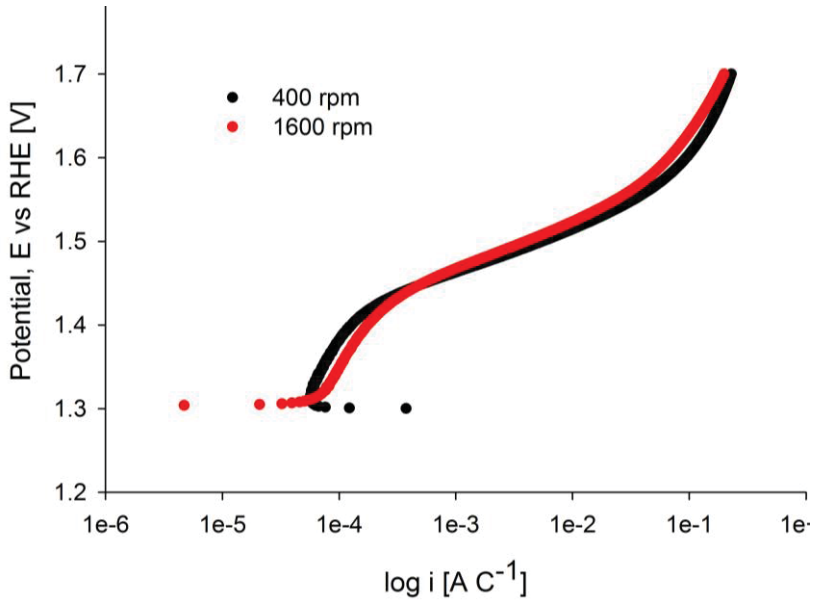

Figure 5.14: Linear sweep voltammetry of the IrO_2 on glassy carbon disc in an electrolyte (0.04 M HNO_3, 3.2 wt% NH_4NO_3) containing 1000 ppm of chloride. The potential was swept from 1.3 V to 1.7 V with a sweep rate of 5 mV min^{-1}. The figure shows results for rotational rates of both 400 rpm and 1600 rpm.

Also for the Pt-IrO_2 RRDE, the current efficiency for chlorine evolution was determined. The time versus potential response on the ring can be seen in Figure 5.15 A, and the time versus current response on the ring can be seen in Figure 5.15 B. In this experiment the disc was cycled between a potential of 0 and 1.7 V with a sweep rate of 100 mV s^{-1}. During the entire experiment, the ring was set at a constant potential of 1.1 V. Using a collection efficiency of 23.5 % (determined by Elizaveta Kuznetsova [65]), the current efficiency for chlorine evolution on iridium oxide was calculated. Some of the calculated values are shown in Table 5.2. As seen in the table below, the current efficiency for chlorine evolution on iridium oxide is in the region of 2.4-3.2 %. Compared to the results from Table 5.1 it is clear that the current efficiency for chlorine evolution on IrO_2 is lower than that for chlorine evolution on Pt.

Table 5.2: Collection efficiencies calculated for some of the experiments carried out using the Pt- IrO_2 RRDE. The temperature was set to 25°C in all experiments.

Rotation rate [rpm]	**Peak current, disc [mA]**	**Peak current, ring [mA]**	**CE [%]**
400	4.8	0.04	3.2
900	4.8	0.03	2.4
2500	4.9	0.03	2.4

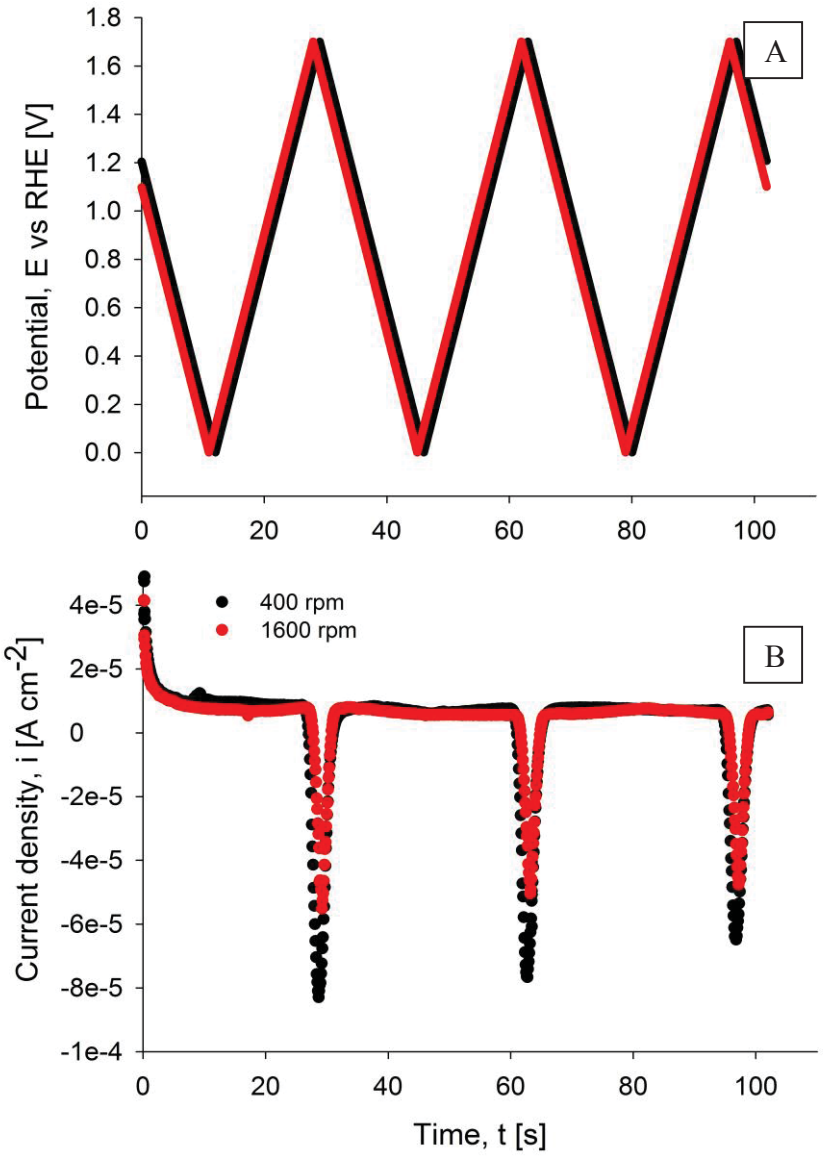

Figure 5.15: Rotating ring disc experiment with electrode consisting of an IrO_2 (on glassy carbon) disc and a Pt ring. The experiment was executed in an electrolyte (0.04 M HNO_3, 3.2 wt% NH_4NO_3) containing 1000 ppm of chloride, for two different rotational rates; 400 and 1600 rpm. ***(A)*** *Potential vs time on the IrO_2 on glassy carbon disc. The potential was swept between 0 and 1.7 V with a sweep rate of 100 mV s^{-1}.* ***(B)*** *Current density response on the ring set at a constant potential of 1.1 V.*

Figure 5.15 clearly shows that the current response on the ring is changing when altering the rotation rate of the electrode. This was also the case for the Pt-Pt electrode (Figure 5.9). This was not to be expected, as the collection efficiency for a rotating ring disc electrode should be independent of the rotation rate [8]. For the ring to detect all the intermediate products generated at the disc (also the unstable ones), it is desirable to narrow the gap between the disc and the

ring. This will reduce the transit time necessary for an intermediate produced at the disc to reach the ring. There is a possibility that the intermediates produced at the disc in these experiments are short-lived, and that these intermediates will oxidize on the disk as the transit time increases. This will result in a higher number of electrons that can be transferred on the ring, causing a higher current response on the ring at lower rotation rates.

There are some sources of error connected to the experiments using IrO_2 on glassy carbon. After the linear sweep voltammograms in the solution containing chloride it seemed as if the coating degraded. This could be seen both with the bare eye, and also from a slight change in the cyclic voltammograms. By comparing Figure 5.13 A with the insert in Figure 5.14, it can be seen that the peaks located at approximately 0.8 V and 1.0 V are less distinct in the latter. A different preparation procedure should be investigated to ensure more reliable results when using this type of electrode in chloride containing electrolytes. A suggestion for change in the preparation procedure may be the use of heat or the use of more Nafion.

5.5 Electrocatalytic layer on titanium substrates

5.5.1 IrO_2-DSA from Permascand

An IrO_2-Ta_2O_5/Ti electrode from Permascand was used for RDE experiments (Figure 4.2), SEM images of the electrode before and after use are shown in Figure 5.16 and Figure 5.17. With some deviations, all of the figures below show a surface coating which exhibits a morphology that is known for IrO_2-Ta_2O_5 coatings [66]. The electrode surface has a standard "mud-cracked" morphology, consisting of cracks, flat areas and particle aggregates. Elemental analysis of the surface area indicated that the aggregates present in Figure 5.16 consisted of iridium oxide, which was to be expected [66, 67]. The EDS analysis also showed that the flat area between the iridium oxide particles consisted of iridium oxide and tantalum oxide.

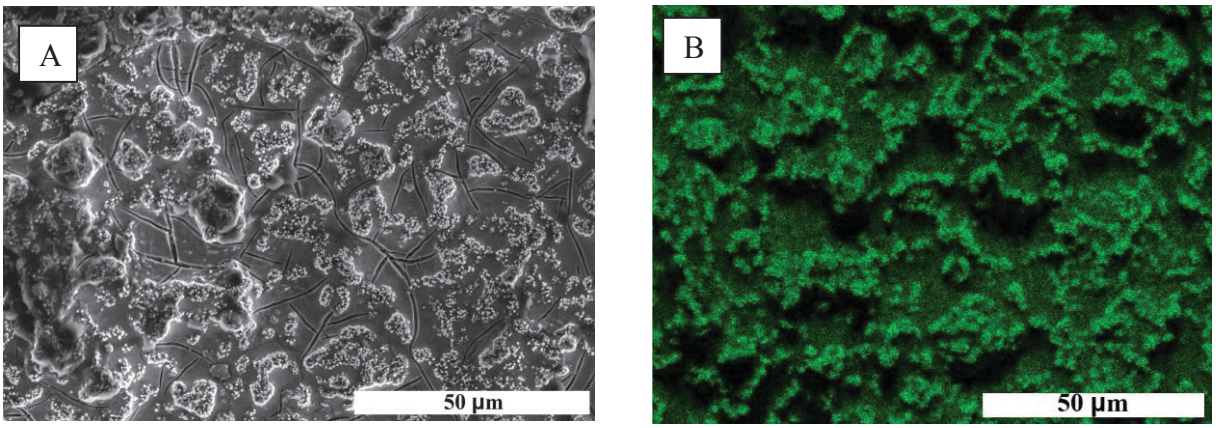

Figure 5.16: SEM images of the IrO_2-Ta_2O_5/Ti electrode from Permascand before use. ***(A)*** *Secondary electron SEM image.* ***(B)*** *EDS map of the iridium present in A. The brighter green areas contain mostly iridium.*

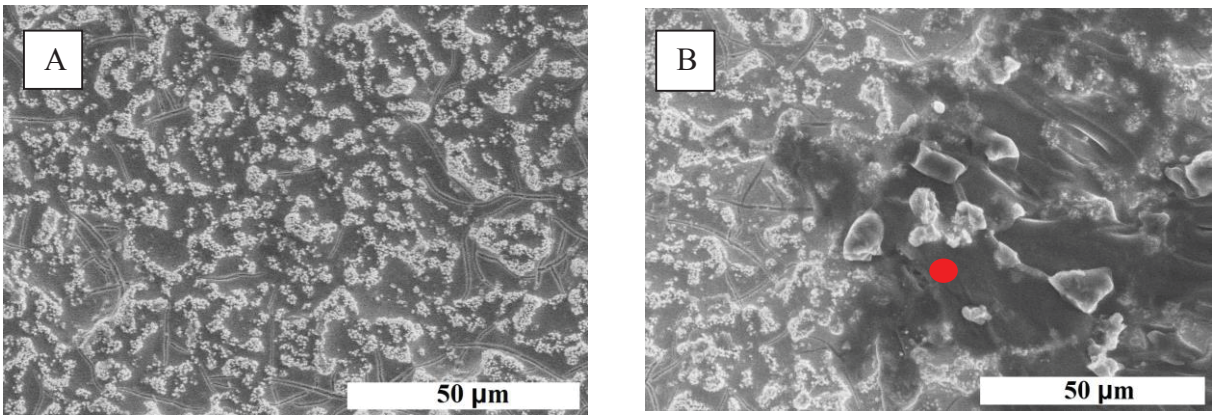

Figure 5.17: SEM images of the IrO_2-Ta_2O_5/Ti electrode from Permascand after use.

SEM and EDS analysis of the electrode after experiments showed areas that looked unchanged (Figure 5.17 A). Areas with a different composition were also detected (Figure 5.17 B). The darker area (marked by a red dot) in Figure 5.17 B was found to contain an amount of 46-52 at% of nitrogen. This may be due to lack of thorough cleaning of the electrode prior to EDS analysis, causing nitrates from the electrolyte drying on to the electrode.

Analysis of the electrode before use was also carried out using XRD. XRD analysis (Figure 5.18) indicated that the sample contained crystalline IrO_2. There was also peaks corresponding to titanium. This was most likely signals from the substrate. Ta_2O_5 was not detected, indicating that the tantalum detected by EDS is amorphous.

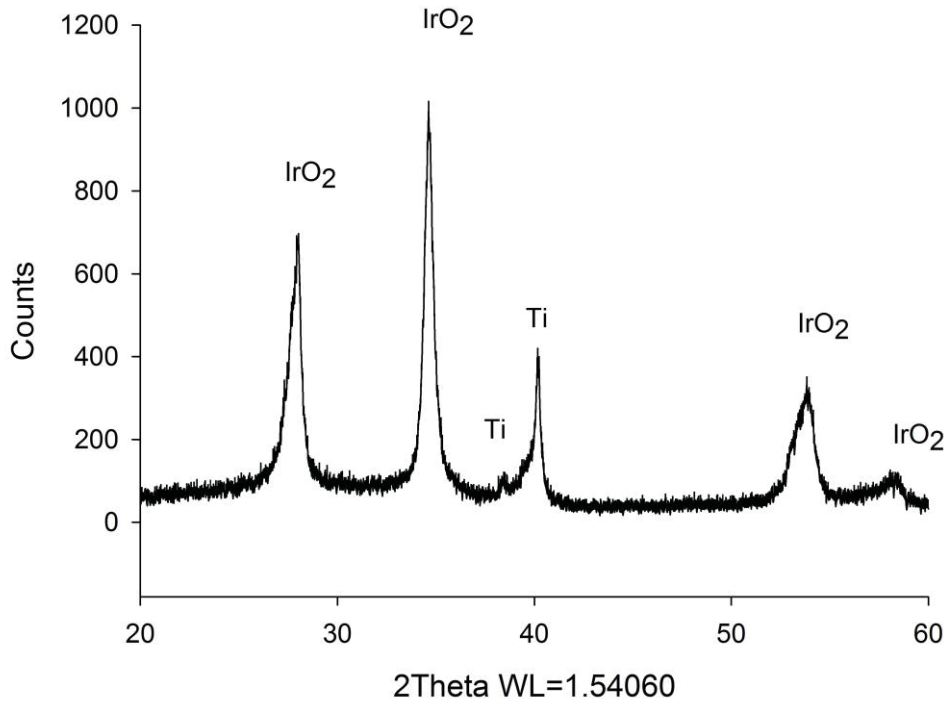

Figure 5.18: XRD of industrial IrO_2-DSA (IrO_2-Ta_2O_5/Ti) from Permascand.

5.5.2 Synthesized IrO_2-DSA prepared by paint brush

SEM images of the IrO_2-DSA where the coating was applied by brush is shown in Figure 5.19. The elements present and the amount of each of them were found by EDS analysis, the data are given in Table 5.3. The element analysis showed an Ir:Ta molar ratio of approximately 60:40. This is a bit lower Ir content than the desired of 70 mol%.

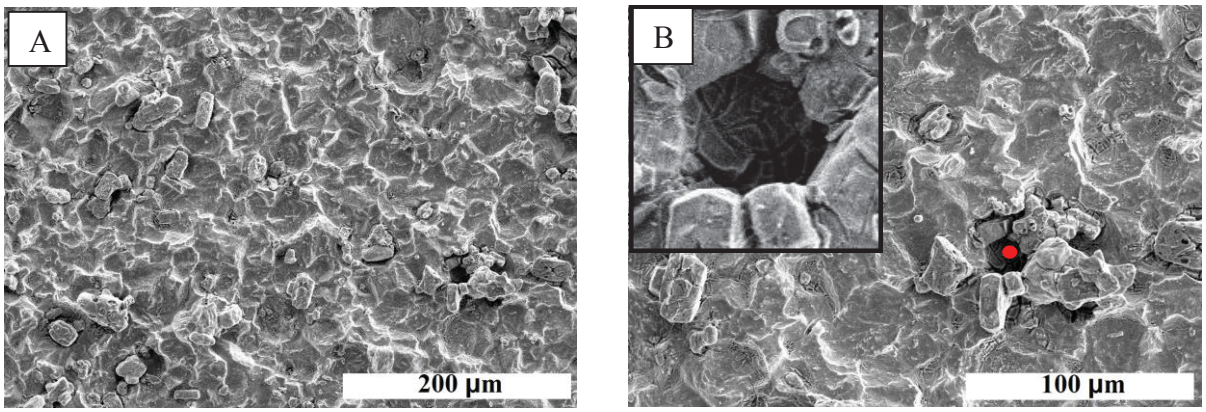

Figure 5.19: SEM images of a DSA (IrO_2 – Ta_2O_5/Ti) electrode. The coating was applied by brush and the electrode was heated at 500°C for 20 minutes. Insert in B: close up of the area marked with a red dot.

Table 5.3: EDS data for the entire area in Figure 5.19 B. Given in atomic percent.

Area	O	Ir	C	Ti	Ta	Cl
Figure 5.19 B	46.5	17.6	16.2	12.9	3.5	3.4

The electrode surface in Figure 5.19 did not show all the well known features of IrO_2-Ti_2O_5 coatings as the commercial electrode (Figure 5.16), but the insert in Figure 5.19 B shows a small area that contain a cracked surface. Figure 5.20 shows the corresponding EDS map of the entire area in Figure 5.19 B. In contrast to the commercial IrO_2-DSA, EDS analysis of the painted electrode indicated a large amount of tantalum in the agglomerates.

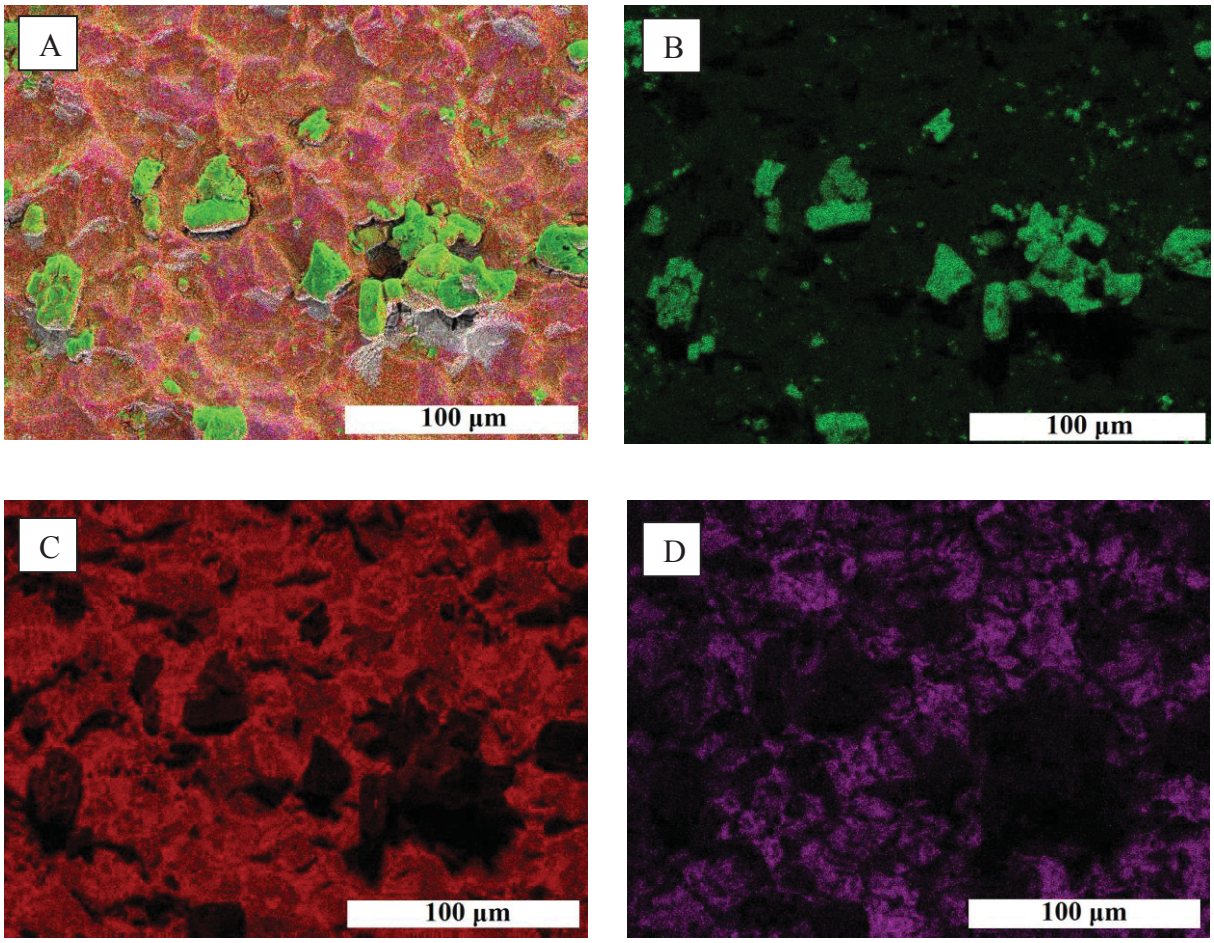

Figure 5.20: EDS maps of the entire area in Figure 5.19 B. The colours represent different elements. Green: tantalum, red: iridium, purple: titanium. (A) Sum of the element maps. (B) Tantalum map. (C) Iridium map. (D) Titanium map.

As Figure 5.20 shows, the painted IrO_2-DSA contained a sufficient amount of agglomerated tantalum. The iridium detected on the electrode seemed to be distributed over the entire surface of the electrode. The characteristic agglomerates of iridium particles were not found. It needs to be pointed out, that agglomerates of iridium particles may be too small for the SEM to detect. Another feature of this electrode was the presence of a large amount of titanium (Figure 5.20 A and C). The presence of titanium will lower the conductivity of the electrode (as TiO_2 has a rather low conductivity) resulting in a lower current for a given potential as an ohimc drop may arise [39]. When an element analysis is carried out by EDS, it is important to mention that the emission volume of the characteristic x-rays is very large. This means that the detected signal will not only come from the surface of the sample. Assuming that the coating of the electrode is very thin, it is reasonable to believe that a large amount of the detected titanium actually is signals coming from the substrate.

Also this electrode was analysed with XRD. Figure 5.21 was similar to the XRD analysis of the industrial electrode, containing all the same peaks for IrO_2, though with a smaller intensity. The discovery of IrO_2 with XRD indicates that the IrO_2 detected by the EDS is actually crystalline, but the particles are too small to see in the microscope. The titanium peaks had a larger intensity in the XRD for the painted electrode. This may indicate that the coating for the electrode synthesized in house is thinner than the commercial electrode. Two additional peaks were observed with XRD of the painted electrode (indicated by stars in Figure 5.21). These peaks are most likely due to crystalline Ta_2O_5, but as the intensity of the peaks is very low, the results are difficult to interpret. The discovery of tantalum agglomerates by EDS supports the findings of crystalline Ta_2O_5 with XRD.

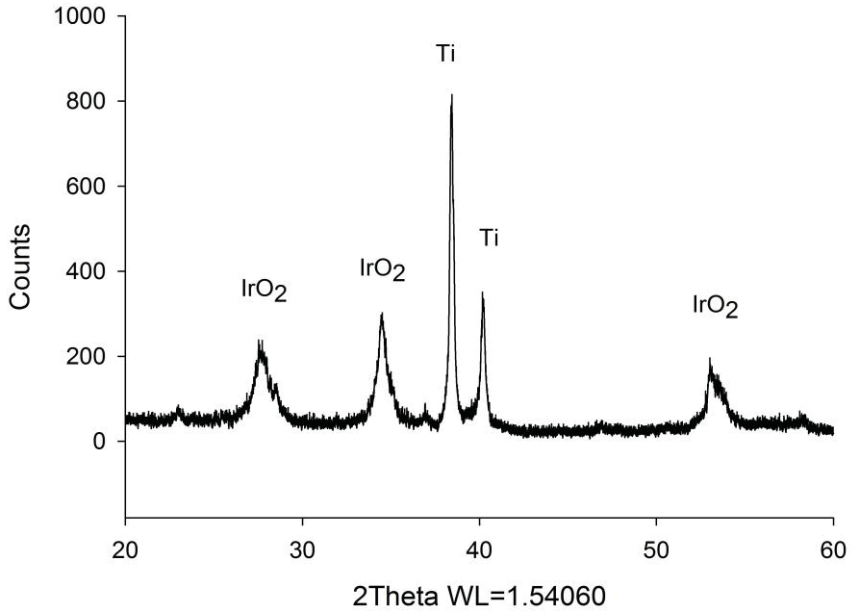

Figure 5.21: XRD of the syntesized IrO_2-DSA (IrO_2-Ta_2O_5/Ti) prepared by painting. The stars indicate peaks that may represent Ta_2O_5.

In addition to analysis by SEM, EDS and XRD, the electrode was also characterized by cyclic voltammetry in 0.5 M H_2SO_4 (Figure 5.22). The voltammogram shows to small current peaks located at approximately 0.8 V and 1.2 V. These peaks are known to be due to solid state redox transitions, as described in Section 3.2.5.

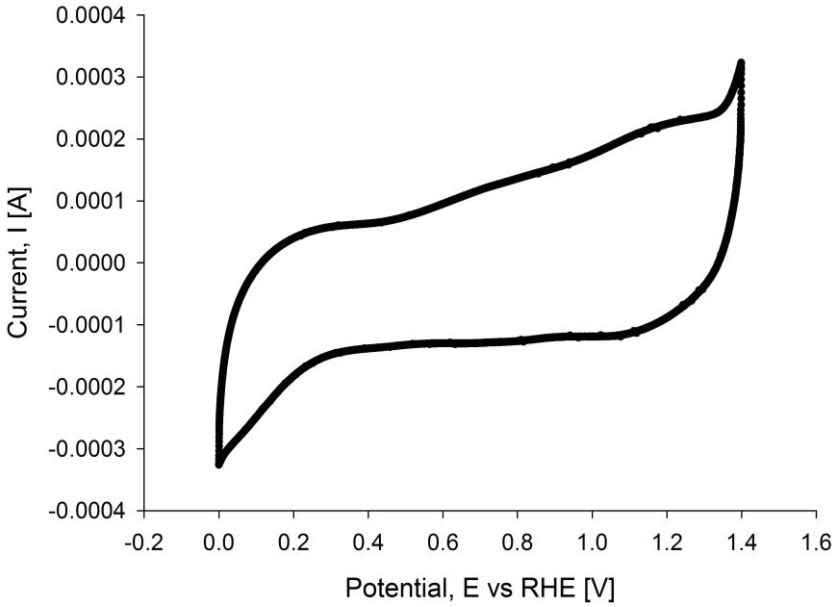

Figure 5.22: Cyclic voltammetry of IrO_2-DSA, prepared by painting, in 0.5 M H_2SO_4. The potential was swept from 0 V to 1.4 V with a sweep rate of 10 mV s^{-1}.

5.5.3 Synthesized IrO_2-DSA prepared by dip coating

SEM images of the circular IrO_2-DSAs, which were dip coated, are shown in Figure 5.23. The EDS analysis gave an indication of the main elements present, in addition to the amount of each of them (Table 5.4). The element analysis showed an Ir:Ta molar ratio of 73:27, which was close to the desired composition of 70:30. The EDS analysis indicated an even distribution of both iridium and tantalum, no particle agglomerates were detected. In addition, the analysis detected a large amount of titanium present in the surface cracks. As for the painted electrode (5.5.2) this is most likely signals from the titanium substrate being exposed in the cracks.

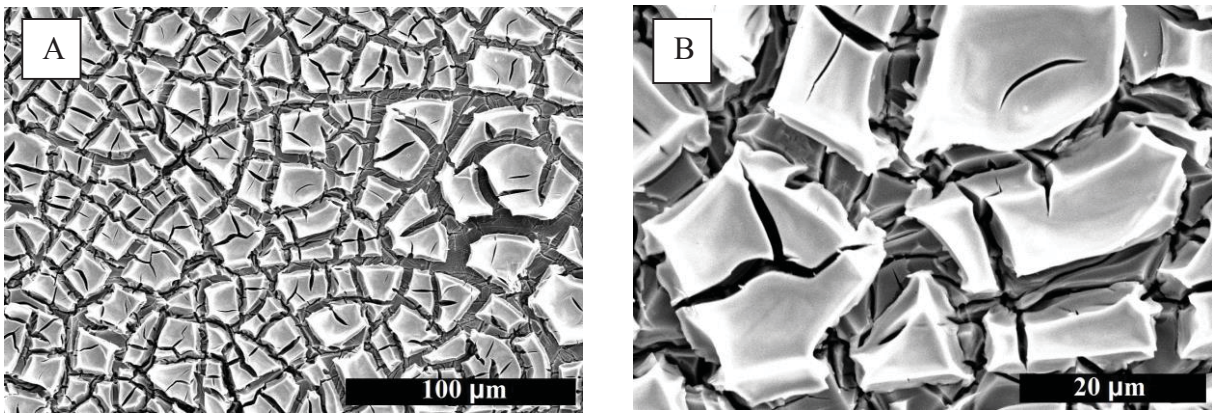

Figure 5.23: SEM images of a DSA (IrO_2 – Ta_2O_5/Ti) electrode. The electrode was dip coated and heated at 470°C for 20 minutes.

Table 5.4: EDS data for Figure 5.23 A. Given in atomic percent.

Area	O	C	Ir	Ta	Cl	Ti
Figure 5.23 A	40.1	19.1	19.6	7.0	7.0	6.6

The circular electrodes were also characterized by cyclic voltammetry in 0.5 M H_2SO_4 (Figure 5.24). The same geometric area of both the dip coated and the painted electrode was exposed for the electrolyte. Figure 5.24 shows a much larger current response than that for the painted electrode (Figure 5.22), indicating that applying coating by dipping results in a larger active surface area. Only by looking at the amount of coating applied by the different methods, this was to be expected. Five dipping treatments resulted in a coating layer of approximately 8 mg cm^{-2}, wheras five painting treatments resulted in a coating layer of approximately 2 mg cm^{-2}.

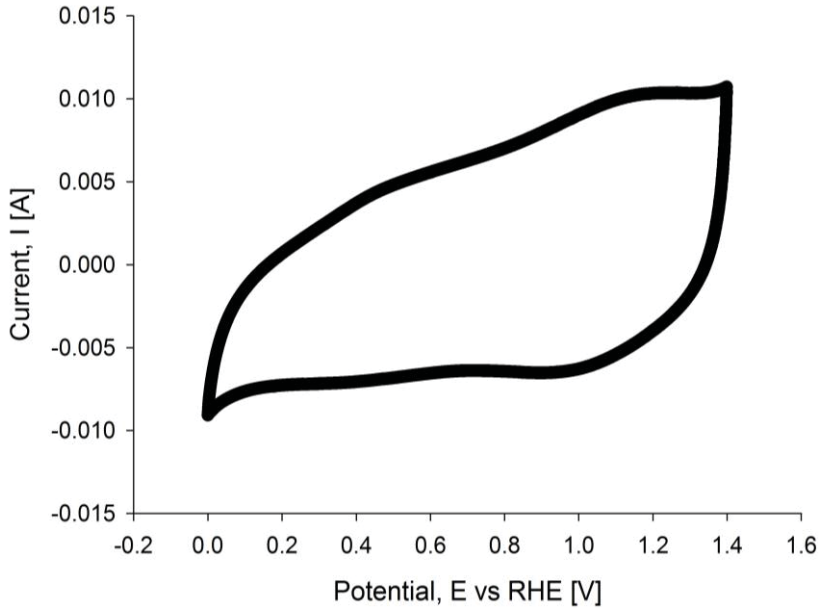

Figure 5.24: Cyclic voltammetry of IrO_2-DSA, prepared by dip coating, in 0.5 M H_2SO_4. The potential was swept from 0 V to 1.4 V with a sweep rate of 10 mV s^{-1}.

In addition to SEM, EDS and cyclic voltammetry, the circular electrodes made by dip coating were also analyzed with XRD. Figure 5.25 shows indistinct peaks with very low intensity. This may be due to noise, it may indicate a too small sample volume or it may result from a sample being amorphous or of low crystallinity. As the dip coating procedure gave a much thicker coating than the painting of the electrodes, the lack of distinct peaks is most likely due to a low degree of crystallinity.

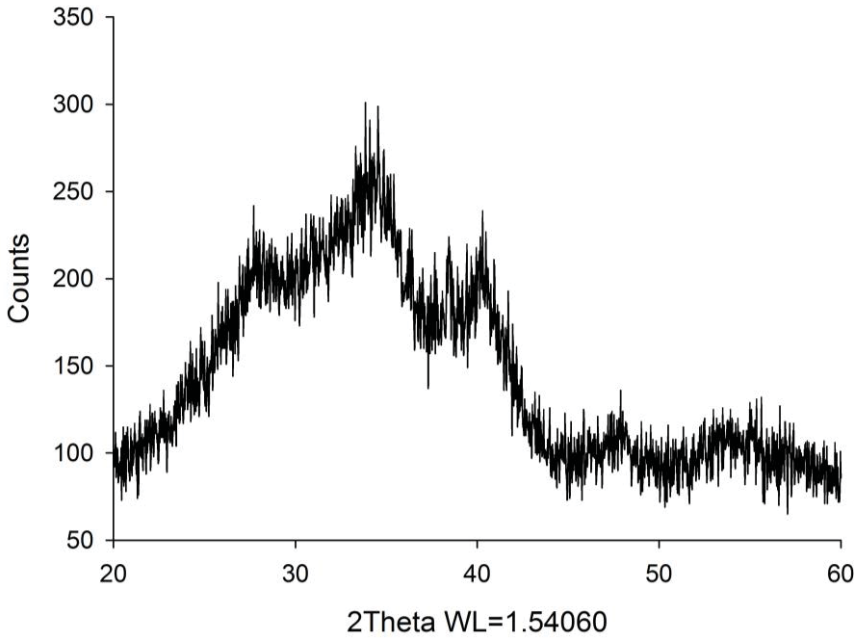

Figure 5.25: XRD of the IrO2-DSA (IrO_2-Ta_2O_5/Ti) prepared by dip coating.

After further examination of the dip coated electrodes it was found that the substrate used for the flow cell electrode was porous. This was not the case for the two circular electrodes, and so the flow cell electrode was examined by SEM after the electrolysis experiments (Figure 5.26). From the figure below it is clear that the morphology of the electrode surface is dependent on the structure of the substrate. Still, the flow cell electrode does contain characteristic cracked areas (Figure 5.26 D). EDS analysis of the electrode showed the presence of both iridium and tantalum, but because of the porosity of the electrode and the penetration depth of the X-rays, a large amount of the signal is most signals from the titanium substrate.

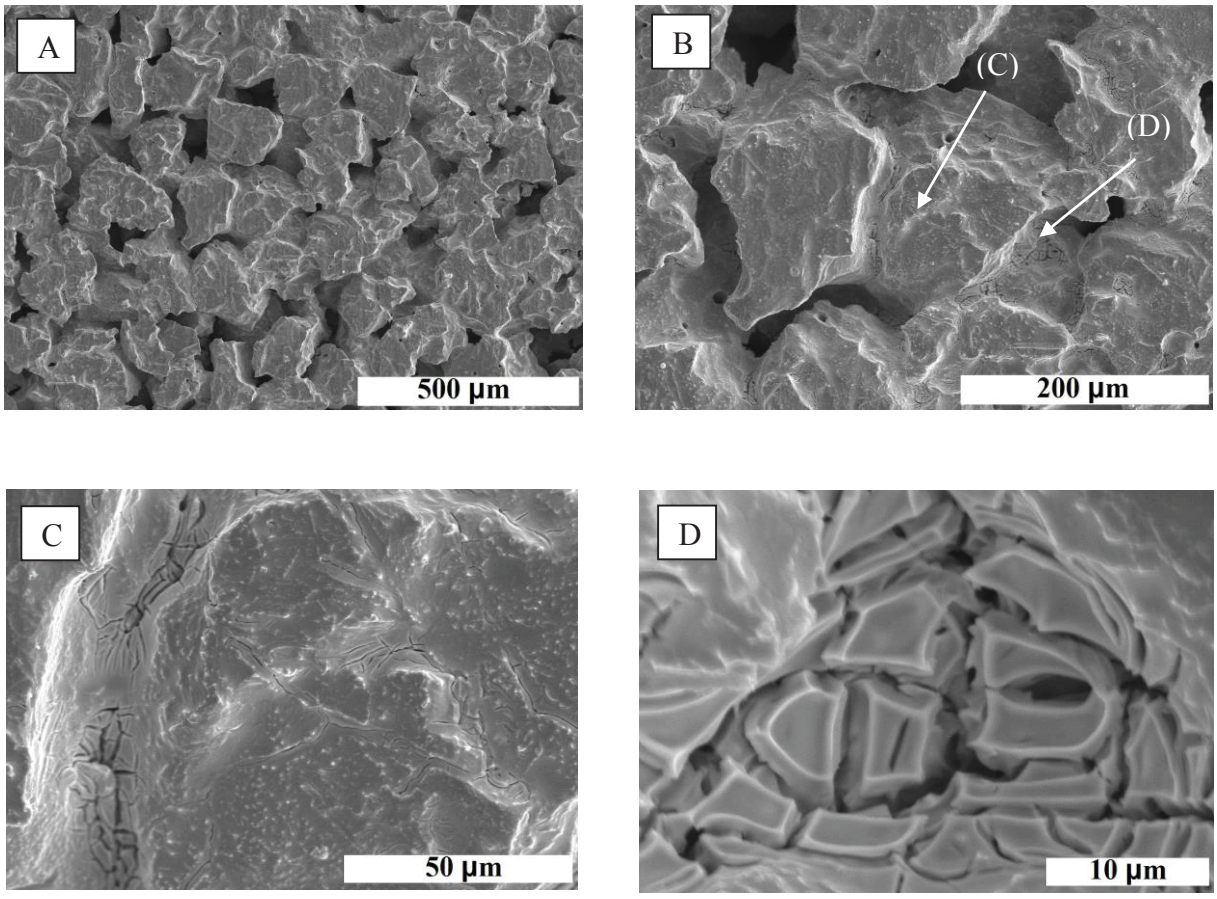

Figure 5.26: SEM images of the coated flow cell electrode. A, B, C and D shows a different magnification of the same area.

5.6 Electrolysis

The preliminary testing of the flow cell (different flow rates and different currents were tested) with the use of the electrode synthesized in house did not give promising results. No reduction of the chloride content was achieved. The synthesized electrode was then further tested in a stagnant cell to exclude this from being inoperative. For comparison, the same experiments were carried out using a commercial RuO_2/IrO_2-mesh from Permascand. The IrO_2-electrode synthesized in house was found not to be as active as the commercial RuO_2/IrO_2-mesh from Permascand. This can be seen from the experiments executed in the stagnant cell (Table 5.6). Because of this, further experiments were only carried out using the commercial electrode.

5.6.1 Electrolysis in a custom made flow cell

The flow cell and its dimensions are shown in the experimental section (Figure 4.4). The core results from the flow cell are shown in Table 5.5. In this table, the electrode synthesized in house is named synth., and the commercial RuO_2/IrO_2-mesh from Permascand is named Ru/Ir. The measured potential as a function of time using the RuO_2/IrO_2-mesh in the flow cell is shown in Figure 5.27. As there was some problems with the chloride containing process water blocking the tube in the flow cell, most of the experiments with this solution were carried out in the stagnant cell (see section 5.6.2).

Table 5.5: Experimental parameters and results for some of the chloride removal experiments executed in the flow cell. T = 25°C.

WE	CE	Electrolyte	Flow rate [mL h^{-1}]	Current [mA]	Average potential [V]	Reduction of chloride content [%]	Current efficiency [%]
Synth.	Steel	1000 ppm	100	50	2.6	0	-
Ru/Ir	Steel	3000 ppm	~10	100	3.7	3	1
Ru/Ir	Steel	process water	~10	100	5.5	23	3

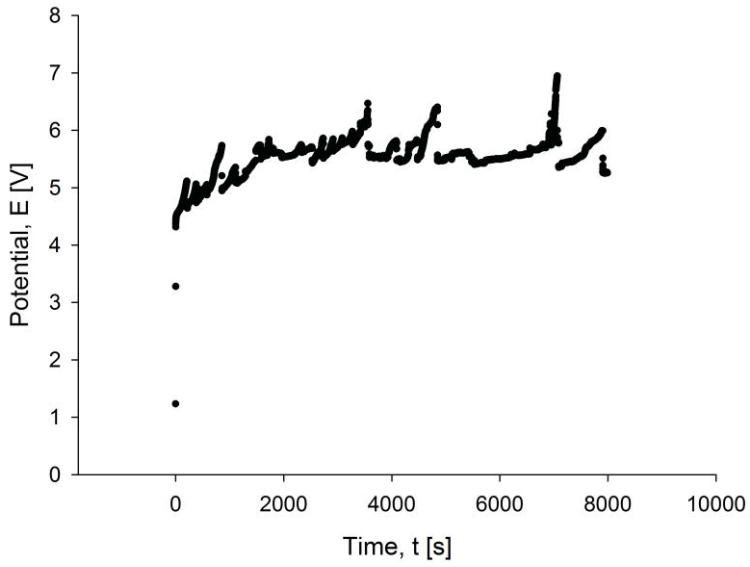

Figure 5.27: Measured potential as a function of time for the flow cell electrolysis experiment where the RuO_2/IrO_2-mesh was used in process water. The current was set to 100 mA.

The current efficiency calculated from the experiments executed in the flow cell was in the range of 1-3 % (Table 5.5). This result is comparable to the current efficiency measurements carried out by RRDE experiments (Section 5.4.2), giving a current efficiency towards chlorine evolution of approximately 3 %. This indicates that the use of rotating ring disc electrodes for current efficiency estimation is suitable for chlorine evolution on iridium oxide based electrodes.

In the project work carried out in the fall of 2013 [14] electrolysis was executed in a stagnant cell using a RuO_2-TiO_2/Ti (70:30) electrode with a diameter of 1 cm placed in a sample holder. The use of a stagnant cell simulates the use of a batch process in the industry. The flow cell was therefore built with the intention of testing a different way to remove the chloride, simulating a continuous chloride removal process. An experiment during the project work (1000 ppm of chloride, 4 hours electrolysis, and current of approximately 10 mA cm^{-1}) gave a reduction in the chloride content of 5 % and a current efficiency of 16 %. Comparing this to the results carried out in the flow cell (Table 5.5) shows a higher chloride reduction in the process water (~1400 ppm chloride) but a lower current efficiency, using the flow cell. These results are dependent both on the size of the electrodes used in the different experiments and on the actual current density applied to the system. A conclusion on whether the use of a flow cell or a stagnant cell is best for chloride removal cannot be drawn only from these results alone. The reader is referred to Section 5.7 for a more thorough discussion on the subject.

For the synthetic electrolyte (3000 ppm) both the reduction of chloride content and the current efficiency were lower than for the experiments using process water. A reason for this is discussed in section 5.6.2.

As can be seen from Table 5.5, electrolysis experiments carried out in the process water yielded a much higher potential than for those carried out in the stagnant electrolyte. This may be due to components in the process water blocking parts of the electrode surface and lowering the activity. The reduction of activity will cause an increase in the overpotential to achieve the same current density.

5.6.2 Electrolysis in stagnant cell

The results from some of the experiments carried out in the stagnant cell are shown in Table 5.6. In this table, the electrode synthesized in house is named synth., and the commercial RuO_2/IrO_2-mesh from Permascand is named Ru/Ir. The measured potential as a function of time for some of the experiments stated in Table 5.6 is shown in Figure 5.28.

Table 5.6: Experimental parameters and results for the chloride removal experiments executed in the stagnant cell. T = 25°C.

WE	CE	Electrolyte	Electrolysis time [h]	Current [mA]	Average potential [V]	Reduction of chloride content [%]	Current efficiency [%]
Synth.	Pt	10 000 ppm	1	50	1.6	0**	-
Ru/Ir	Pt	10 000 ppm	1	50	1.8	0	-
Ru/Ir	Pt	10 000 ppm	1	100	1.8	0.6**	4
Ru/Ir	Pt	10 000 ppm	4.6	100	2.8	24*	14
Synth.	Pt	3000 ppm	1	200	2.4	0.6**	0.7
Synth.	Pt	3000 ppm	15	100	2.8	3	0.5
Ru/Ir	Steel	3000 ppm	1	100	2.1	3	6
Ru/Ir	Steel	3000 ppm	3	100	2.2	10	8
Ru/Ir	Pt	3000 ppm	15	100	2.5	68	10
Ru/Ir	Steel	process water	3	100	3.1	28	10
Ru/Ir	Pt	process water	15	100	3.2	98	7

* The electrolyte was bubbled with Ar gas during the experiment.

** A flow of Ar gas was placed above the cell during the experiment.

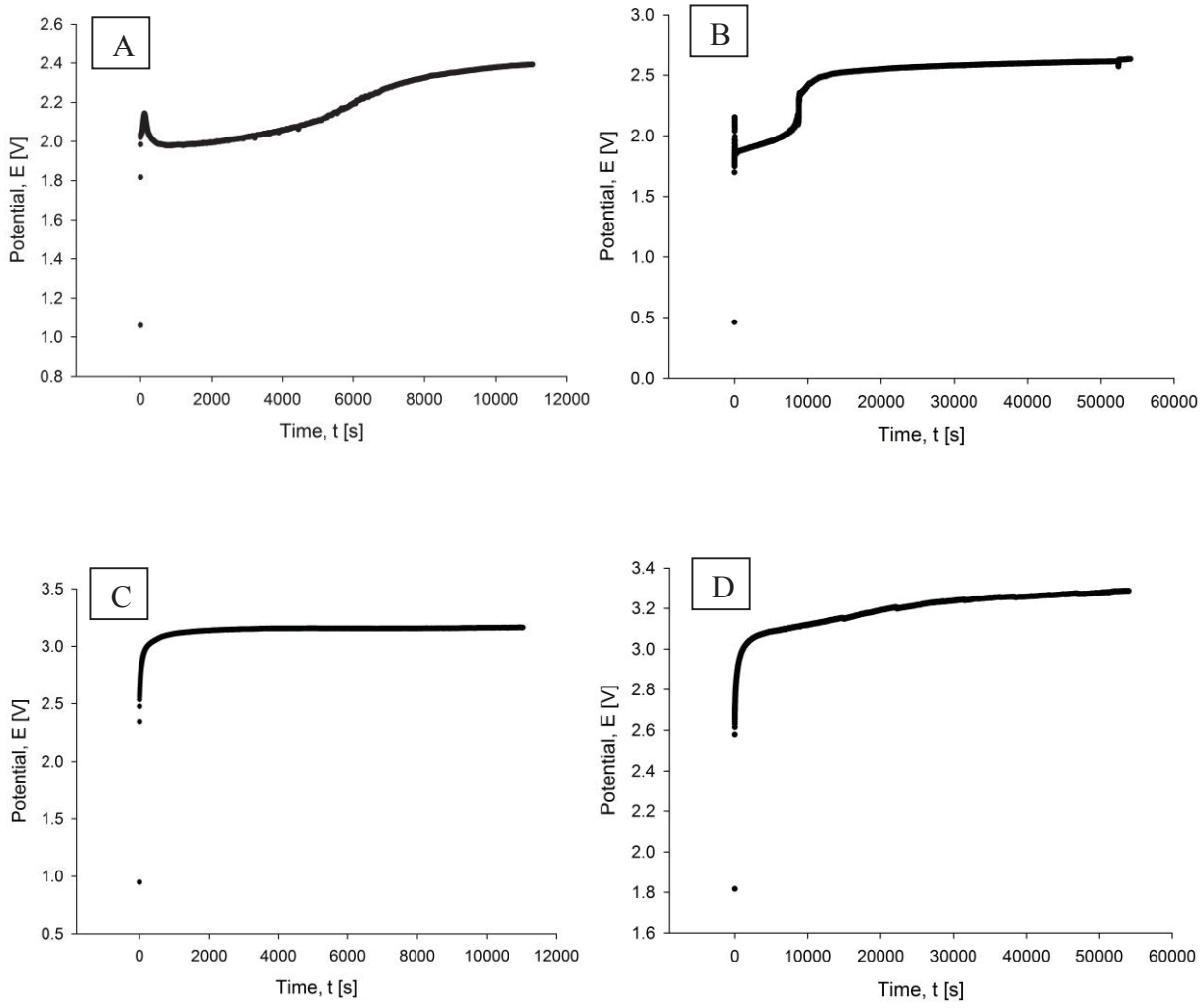

Figure 5.28: Measured potential as a function of time for some of the experiments, using the RuO_2/IrO_2-mesh, stated in Table 5.6. A current of 100 mA was used in all of the stated experiments. (A) Synthetic electrolyte containing 3000 ppm of chloride, 3 hours of electrolysis. (B) Synthetic electrolyte containing 3000 ppm of chloride, 15 hours of electrolysis. (C) Process water, 3 hours of electrolysis. (D) Process water, 15 hours of electrolysis.

The experiments executed in a stagnant cell (Table 5.6) gave a lower current efficiency compared to the experiments carried out during authors the project work in the fall of 2013 [14]. This is believed to be due to the difference in actual current density. In all of the experiments described above the electrodes had a geometric surface area of approximately 32 cm^2 (assuming a solid electrode). This implies that the current used in these experiments is in the range of 3 mA per cm^2 electrode. Because of a high ohmic drop in the electrolyte, causing the potential to become very high, it was not possible to use a higher current. In the project work, on the other hand, all of the electrolysis experiments were run at a constant potential of

1.7 V giving a current density of 10 – 22 mA cm^{-2} [14]. Comparing these results, the current efficiency was expected to be lower in the present work as the actual current density was very small.

Analysing the results in Table 5.6 regarding the chloride concentration in the electrolyte, there was expected an increase in the current efficiency with increasing chloride concentration. The increase in current efficiency with increasing chloride concentration has been described in different literature [34, 53], and was also supported by the authors project work in the fall of 2013 [14]. Why this trend was not observed in the results presented in Table 5.6 is not known. An explanation may be that the commercial electrode needs time to be activated, resulting in a lower current efficiency for chlorine evolution at the start of its service life. The experiments using an electrolyte containing 10 000 ppm of chloride was the first to be run in the stagnant cell. It may be that a similar experiment executed at the end of the experiment series would have resulted in a larger current efficiency.

For the reduction of chloride content, a much better result was achieved during the experiments carried out recently, compared to the results from the project work [14]. This is believed to be due to the electrode area used in these experiments. A larger electrode area, which was used in the present work, should result in a larger reduction of the chloride content. In the project work the electrode area was much smaller with a geometry based area of only 1 cm^2, resulting in a chloride reduction of only 5 %.

Another important aspect of the experiments carried out in the stagnant cell was the observation of bubble growth on the electrode surface. During the electrolysis experiments of 1 hour it was discovered that the gas bubbles formed on the working electrode did not easily detach from the electrode surface. If this is the case, the active surface area of the electrode will decrease during operation and there is also a possibility of additional ohmic drops [12]. When the electrolysis was carried out for longer than 1 hour, using the commercial electrode, it seemed as if the bubble problem disappeared after a while. Then most of the gas bubbles formed at the electrode were released and reached the surface of the electrolyte. As discussed earlier in this section, it is suggested that the coating of the electrode needs time to be activated. For the electrode synthesized in house the bubble growth seemed large, independent of the electrolysis time. This electrode had a rougher surface than the commercial electrode. It is believed that the use of

larger electrodes in the industry as well as flow of the electrolyte will minimize this problem by “bubble drag”. Bubbles detaching from the bottom of the anode will drag other bubbles of the surface as they rise up the cell.

From Table 5.5 and Table 5.6 it can be seen that there is a large difference in the results from the electrolysis carried out in the process water compared to those carried out in the synthetic electrolyte. The reason for this is not known, but it may be caused by a different pH in the process water. As discussed in section 2.2, a lowering of the pH will cause a retardation of the oxygen evolution causing the current efficiency for chlorine evolution to increase. In addition, according to the Pourbaix diagram (Figure 2.2), chlorine gas is more stable at low pH.

5.6.3 Activity of the electrode synthesized in house

As shown in Table 5.5 and Table 5.6 the IrO_2-DSA (IrO_2-Ta_2O_5/Ti) electrode synthesized in house exhibits a low selectivity towards chlorine evolution compared to the commercial RuO_2/IrO_2-mesh.

Studies [68, 69] have shown that controlling the amorphization of the IrO_2-Ta_2O_5 coating has been effective for the inhibition of unwanted side reactions like PbO_2 deposition. This has been done by lowering the thermal decomposition temperature. Kawaguchi [69] found the oxygen evolution to accelerate by use of electrodes containing a large amount of iridium as the coating became amorphous.

Whether Kawaguchi’s observations would be discovered in a chloride-containing electrolyte is not known. Assuming that this is the case, the high selectivity for oxygen evolution using the electrode synthesized in house may be due to the probable amorphization of the electrode, discovered by XRD (see Section 5.5.3).

Studies of ruthenium oxide electrodes has shown that micro pores favour oxygen evolution [36, 70], indicating that the oxygen evolution reaction is not a simple surface process. These micro pores were found not to be accessible for the large chloride ions, causing a low selectivity towards chlorine evolution if a porous coating is used. As described in Section 5.5.3, the titanium substrate used for the flow cell electrode appeared to be porous. This will lead to the IrO_2-Ta_2O_5 coating of the electrode also being porous, as shown in Figure 5.26. Assuming that

the results from the mentioned studies are also applicable to IrO_2 typed electrodes; it may be that the observed low selectivity towards chlorine evolution is due to a porous surface structure of the synthesized electrode.

Further testing of amorphous and porous coatings used in chloride-containing electrolytes is necessary to draw a conclusion regarding the influence of amorphization and porosity on the chlorine selectivity.

5.6.4 Cell design

Even though the results of this work show better results in a stagnant cell it is still believed that a flow cell, with some optimization, would be the best alternative. The anode compartment was made so that the electrode would fill most of the space. In that way all of the electrolyte flowing through the cell would be in contact with the electrode. The separator placed between the anode and cathode compartment (Figure 4.5) was made to hinder flow of gases from one side to the other. There was also a hope that the electrolyte would only flow through the anode compartment on its way through the cell. As the current efficiency obtained during the experiments was very low, it is assumed that the electrolyte also flows through the cathode compartment, making the volume of the cell much larger than intended. An idea for optimization of the flow cell is to replace the separator with a diaphragm.

Another aspect of the cell design is the potential risk of explosion as the oxygen formed at the anode, and the hydrogen formed at the cathode may mix. Because of this it is of high importance to separate the gases produced at the electrodes in the cell. Another possibility is to remove the the hydrogen evolution from the cathode. Kiros and Bursell [71] has been testing an air/ oxygen gas diffusion electrode, which replaced the hydrogen evolving cathode in a chlor-alkali cell. In addition, chlorine production is one of the most energy demanding processes in the world [2]. Changing from the traditional hydrogen producing cathodes to the so called oxygen depolarized cathodes will lower the energy consumption [2].

As for the current efficiency, it was mentioned that a flow cell with a large electrode to electrolyte ratio might improve this. Another aspect of the electrolytical removal of chloride is the removal of the produced chlorine gas. From an HSE point of view, as chlorine gas is toxic, proper ventilation and handling of the gas is necessary.

5.6.5 Chloride removal as a function of temperature

The commercial RuO_2/IrO_2-mesh from Permascand was also tested using different temperatures. This was done to study the influence of temperature on the chloride removal. The experiments were executed in a stagnant electrolyte containing 3000 ppm of chloride. In all experiments steel was used as the counter electrode, the electrolysis time was set to three hours, and a current of 100 mA was used. The results from the temperature dependent experiments are shown in Table 5.7.

Table 5.7: Results from the temperature dependent electrolysis experiments. WE: RuO_2/IrO_2-mesh, CE: steel, electrolysis time: 3h, current: 100mA.

Temperature [°C]	Reduction of chloride content [%]	Current efficiency [%]
25	10	8
35	12	8
60	2	1

As can be seen from Table 5.7, a temperature increase of 10 degrees from 25°C to 35°C did not give a large change in the reduction of chloride content nor the current efficiency. This is to be expected, as the kinetics of the oxygen evolution reaction as well as the chlorine evolution reaction will increase with an increase in temperature. Increasing the temperature up to 60°C caused a severe drop in the amount of chloride to be removed and in the current efficiency. This effect is believed to come from deactivation of the electrode. After the experiment was finished, the electrolyte had a yellowish colour and the counter electrode was coated with a grey substance (see Figure 5.29) which was not soluble in water.

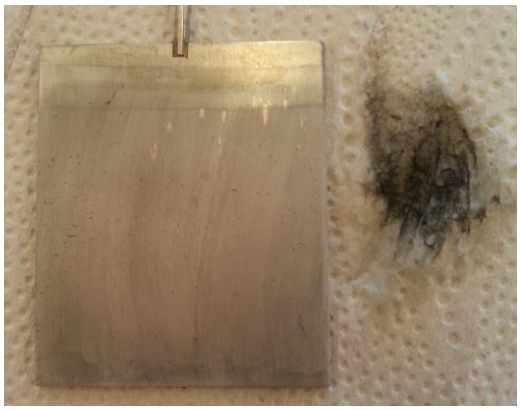

Figure 5.29: Counter electrode after electrolysis at 60°

5.6.6 Electrode deposit

After long time electrolysis in process water, white deposits (Figure 5.30) were detected on the counter electrode, and also some in the electrolyte. With an average current of approximately 3 mA the deposits were visible after five hours. The electrode was checked again after an electrolysis time of 20 hours. Now the deposits had a dendritic shape.

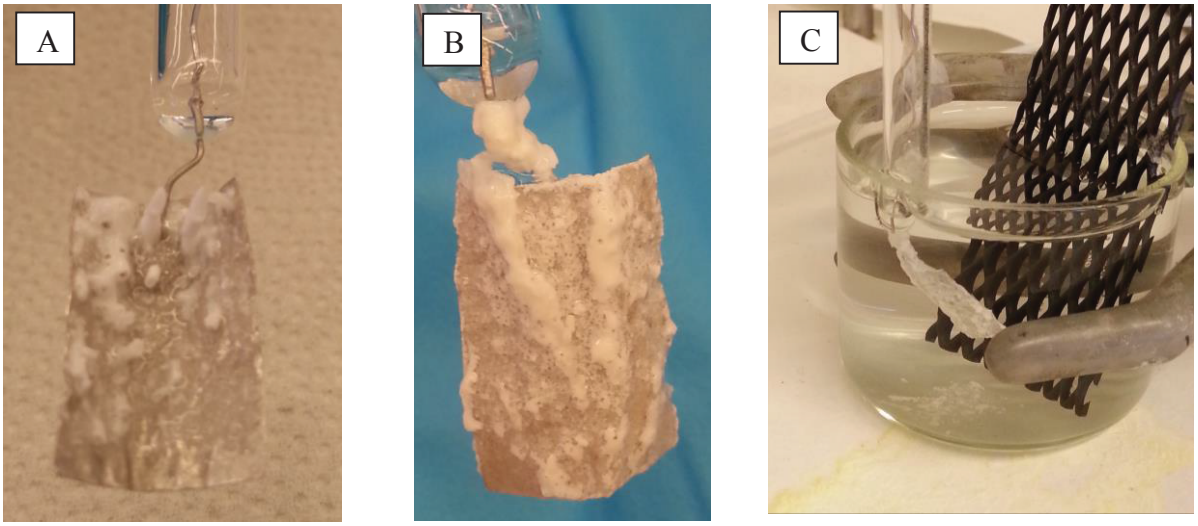

Figure 5.30: Scaling on the counter electrode after long time electrolysis in process water. (A) After 20 hours at 3mA. (B) After 15 hours at 100 mA. (C) Deposits were also detected in the electrolyte after 15 hours at 100 mA.

The deposit was mechanically removed from the electrode and then left to dry before it was examined with XRD. This did not give any results, implying that the deposit was partly or fully amorphous. The deposit was further examined by EDS, by dispersing the dried powder in water

and then coating it with carbon. This gave a clear indication that the deposit mostly consisted of calcium phosphates, as can be seen in Figure 5.31. The EDS analysis of the entire area gave a composition as stated in Table 5.8. With a solubility product in the order of 10^{-29} for $Ca_3(PO_4)_2$ [13] the idea that the deposit was a calcium phosphate salt is supported. Other possible salts and their solubility product constants are given in Table 5.9.

As discussed in Section 5.6.1, the potential measured during electrolysis in the process water was much higher than that in the synthetic electrolyte. This was explained as parts of the surface area of the electrode being blocked by components in the process water, lowering the activity of the electrode. Phosphate ions are known to adsorb stronger on to oxide surfaces (compared to other ions), blocking active sites for intermediates to form [64]. Given that the deposit on the counter electrode was determined to be calcium phosphate, the explanation above is reasonable.

Table 5.8: EDS data for Figure 5.31 A.

Area	O	Ca	P	Mg	Sr	K
Figure 5.31 A	80.8	10.2	7.6	0.9	0.3	0.2

Table 5.9: Solubility product constants at 25°C [13].

Ca(OH)2	$Ca_3(PO_4)_2$	CaF_2	$CaCO_3$
$6.4 \cdot 10^{-6}$	$2.07 \cdot 10^{-29}$	$3.2 \cdot 10^{-11}$	$3.3 \cdot 10^{-9}$

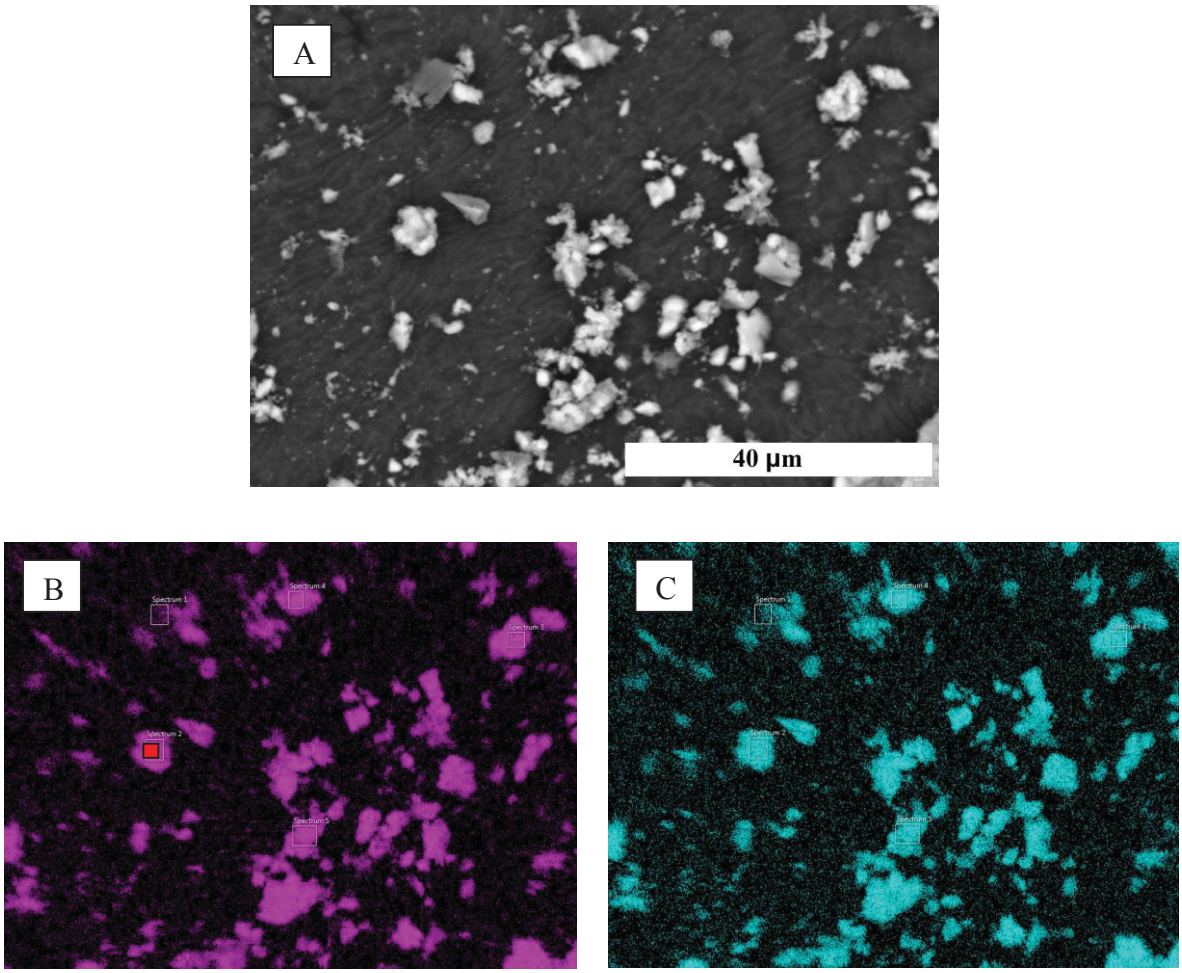

Figure 5.31: ***(A)*** *SEM image of deposit found at the cathode after long time electrolysis. The particles was coated in carbon.* ***(B)*** *Calcium map from the EDS analysis. The bright purple areas are Ca.* ***(C)*** *Phosphorus map from the EDS analysis. The bright blue areas are P.*

An EDS spectrum from the red point in Figure 5.31 B is shown in Figure 5.32.

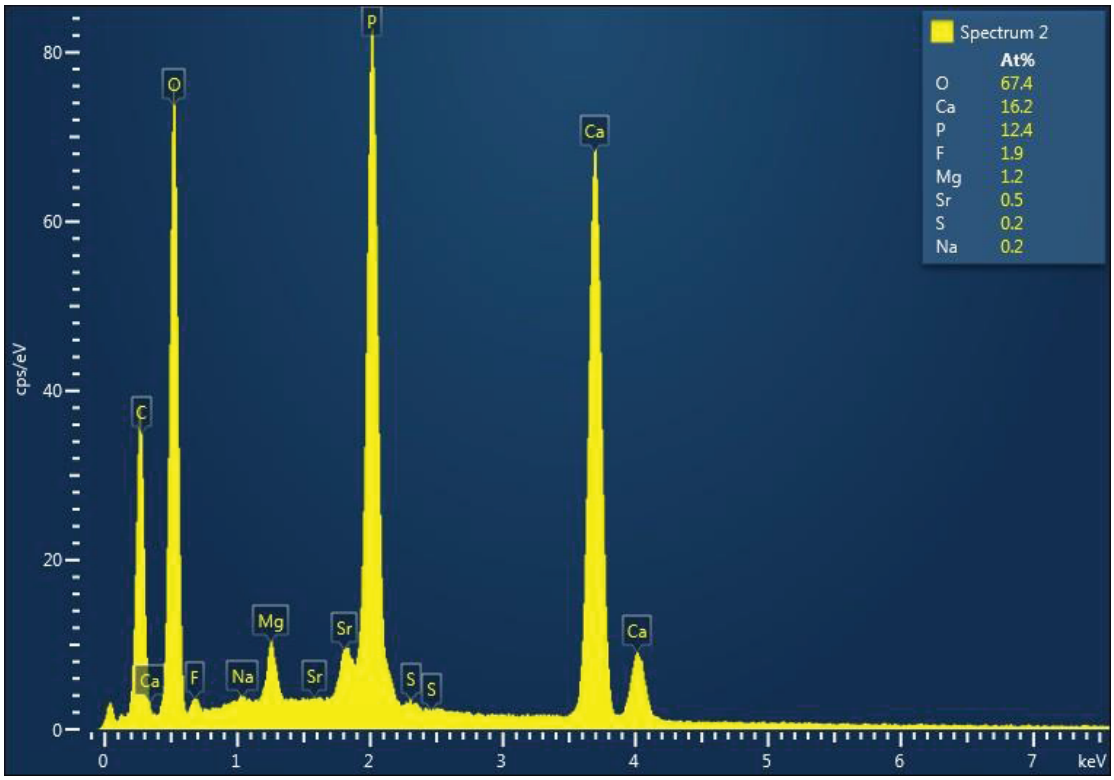

Figure 5.32: EDS spectrum of the red point marked in Figure 5.31 B.

During the long term electrolysis experiments in both synthetic electrolyte and process water there was observed some white deposit on the working electrode as well. As can be seen in Figure 5.33, the deposit was located above the electrolyte level. The composition of this deposit is not known, but is believed to be nitrates from the electrolyte.

Figure 5.33: Deposit discovered on the working electrode after long time electrolysis in both synthetic electrolyte and process water.

5.6.7 Sources of error

The results from the electrolysis experiments are stated with a maximum of two significant numbers as the error in the titration method is assumed to be of essential importance. As there was used a standard burette for the titration, there may be discrepancies in the results due to reading errors. In addition, there was used a 0.1 M silver nitrate solution independent of the chloride concentration, and therefore the inaccuracy in the results would increase with decreasing chloride content. To improve the reliability of the results, it is necessary to improve the titration method by using a lower concentration of silver nitrate when determining the chloride concentration of solutions containing below 1000 ppm of chloride. Also, use of a more accurate titrator, preferably an autotitrator, should be assessed.

5.7 Industrial considerations

In the experiments carried out in this thesis it was found that chlorine evolution on iridium oxide based DSAs is only to a small degree affected by mass transport. As discussed earlier, there may be mass transport effects present which is masked by the dominating oxygen reaction. In an industrial scale, the mass transport effects would be optimized by a large production of gas at the electrodes, causing an effective stirring between the anode and cathode in the cell. However, there is also a problem related to the large gas evolution at the electrodes, the production of acid mist. Acid mists is known to be generated as a result of gas bubbles bursting at the electrolyte-air interface [72]. The bursting gas bubbles results in particles mixing with the air causing toxic aerosols. This may cause health problems for operators in the area due to inhalation of the aerosols.

As mentioned in Section 5.6, there are different ways of implementing electrolytic removal of chloride in an industrial process. One being a batch process, removing the chloride in a stagnant cell. Another way, using a flow cell, is to continuously remove chloride from the process water. Both of these methods have been simulated in this thesis. The results in Table 5.6 indicates that the current efficiency for chlorine evolution is relatively stable independent of the chloride concentration. If the same result is achieved in an industrial scale, the batch process is to be preferred. The use of a batch process will for instance simplify the procedure of removing the deposit of the counter electrode, which is formed during electrolysis.

When implementing a new process in the industry, the cost of this implementation is of prime importance. Of course, there will be a high cost connected to the investment in new equipment. As this is usually a one-time payment the cost that is most important to monitor is the one connected to the run-time of the process. In a project like this, the highest expense item will be the electrical energy consumption connected to the electrolysis. This can be calculated by use of equation (5.2). Here W_{el} is the electrical consumption in kWh kg^{-1}, U is the total cell voltage in volts, CE_x is the current efficiency and M_x is the mol weight of the product.

$$W_{el} = \frac{nFU}{CE_x \cdot M_x \cdot 3600} \tag{5.2}$$

As discussed in Section 2.1, the cell voltage is dependent not only on the reversible potential of the reaction, but also on the overpotential and other potential losses. When current is flowing through an electrochemical cell, there will always be a potential drop between the reference electrode and the working electrode. This voltage drop is known as an ohimc drop or iR drop [9], and is dependent on the electrolyte conductivity, the distance between electrodes and the magnitude of the current. As can be seen from equation (5.2), lowering of the cell voltage will cause a reduction in the electrical energy necessary and therefore also the cost will be reduced. To minimize the ohmic losses, and then reduce the cell voltage, it is important to ensure that the electrolyte is highly conducting, that the electrodes are of even dimensions and that they are placed as close as possible.

As an example, the chlorate process has an electrical energy consumption of approximately 5.4 kWh per kilogram product, with a current efficiency of 95 % [4]. The cell voltage of the process is usually around 3.1 V with an ohmic voltage drop of 0.44 V and a current density of approximately 3 kA m^{-2}. Assuming a price of 0.3 NOK/kWh [73] and an annual production rate of 750 000 tonnes chlorate, a reduction in the ohmic voltage drop by a factor of 2 will reduce the annual electricity costs by 90 million NOK.

As pointed out earlier, the electrolytic removal of chloride has a downside regarding health, environment and safety as toxic chlorine gas is formed during the process. The outlet of chlorine products to the atmosphere needs to be avoided, as halogens like chlorine are known to reduce the amount of ozone in the atmosphere [74]. Causing a degradation of the ozone layer, which

protects the earth from most of the ultraviolet radiation. One way to handle the chlorine gas produced, is by installing a scrubber system. A chlorine scrubber is a device for removal of chlorine by the addition of a scrubbing agent in the gas flow. Usually a base like sodium hydroxide is added [75]. The presence of sodium hydroxide will give the reaction given in equation (5.3) [75].

$$Cl_2 + 2NaOH \rightarrow NaOCl + NaCl + H_2O \qquad (5.3)$$

6 Conclusion

Experiments carried out in this work indicated that the kinetics of the chlorine evolution reaction on IrO_2-Ta_2O_5/Ti electrodes is only to a small degree dependent on rotation rate, and the effect of mass transport is therefore limited.

Rotating ring disc experiments were executed in a chloride containing electrolyte (0.04 M HNO_3, 3.2 wt% NH_4NO_3) for current efficiency measurements. These experiments yielded for platinum a current efficiency (towards chlorine evolution) of 23-32%, and for iridium oxide; 2.4-3.2 %. Cyclic voltammetry using platinum showed a peak current at approximately 1.6 V vs RHE, related to the chloride present in the electrolyte. The peak is believed to be connected to a change in the surface state of platinum. An explanation may be the formation of a platinum-chloro-complex.

The removal of chloride, from an acidic nitrate solution, was successfully carried out in both a stagnant cell and a flow cell, using a commercial RuO_2/IrO_2-mesh electrode from Permascand. The IrO_2-DSA (IrO_2-Ta_2O_5/Ti) synthesized in house, by thermal decomposition, showed very low selectivity towards chlorine evolution. This may be due to low crystallinity of the coating or because of the porosity of the titanium substrate.

For the synthetic electrolyte (0.04 M HNO_3, 3.2 wt% NH_4NO_3, 3000 ppm of chloride), electrolysis in the designed flow cell (RuO_2/IrO_2-mesh), yielded a chloride reduction of 3 % and a current efficiency of 1 %. The electrolysis was run galvanostatically with a current of 100 mA and a flow rate of approximately 10 mL h^{-1}. The three hour, stagnant electrolysis (100 mA) gave a chloride reduction of 10 % and a current efficiency of 8 %. For the process water, the same electrolysis experiment yielded a chloride reduction of 23 % and a current efficiency of 3 % in the flow cell. The three hour, stagnant electrolysis gave a chloride reduction of 28 % and a current efficiency of 10 %.

The electrolysis experiments executed in the process water resulted in deposits on the counter electrode. By EDS analysis, the deposit was determined to consist of mostly calcium phosphate.

7 Further work

This work has indicated that chlorine evolution on IrO_2-Ta_2O_5/Ti electrodes is only to a small degree influenced by mass transport. A more in depth study of the kinetics of the chlorine evolution reaction is important to confirm or invalidate this conclusion. A study of the kinetics is especially important regarding the influence that pH and temperature has on the selectivity towards chlorine evolution.

To optimize the chloride reduction by electrolysis, both cell design and electrode design need improvement. Regarding cell design, it is still believed that a flow cell is the best alternative for efficient chloride removal. If it really is the case that the current efficiency for chlorine evolution is stable independent of the chloride concentration (Table 5.6), the use of a batch process should be assessed. Experiments confirming these results should be carried out, as there may be an "activation problem" of the electrode causing these trends. It is also of interest to study the effect of a membrane or diaphragm in the electrolysis cell. Also, if implementing a flow cell a series of electrolysers is believed to increase the chloride removal. As for the working electrode, a more thorough study of different catalytic coatings is necessary. This to find the most suitable electrode for chloride removal in electrolytes containing low amounts of chloride. In addition to the study of different coating compositions, different preparation procedures and heat treatments should be addressed. It is also of interest to study the effect that porous and amorphous coatings would have on the chlorine selectivity (as discussed in Section 5.6.3).

8 References

1. O'Brien TF, Bommaraju TV, Hine F. *Handbook of Chlor-Alkali Technology: Volume I: Fundamentals*. Boston, MA: Springer Science+Business Media, Inc; 2005. : v.: digital p.
2. Moussallem I, Joerissen J, Kunz U, Pinnow S, Turek T. *Chlor-alkali electrolysis with oxygen depolarized cathodes: history, present status and future prospects*. Journal of Applied Electrochemistry. 2008;38(9):1177-94.
3. Cornell A. *Electrode reactions in the chlorate process* Stockholm: Royal Institute of Technology; 2002.
4. Thonstad J. *Fag 53541 Elektrolyseprosesser*: Institutt for teknisk elektrokjemi, Norges teknisk-naturvitenskapelige universitet CY - [Trondheim]; 1998. 1 b. (flere pag.) : ill. p.
5. Fauvarque J. *The chlorine industry*. Pure and Applied Chemistry. 1996;68(9):1713-20.
6. Beer HB. *The invention and industrial-development of metal anodes*. Journal of the Electrochemical Society. 1980;127(8):C303-C7.
7. Beer HB, *Electrode and Coating therefor,*U.S Pat. 3,632,298. 1972.
8. Bard AJ, Faulkner LR. *Electrochemical methods: fundamentals and applications*. New York: Wiley; 1980. xviii,718 s. : fig., tab., diagr. p.
9. http://www.metrohm-autolab.co.uk/Applications/applications - *Ohmic drop, basic principles* [cited 2014 7th of June].
10. Tunold R, Thonstad J, Hagen G. *Elektrokjemi: videregående kurs : forelesningsreferat vårsemester 1985*. Trondheim: Universitetet i Trondheim, Norges tekniske høgskole, Institutt for teknisk elektrokjemi; 1985. 1 b. (flere pag.) : ill. p.
11. Hamann CH, Hamnett A, Vielstich W. *Electrochemistry*. Weinheim: Wiley; 2007. XVIII, 531 s. : ill. p.
12. Trasatti S. *Progress in the understanding of the mechanism of chlorine evolution at oxide electrodes*. Electrochimica Acta. 1987;32(3):369-82.
13. Aylward G, Findlay, T. *SI Chemical Data*. 6th ed: Wiley; 2008.
14. Sandland M. *Chlorine evolution for removal of chloride from aqueous nitrate solution*. [Project thesis]. In press 2013.
15. Jerkiewicz G, Vatankhah G, Lessard J, Soriaga MP, Park YS. *Surface-oxide growth at platinum electrodes in aqueous H_2SO_4 - Reexamination of its mechanism through combined cyclic-voltammetry, electrochemical quartz-crystal nanobalance, and Auger electron spectroscopy measurements*. Electrochimica Acta. 2004;49(9-10):1451-9.

16. Pletcher D. *A first course in electrode processes*. Romsey: Electrochemical Consultancy; 1991. 274 s. : ill. p.
17. Nikolic J, Expósito E, Inesta J, González-Garzia J, Montiel V. *Theoretical concepts and applications of a rotating disk electrode*. J Chem Educ. 2000;77(9):1191 - 4.
18. http://www.pineinst.com [cited 2014 March 28.].
19. Albery WJ, Hitchman ML. *Ring-disc electrodes*. Oxford: Clarendon Press; 1971.
20. Lein HL. *Laboratoriekurs i generell kjemi*. Trondheim: Tapir akademisk; 2010. 145 s. : ill. ; 30 cm p.
21. Hjelen J. *Scanning elektron-mikroskopi*. Trondheim: SINTEF; 1989. 106 s. : ill. p.
22. Lloyd GE. *Atomic-number and crystallographic contrast images with the sem - a review of backscattered electron techniques*. Mineralogical Magazine. 1987;51(359):3-19.
23. Callister WDaR, D.G. *Materials Science and Engineering*. 8th ed2011.
24. West AR. *Crystallography and Diffraction Teqhniques.* Basic Solid State Chemistry1999.
25. Tolchard J, Grande, T. *"Powder X-ray Diffraction" from the course TMT4166*. 2013.
26. Trasatti S. *Physical electrochemistry of ceramic oxides*. Electrochimica Acta. 1991;36(2):225-41.
27. Trasatti S. *Electrocatalysis: Understanding the success of DSA®*. Electrochimica Acta. 2000;45(15-16):2377-85.
28. Trasatti S. *Electrocatalysis in the anodic evolution of oxygen and chlorine*. Electrochimica Acta. 1984;29(11):1503-12.
29. Vercesi GP, Rolewicz J, Comninellis C, Hinden J. *Characterization of dsa-type oxygen evolving electrodes - choice of base-metal*. Thermochimica Acta. 1991;176:31-47.
30. Comninellis C, Vercesi GP. *Characterization of dsa-type oxygen evolving electrodes - choice of a coating*. Journal of Applied Electrochemistry. 1991;21(4):335-45.
31. Hayfield PCS. *Development of the Noble Metal/Oxide Coated Titanium Electrode*. Platinum Metals Review. 1998;42(2):46-55.
32. Comninellis C, Vercesi GP. *Problems in dsa coating deposition by thermal-decomposition*. Journal of Applied Electrochemistry. 1991;21(2):136-42.
33. Nidola A. *Technological impact of metallic oxides as anodes.* In: Trasatti S, editor. Electrodes of conductive metallic oxides, part B. Amsterdam: Elsevier; 1980. p. 626-59.
34. Trasatti S, Lodi G. *Oxygen and Chlorine Evolution at Conductive Metallic Oxide Anodes.* In: Trasatti S, editor. Electrodes of conductive metallic oxides, part B. Amsterdam: Elsevier; 1981.

35. Åkre T. *Electrowinning of Cobalt from Chloride Solutions: Anodic Deposition of Cobalt Oxide on DSA*. Trondheim: Norwegian University of Science and Technology; 2008.
36. Lodi G, Sivieri E, Debattisti A, Trasatti S. *Ruthenium dioxide-based film electrodes .3. Effect of chemical composition and surface morphology on oxygen evolution in acid-solutions*. Journal of Applied Electrochemistry. 1978;8(2):135-43.
37. Galizzio.D, Tantardi.F, Trasatti S. *Ruthenium dioxide - new electrode material .1. Behavior in acid solutions of inert electrolytes*. Journal of Applied Electrochemistry. 1974;4(1):57-67.
38. Trasatti S, Lodi G. *Properties of Conductive Transition Metal Oxides with Rutile-type structure.* In: Trasatti S, editor. Electrodes of Conductive Metallic Oxides, part A. Amsterdam: Elsevier; 1980.
39. Trasatti S. *The oxygen evolution reaction.* In: Wendt H, editor. Electrochemical hydrogen technologies: electrochemical production and combustion of hydrogen. Amsterdam: Elsevier; 1990. p. xx, 512 s. : ill.
40. Hu JM, Zhang JQ, Cao CN. *Oxygen evolution reaction on IrO_2-based DSA (R) type electrodes: kinetics analysis of Tafel lines and EIS*. International Journal of Hydrogen Energy. 2004;29(8):791-7.
41. Mraz R, Krysa J. *Long service life IrO_2/Ta_2O_5 electrodes for electroflotation*. Journal of Applied Electrochemistry. 1994;24(12):1262-6.
42. Kotz R, Stucki S. *Stabilization of RuO_2 by IrO_2 for anodic oxygen evolution in acid-media*. Electrochimica Acta. 1986;31(10):1311-6.
43. Hansen HA, Man IC, Studt F, Abild-Pedersen F, Bligaard T, Rossmeisl J. *Electrochemical chlorine evolution at rutile oxide (110) surfaces*. Physical Chemistry Chemical Physics. 2010;12(1):283-90.
44. Faita G, Fiori G. *Anodic discharge of chloride ions on oxide electrodes*. Journal of Applied Electrochemistry. 1972;2:31-5.
45. Kotz R, Lewerenz HJ, Stucki S. *XPS studies of oxygen evolution on Ru and RuO_2 anodes*. Journal of the Electrochemical Society. 1983;130(4):825-9.
46. Martelli GN, Ornelas R, Faita G. *Deactivation mechanisms of oxygen-evolving anodes at high-current densities*. Electrochimica Acta. 1994;39(11-12):1551-8.
47. Hine F, Yasuda M, Noda T, Yoshida T, Okuda J. *Electrochemical behavior of the oxide-coated metal anodes*. Journal of the Electrochemical Society. 1979;126(9):1439-45.

48. Cornell A, Hakansson B, Lindbergh G. *Ruthenium based DSA((R)) in chlorate electrolysis - critical anode potential and reaction kinetics*. Electrochimica Acta. 2003;48(5):473-81.
49. Takasu Y, Sugimoto W, Nishiki Y, Nakamatsu S. *Structural analyses of RuO_2-TiO_2/Ti and IrO_2-RuO_2-TiO_2/Ti anodes used in industrial chlor-alkali membrane processes*. Journal of Applied Electrochemistry. 2010;40(10):1789-95.
50. Marshall A. *Electrocatalysts for the oxygen evolution electrode in water electrolyseres using proton exchange membranes: synthesis and characterisation*. Trondheim: Norwegian University of Science and Technology; 2005.
51. Michell D, Rand DAJ, Woods R. *Study of ruthenium electrodes by cyclic voltammetry and X-ray-emission spectroscopy*. J Electroanal Chem. 1978;89(1):11-27.
52. Miles MH, Huang YH, Srinivasan S. *Oxygen-electrode reaction in alkaline-solutions on oxide electrodes prepared by thermal-decomposition method*. Journal of the Electrochemical Society. 1978;125(12):1931-4.
53. Arikawa T, Murakami Y, Takasu Y. *Simultaneous determination of chlorine and oxygen evolving at RuO_2/Ti and RuO_2-TiO_2/Ti anodes by differential electrochemical mass spectroscopy*. Journal of Applied Electrochemistry. 1998;28(5):511-6.
54. Kuhn AT, Mortimer CJ. *The efficiency of chlorine evolution in dilute brines on ruthenium dioxide electrodes*. Journal of Applied Electrochemistry. 1972;2:283-7.
55. Marshall A, Borresen B, Hagen G, Sunde S, Tsypkin M, Tunold R. *Iridium oxide-based nanocrystalline particles as oxygen evolution electrocatalysts*. Russian Journal of Electrochemistry. 2006;42(10):1134-40.
56. Takasu Y, Onoue S, Kameyama K, Murakami Y, Yahikozawa K. *Preparation of ultrafine RuO_2-IrO_2-TiO_2 oxide particles by a sol-gel process*. Electrochimica Acta. 1994;39(13):1993-7.
57. Marshall A, Borresen B, Hagen G, Tsypkin M, Tunold R. *Electrochemical characterisation of $Ir_xSn_{1-x}O_2$ powders as oxygen evolution electrocatalysts*. Electrochimica Acta. 2006;51(15):3161-7.
58. Kurihara LK, Chow GM, Schoen PE. *Nanocrystalline metallic powders and films produced by the polyol method*. Nanostructured Materials. 1995;5(6):607-13.
59. Lervik IA, Tsypkin M, Owe L-E, Sunde S. *Electronic structure vs. electrocatalytic activity of iridium oxide*. J Electroanal Chem. 2010;645(2):135-42.
60. Kawaguchi K. *Electrocatalysis and Novel Functions of Nano-Structured IrO_2-Ta_2O_5/Ti Anodes*. Trondheim: Norwegian University of Science and Technology; 2013.

61. Yadav AP, Nishikata A, Tsuru T. *Effect of halogen ions on platinum dissolution under potential cycling in 0.5 M H2SO4 solution*. Electrochimica Acta. 2007;52(26):7444-52.
62. Ofstad AB, Thomassen MS, de la Fuente JLG, Seland F, Moller-Holst S, Sunde S. *Assessment of Platinum Dissolution from a Pt/C Fuel Cell Catalyst: An Electrochemical Quartz Crystal Microbalance Study*. Journal of the Electrochemical Society. 2010;157(5):B621-B7.
63. Ginstrup O, Leden I. *Emf measurements on system platinum(4) /platinum(2) in a chloride ion medium at 60 degrees C*. Acta Chemica Scandinavica. 1968;22(4):1163-&.
64. Owe LE. *Characterisation of Iridium Oxides for Acidic Water Electrolysis*. Trondheim: Norwegian University of Science and Technology; 2011.
65. Kuznetsova E. *Structure, Selectivity and Electrocatalytic Activity of Iridium-Based Oxides for Oxygen Evolution*. Trondheim: Norwegian University of Science and Technology; 2014.
66. Otogawa R, Morimitsu M, Matsunaga M. *Effects of microstructure of IrO_2-based anodes on electrocatalytic properties*. Electrochimica Acta. 1998;44(8-9):1509-13.
67. Hu JM, Zhang JQ, Meng HM, Cao CN. *Microstructure, electrochemical surface and electrocatalytic properties of IrO_2+Ta_2O_5 oxide electrodes*. Journal of Materials Science. 2003;38(4):705-12.
68. Morimitsu M, Matsumoto, K., Otogawa, R., Matsunaga, M., editor Intelligent electrodes to distinguish between wanted and unwanted reactions. 210th ECS Meeting; 2006; Cancun.
69. Kawaguchi K, Haarberg, G.M., Morimitsu, M. *Control of Amorphization of IrO_2-Ta_2O_5/Ti Electrodes to Suppress Unwanted Side Reactions*. ECS Trans. 2009;16(39).
70. Ardizzone S, Carugati A, Lodi G, Trasatti S. *Surface-structure of ruthenium dioxide electrodes and kinetics of chlorine evolution*. Journal of the Electrochemical Society. 1982;129(8):1689-93.
71. Kiros Y, Bursell M. *Low energy consumption in chlor-alkali cells using oxygen reduction electrodes*. International Journal of Electrochemical Science. 2008;3(4):444-51.
72. McGinnity JJ, Nicol MJ. *Sulfuric Acid Mist: Generation, Suppression, Health Aspects, and Analysis*. Mineral Processing and Extractive Metallurgy Review. 2014;35(3):149-92.
73. http://www.ssb.no/elkraftpris/ [cited 2014 8th of June].
74. Cambridge University. http://www.atm.ch.cam.ac.uk/tour/part3.html 1998 [cited 2014 13th of June].

75. http://worldchlorine.org/publications/index.html - *Chlorine Safety Scrubbing Systems* 2011 [cited 2014 8th of June].
76. Savinell RF, Zeller RL, Adams JA. *Electrochemically active surface-area - voltammetric charge correlations for ruthenium and iridium dioxide electrodes*. Journal of the Electrochemical Society. 1990;137(2):489-94.
77. Ardizzone S, Fregonara G, Trasatti S. *Inner and outer active surface of RuO_2 electrodes*. Electrochimica Acta. 1990;35(1):263-7.

A Preparation of a reversible hydrogen electrode (RHE)

The reference electrode used in the voltammetry experiments was a reversible hydrogen electrode (RHE) as shown in Figure A.1. To prepare the electrode the lower part of the electrode was filled with a solution of nitric acid with the same pH as the electrolyte (0.04M). The hydrogen electrode was then placed in the same solution of nitric acid with a platinum electrode working as both the counter electrode and the reference electrode, see Figure A.2. A potential of -4.0 V was applied to the system until approximately 50 % of the electrode was filled with hydrogen gas. The compartment for the hydrogen electrode to be situated in was further filled with fresh nitric acid (0.04M) before the hydrogen electrode was positioned.

Figure A.1: Reference electrode.

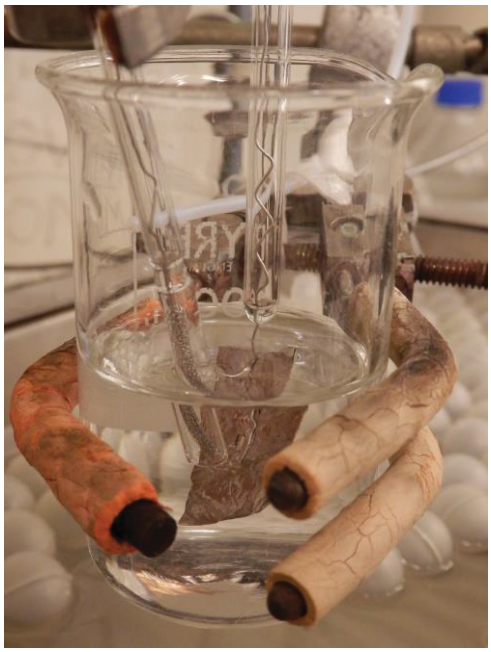

Figure A.2: Setup for making of the reference electrode.

B Normalising electrochemical measurements

When comparing different electrodes it is usually an advantage to normalise them with respect to the active sites on the electrode as the geometric surface area usually differ from the active surface area.

The platinum electrode

From a cyclic voltammogram like that in Figure B1, using the adsorption peaks for hydrogen (green area), the active surface area of platinum can be calculated. This is done by assuming that each platinum atom only adsorbs one hydrogen atom, and that for each adsorbed hydrogen atom it is associated a charge which is consumed or released in either the adsorption or desorption process [11]. For a complete platinum monolayer, the most accepted charge is 220 μC cm^{-2} [11]. By using these assumptions, the active surface area of a platinum electrode can be calculated from equation (A1).

$$A = \frac{Q_H}{q_{Pt}} = \frac{Q_H}{220 \mu C cm^{-2}} \qquad \text{(A1)}$$

,where Q_H is the charge associated with the hydrogen adsorption, and can be calculated from the area under the hydrogen adsorption peaks in the cyclic voltammogram.

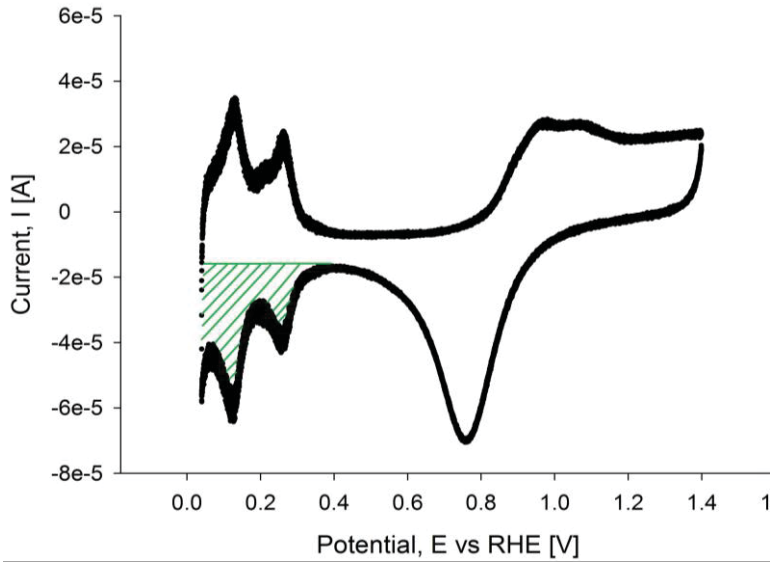

Figure B1: Cyclic voltammogram of Pt in 0.5 M H2SO4. Sweeping from 0 V to 1.4 V with a sweep rate of 100 mV s-1.

The IrO_2-DSA

Cyclic voltammograms of noble metal oxides can give information on the active surface area of these materials. It has been found that the electrochemically accessible surface area shows a linear dependency of voltammetric charge [76]. The charge of the electrode can be found by integrating the voltammetry curve (normally between 0 - 1.4 V) as described by Ardizzone [77]. The charge related to the voltammetric curve of oxides is several times smaller than that of the same metal. This is because the surface of thermal oxides is hydrated and the exchange of protons with the solution will only take place there [39].

There are two different types of charge related to the electrode. The inner charge represent the surface area that are hard to get at while the outer charge represent the surface area that are easily available. The total charge of the electrode are thus the total number of active sites on the electrode. Recording cyclic voltammograms using a high sweep rate, only the easily available sights will be responsible for the current. Using a low sweep rate, almost all of the sites will be active. This means that the total charge of the electrode can be found by plotting the inverse of the integrated charge against the square root of the sweep rate. Extrapolating the straight curve to zero will give the total charge, which is proportional to the number of active sites and thus the active surface area.

C Rotating ring disc electrode dimensions

The numbers given in Table C1 below, are derived from "Document LMECE6". The document was taken from the manufactorers (Pine Instrumentation) web page [18], and contain information on the RRDE (E6 series) used in this work.

Table C1: Rotating ring disc dimensions.

Parameter	**Value**
Disc outer diameter [mm]	5.0
Ring inner diameter [mm]	6.5
Ring outer diameter [mm]	7.5
Collection efficiency	26 %

D XRD data for IrO_2 hydrolysis powder

The XRD data for the IrO_2 powder used for RRDE experiments are shown in Figure D.1. Both the making of the powder as well as the XRD analysis were made by Anita Reksten.

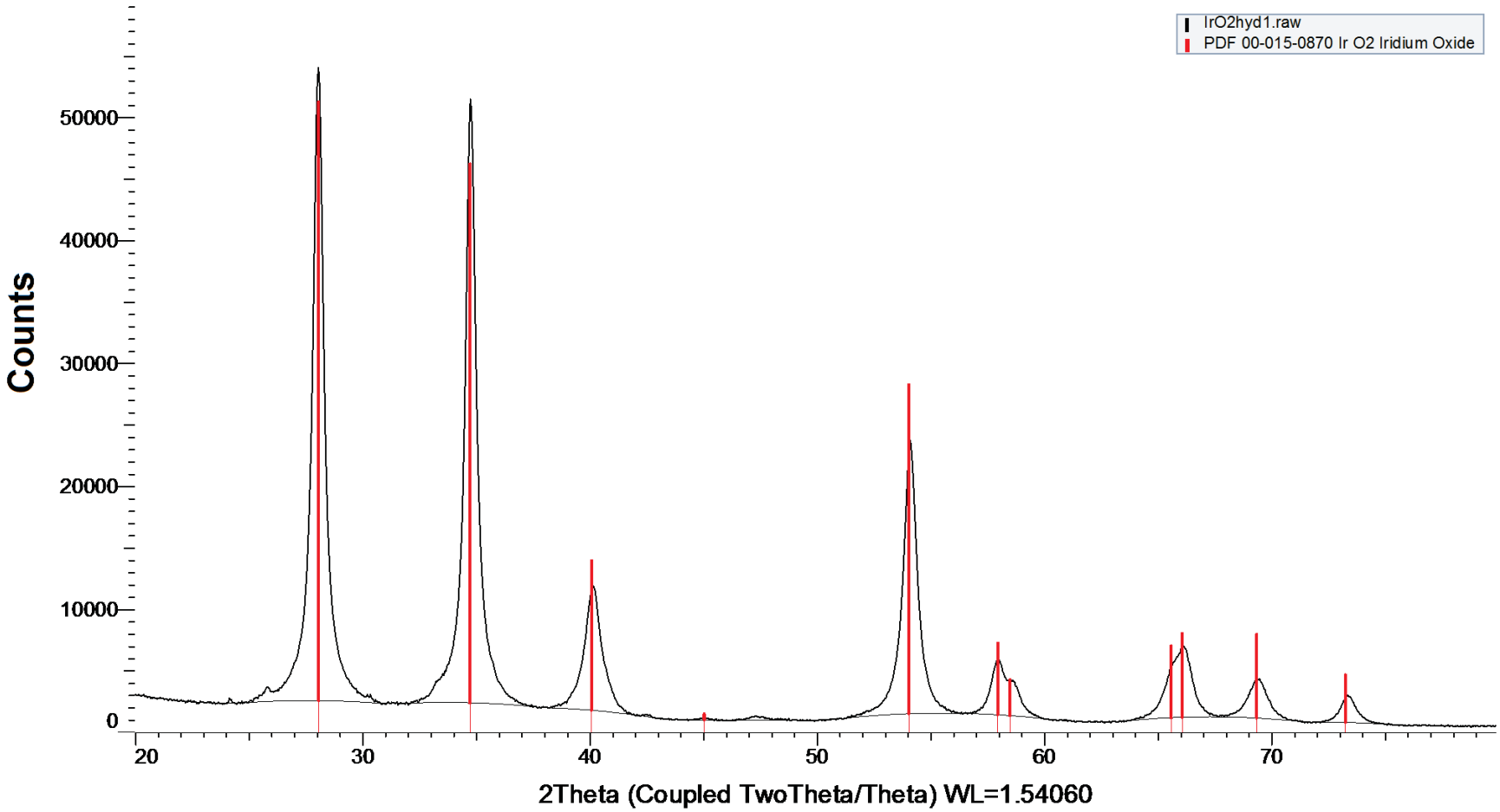

Figure D.1: XRD data for iridium oxide powder used for RRDE experiments. The powder were made by Anita Reksten, using the hydrolysis method.